

T.C.

UNIVERSITY OF TURKISH AERONAUTICAL ASSOCIATION

SCIENCE AND TECHNOLOGY INSTITUTE

**SIMILARTY ANALYSIS OF UNSTEEADY LAMINAR INCOMPRESSIBLE
STAGNATION POINT FLOW BOUNDARY LAYER IN PRESENCE OF
OSCILLATING MOTION**

PhD. THESIS

Ali BELHAJ

1303947010

Thesis Supervisor: Asst. Prof. Dr. Mustafa KAYA

DEPARTMENT OF MECHANICAL AND AERONAUTICAL ENGINEERING

December 2018

Ali Mohamed Ali Belhaj, having student number 1303947010 and enrolled in the Ph.D. Program at the Institute of Science and Technology at the University of Turkish Aeronautical Association, after meeting all of the required condition in the related regulations, has successfully accomplished, in front of the jury, the presentation of the thesis prepared with the title of “Similarity analysis of unsteady laminar incompressible stagnation point flow boundary layer in presence of oscillating motion”.

Thesis Supervisor: Assist. Prof. Dr. Mustafa Kaya
Ankara Yıldırım Beyazıt University

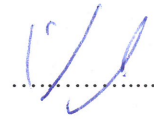
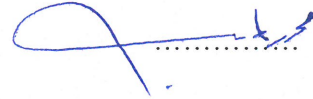
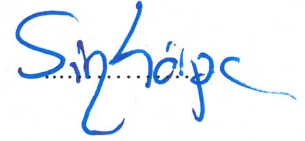
Jury Members:

Assoc. Prof. Dr. Murat DEMIRAL
University of Turkish Aeronautical Association

Assist. Prof. Dr. Durmuş Sinan KÖRPE
University of Turkish Aeronautical Association

Assist. Prof. Dr. Mohamed Salem EIMNEFI
University of Turkish Aeronautical Association

Assist. Prof. Dr. Munir ELFARRA
Ankara Yıldırım Beyazıt University



Thesis Defense Date: 28 Dec. 2018

OF UNIVERSITY OF TURKISH AERONAUTICAL ASSOCIATION

INSTITUTE OF SCIENCE AND TECHNOLOGY

STATEMENT NON-PLAGIARISM

I hereby declare that all information in this study I present as my Ph.D. thesis, entitled “*Similarity analysis of unsteady laminar incompressible stagnation point flow boundary layer in presence of oscillating motion*”, has been presented in accordance with the academic rules and ethical conduct. I also declare and certify with my honor that I have fully cited and referenced all sources utilized in this study.

28 Dec. 2018.

Ali Mohamed Belhaj



ABSTRACT

Similarity analysis of unsteady Laminar Incompressible Stagnation Point Flow Boundary Layer in Presence of Oscillating Motion

BELHAJ, Ali

Ph.D., Mechanical and Aeronautical Engineering

Thesis Supervisor: Assist. Prof. Dr. Mustafa KAYA

December-2018, 102 pages

The similarity solutions of Navier-Stokes equations describe incompressible laminar flows over semi-infinite plates. A special case is the classical Hiemenz problem which deals with the steady two-dimensional stagnation point flow on a vertical solid wall. There are also recent studies on the unsteady version of the Hiemenz problem. In this thesis work, the unsteadiness of the stagnation point flow is generalized using a harmonically oscillating plate and a time-dependent freestream flow. For this purpose, the unsteadiness parameter, oscillating frequency and amplitude are introduced. The similarity solutions are computed for the values of these parameters in various combinations. It is observed that, for any given oscillation amplitude, there exists a threshold frequency above which the flow is regular and periodic. The solution is unstable for the frequency below that value.

Keywords: stagnation point flow, similarity solutions, unsteady flow, oscillating plate, blowing

ÖZET

Salınım Hareketi Durumunda Zamana Bağlı Sıkışamaz Durma Noktası Akışının Sınır Tabakası

BELHAJ, Ali

Doktora, Makina ve Havacılık Mühendisliği

Tez Danışmanı: Dr. Öğr. Üyesi Mustafa KAYA

Aralık-2018, 102 sayfa

Navier-Stokes denklemlerinin benzerlik çözümleri, yarı-sonsuz plakalar üzerindeki sıkışamaz laminer akışları tarif eder. Bu çözümlerin özel bir durumu, yatay bir katı duvar üzerindeki zamandan bağımsız iki-boyutlu durma noktası akışının incelendiği klasik Hiemenz problemi. Hiemenz probleminin zamana bağlı versiyonları üzerine yeni çalışmalar da bulunmaktadır. Bu tez çalışmasında, durma noktası akışının zamana bağlı olma durumu genelleştirilmiştir. Genelleştirme, harmonik olarak salınan bir plaka ve zamana bağlı serbestakım akışı kullanılarak yapılmıştır. Bu amaç doğrultusunda, zamana bağlılık parametresi, salınım frekansı ve genliği değerlendirilmiştir. Benzerlik çözümleri, bu parametrelerin çeşitli kombinasyonlardaki değerleri için hesaplanmıştır. Verilen bir salınım genliği için, akışın düzgün ve periyodik olduğu eşik frekansının varlığı gözlenmiştir. Bu frekans değerinin altında çözüm kararsız olmaktadır.

Anahtar Kelimeler: durma noktası akışı, benzerlik çözümleri, zamana bağlı akış, salınan plaka, üfleme

ACKNOWLEDGEMENTS

I would like to thank my supervising Assist. Prof. Dr. Mustafa Kaya for constantly motivating and encouraging me, and also for his invaluable advice during my doctoral studies. I wish to thank my academic advisors, Assist. Prof. Dr. Sinan korpe, Assist. Prof. Dr. Mohamed Elmnifi, Assist. Prof. Dr. Munir Elffara, and Assoc. Prof. Dr. Murat Demiral for their interest in my research and for taking time to serve in my dissertation committee and reviewing this thesis.

Finally, I would like to express my deep gratitude to my parents who have prayed and inspired me and sponsored my undergraduate and graduate studies. I am extremely fortunate to be so blessed. I am also extremely grateful to my wife care, sacrifice, encouragement and patience. I also thank several of my friends who have helped me throughout my career.

December 15, 2018

Contents

ABSTRACT	iv
ÖZET	vi
CONTENTS	vii
LIST OF FIGURES	x
LIST OF TABLES	xiv
NOMENCLATURE	xv
Chapter 1: Introduction	
1.1: Motivation and objectives.....	1
1.1.1: Problem of thesis motivation.....	1
1.1.2: Thesis objectives.....	1
1.2: Stagnation point flows (literature review)	2
1.3: Problem of the current study.....	8
1.4: Order of thesis.....	12
Chapter 2: General Background Knowledge	
2.1: Similarity Transformations.....	13
2.1.1: Two-Dimensional Similarity Solutions: The Falkner-Skan Equation.....	13
2.1.2: Three Dimensional Similarity Solution.....	17
2.2: Steady stagnation point flows	21
2.2.1: The classical Hiemenz (1911) solution.....	21
2.2.2: Oblique stagnation-point flows.....	23
2.2.3: Two-fluid stagnation-point flow	23
2.2.4: The classical Homann solution.....	24
2,3: General review of unsteady Stagnation point flows.....	25
2.3.1: Orthogonal oscillations.....	26
2.3.2: The Homann flow against an oscillating plate.....	27
2.3.3: Three-dimensional stagnation-point flow.....	28

Chapter 3: Similarity Transformation and Numerical Solution

3.1: Similarity transformations.....	30
3.2: Numerical procedure to solve (PDE) similarity equations.....	36

Chapter 4: Results and Discussion

4.1: Comparison and investigation.....	39
4.1.1: Comparison (PDE & ODE) solutions.....	41
4.1.2: Comparison (PDE & CFD) solutions	45
4.2: Flow parameters regions and regimes.....	43
4.2.1: Regions of stable and unstable flow parameters regions.....	43
4.2.2: Regions of reversed and non-reversed flows at: $\eta = 0$	47
4.2.3: Matching regions of stable periodic and unstable flow parameters with regions of reversed and non-reversed flow parameters.....	51
4.3: The effect of flow parameters on $f - profile$	55
4.3.1: The effect of blowing parameter on $f - profile$	55
4.3.2: The effect of oscillation frequency on $f - profile$	56
4.3.3: The effect of unsteadiness parameter on $f - profile$	57
4.4: The effect of flow parameters on $f_{\eta} - profile$	59
4.4.1: The effect of blowing parameter on $f_{\eta} - profile$	59
4.4.2: The effect of oscillation frequency on $f_{\eta} - profile$	63
4.4.3: The effect of unsteadiness parameter on $f_{\eta} - profile$	66
4.5: The effect of flow parameters on $f_{\eta\eta} - profile$	69
4.5.1: The effect of blowing parameter on $f_{\eta\eta} - profile$	69
4.5.2: The effect of oscillation frequency on $f_{\eta\eta} - profile$	72

4.5.3: The effect of unsteadiness parameter on $f_{\eta\eta}$ – profile	74
4.6: The effect of flow parameters on shear stress distribution.....	76
4.6.1: Effect of blowing parameter on the wall shear stress.....	76
4.6.2: Effect of unsteadiness parameter on the shear stress.....	78
4.6.3: The observation of the time of maximum shear stress.....	80
Chapter 5: Conclusion and Future Work.	
5.1: Concluding Remarks.....	82
5.2: Further work.....	83
References	84

List of Figures:

Fig.1.1: Stagnation point flow (Hiemens 1911).....	2
Fig.1.2: Stability and instability of the flow. The lower curve corresponds to the small amplitude predictions of this boundary and the upper curve corresponds to the onset of quasi-periodicity, The diamonds correspond to the boundary between stable and unstable regions (P. Hall and D. T. Papageorgiou 1999)	4
Fig.1.3: The barrier in (Δ, σ) parameter space between regular periodic solutions and those which blow up in finite time. The lower graph shows the barrier close to $\sigma = 0$. The upper graph includes the asymptotic approximation for large σ (Blyth & Hall 2003).....	5
Fig.3.1: Grid points	36
Fig.3.2: Explicit and Implicit schemes.....	37
Fig.4.1: Compression PDE solution with ODE solution for horizontal velocity profile	40
Fig 4.2: Compression PDE solution with ODE solution for vertical velocity profile ...	40
Fig.4.3: Velocity field stream lines	41
Fig.4.4: Variation of the velocity component parallel to the wall near the stagnation point.....	42
Fig.4.5: Variation of the velocity component vertical to the wall near the stagnation point.....	42
Fig.4.6: Stable periodic & unstable flow parameters regions	44
Fig.4.7: Regular periodic structure for f -profile.....	45
Fig.4.8: Regular periodic structure for $f_\eta - profile$ (example1).....	45
Fig.4.9: Regular periodic structure for $f_\eta - profile$ (example2).....	46
Fig.4.10: Regular periodic structure for $f_{\eta\eta} - profile$ (example1).....	46
Fig.4.11: Regular quasi-periodic structure for $f_{\eta\eta} - profile$ (example2)	47
Fig.4.12: reversed and non-reversed regions of parameters at the wall (reversed flow at the wall exists at definite time).....	511
Fig.4.13: Matching regions of stable periodic and unstable flow parameters with regions of reversed and non-reversed flow parameters at the wall.....	52

Fig.4.14:Maximum reversal wall shear stress vs. oscillating frequency increasing
(at $\eta=0$, unsteadiness parameter $D=2$, blowing parameter $k=100$)..... 54

Fig.4.15:Reversalflow interval starting time vs. oscillating frequency
(at $\eta=0$, unsteadiness parameter $D=2$, blowing parameter $k=100$)..... 54

Fig.4.16:Slope of f-profile vs blowing parameter k(at unsteadiness parameter
 $D=4$, oscillation frequency $\omega=100$ 1/s) during the period $t = (5.81 \text{ s} - 5.85 \text{ s})$.55

Fig.4.17:Structures of (f-velocity profile) during a definite period of time
at(unsteadiness parameter $D=4$, oscillation frequency $\omega=100$ 1/s, blowing
parameter $k=0, 10$ respetively) 56

Fig.4.18:Structures of (f-profile) under the effect of (blowing parameter
 $k=60$, unsteadiness parameter $D=4$, oscillation frequency $\omega=10$ 1/s, 100
1/s)respectively at different times 56

Fig.4.19: Changing of unsteadiness parameter D on f-profile structure (blowing
parameter $k=30$ s cillation frequency $\omega=201$ /s) at $\omega t=4.3 \text{ rad}$ 57

Fig.4.20: Changing of unsteadiness parameter D on f-profile structure blowing parameter
 $k=30$ scillation frequency $\omega=50$ 1/s) at $\omega t=5.8 \text{ rad}$58

Fig.4.21:Changing of unsteadiness parameter D on f-profile structure at (blowing
parameter $k=30$ scillation frequency $\omega=100$ 1/s) at $\omega t=1.62 \text{ rad}$ 59

Fig.4.22:Changing of blowing parameter k effect on f_{η} -profile structure at
(unsteadiness parameter $D=4$, scillation frequency $\omega=30$ 1/s) at $\omega t=5.7 \text{ rad}$.600

Fig.4.23:Structures of f_{η} -profile at (blowing parameter $k=10$, unsteadiness parameter
 $D=4$) at different values of ωt 61

Fig.4.24: Structures of f_{η} -profile at (blowing parameter $k=60$ unsteadiness parameter
 $D=4$) at different values of ωt 62

Fig.4.25: Structures of f_{η} -profile at (blowing parameter $k=160$, unsteadiness parameter
 $D=4$) at different values of ωt 62

Fig.4.26: Structures of f_{η} -profile at (blowing parameter $k=500$, unsteadiness
parameter $D=4$) at different values of ωt 63

Fig.3.27: Structures of f_{η} -profile at (blowing parameter $k=60$, unsteadiness parameter
 $D=4$) at different values of ωt 64

Fig.4.28: Structures of f_{η} -profile at (blowing parameter $k=60$, unsteadiness parameter
 $D=4$, oscillation frequency $\omega=30$ 1/s 64

Fig.4.29: Structures of $f\eta$ -profile at (blowing parameter $k=60$, unsteadiness parameter $D=4$,oscillation frequency $\omega=100$ 1/s)..... 65

Fig.4.30: Structures of $f\eta$ -profile at (blowing parameter $k=60$, unsteadiness parameter $D=4$,oscillation frequency $\omega=300$ 1/s)..... 65

Fig.4.31: Structures of $f\eta$ -profile at (blowing parameter $k=60$, unsteadiness parameter $D=4$,oscillation frequency $\omega=700$ 1/s)..... 66

Fig.4.32: Structures of $f\eta$ -profile at ($\omega t=1.55$ rad) and (blowing parameter $k=60$, oscillation frequency $\omega=160$ 1/s) at different values of unsteadiness parameter D 67

Fig.4.33: Structures of $f\eta$ -profile at ($\omega t=4.82$ rad) and (blowing parameter $k=60$ oscillation frequency $\omega=160$ 1/s) at different values of unsteadiness parameter D67

Fig.4.34: Structures of $f\eta$ -profile at (blowing parameter $k=60$,unsteadiness parameter $D=0.5$, oscillation frequency $\omega=160$ 1/s) , at different times..... 68

Fig.4.35: Structures of $f\eta$ -profile at (blowing parameter $k=60$,unsteadiness parameter $D=2$, oscillation frequency $\omega=160$ 1/s) , at different times..... 68

Fig.4.36: Structures of $f\eta$ -profile at (unsteadiness parameter $D=4$, oscillation frequency $\omega=60$ 1/s) , at different values of blowing parameter. 70

Fig.4.37: Structures of $f\eta$ -profile at (unsteadiness parameter $D=4$, oscillation frequency $\omega=300$ 1/s), at different values of blowing parameter. 70

Fig.4.38: Structures of $f\eta$ -profile at (unsteadiness parameter $D=4$, blowing parameter= 300 ,at different values of oscillation frequency 71

Fig.4.39: Structures of $f\eta$ -profile at(unsteadiness parameter $D=4$,oscillation frequency $\omega=300$ 1/s), at different values of blowing parameter.....72

Fig.4.40: Structures of $f\eta$ -profile at(unsteadiness parameter $D=4$,blowing parameter $k=60$) at different values of oscillation frequency ($\omega=5,50,70,80,150$ 1/s).. 73

Fig.4.41: Structures of $f\eta$ -profile at(unsteadiness parameter $D=4$,blowing parameter $k=60$) at different values of oscillation frequency ($\omega=30,40,100,200$ 1/s)... 73

Fig.4.42: Structures of $f\eta$ -profile at(blowing parameter $k=60$, oscillation frequency $\omega=50$ 1/s)at different values of unsteadiness parameter D 74

Fig.4.43: Structures of $f\eta$ -profile at(blowing parameter $k=60$, oscillation frequency $\omega=100$ 1/s)at different values of unsteadiness parameter D 75

Fig.4.44: Structures of $f\eta$ -profile at(blowing parameter $k=60$, oscillation frequency $\omega=200$ 1/s)at different values of unsteadiness parameter D 75

Fig.4.45: Structures of $f\eta$ -profile at(blowing parameter $k=60$, oscillation frequency $\omega=400$ 1/s)at different values of unsteadiness parameter D 76

Fig.4.46: Maximum values of $f\eta$ -profile indicates maximum shear stress $f_{\eta}(\eta)_{(max.)}$ vs. oscillation frequency ω at different values of blowing parameter k at unsteadiness parameter $D=2$ 78

Fig.4.47: Maximum values of $f\eta$ -profile indicates maximum shear stress $f_{\eta}(\eta)_{(max.)}$ vs. oscillation frequency ω ,blowing parameter $k=100$ at at different values of unsteadiness parameter D 800

Fig. 4.48:The time at which $f\eta$ -profile maximum value occurs vs. oscillation frequency ω ,blowing parameter $k=100$ at at different values of unsteadiness parameter D 81

List of Tables

Table (1.1): Generalization of the previous studies.....	12
Table (2.1): Flow types due to the stream wise pressure gradient parameter	17
Table (4.1): Stable periodic & unstable flow parameters regions.....	44
Table (4.2): Regions of reversed & non-reversed flows (ODE solution)	48
Table (4.3): Regions of reversed & non-reversed flows (due to our assumptions)	49
Table (4.4): Values of ω^* at which the point separates reversed and non-reversed regions of parameters at the wall (reversed flow at the wall exists at definite time)	50
Table (4.5): Intervals of reversed flow & $f_{\eta\eta}(0)_{\max-\text{rev}}$ at the first period of cillation.....	53
Table (4.6): $f_{\eta\eta}$ – profile maximum values indicates maximum shear stress $f_{\eta\eta}(\eta)_{\max}$. vs. oscillation frequency ω at different values of blowing parameter k at unsteadiness parameter D	77
Table (4.7): $f_{\eta\eta}$ – profile maximum values indicates maximum shear stress $f_{\eta\eta}(\eta)_{\max}$. vs. oscillation frequency ω , blowing parameter $k = 100$ at different values of unsteadiness parameter D	79
Table (3.8): $f_{\eta\eta}$ – profile maximum value occurrence time vs. oscillation frequency ω , blowing parameter $k = 100$ at different values of unsteadiness parameter.....	81

Nomenclature:

symbol	Description
β	pressure gradient parameter
u	Velocity in the x-direction (ms^{-1})
v	Velocity in the y-direction (ms^{-1})
U_e	Potential flow velocity in the x-direction (ms^{-1})
V_e	Potential flow velocity in the y-direction (ms^{-1})
W_e	Potential flow velocity in the z-direction (ms^{-1})
x, y, z	Basic Cartesian coordinate
Re	Reynolds number
$\delta(x)$	function proportional to the boundary-layer thickness
ψ	Stream function
η	Similarity variable in the y-direction
f	Similarity function
f_η	First derivative of similarity function
$f_{\eta\eta}$	Second derivative of similarity function
$f_{\eta\eta\eta}$	Third derivative of similarity function
g	Similarity function
g_η	First derivative of similarity function
$g_{\eta\eta}$	Second derivative of similarity function
$g_{\eta\eta\eta}$	Third derivative of similarity function
C	Constant of three-dimensionality
A	Constant related to the geometry of the body
B	Constant related to the geometry of the body
ν	Viscosity (m^2s^{-1})
P_0	Stagnation pressure (Nm^{-2})
P	Pressure (Nm^{-2})
ρ	Density (kgm^{-3})
u_w	Flow velocity at the wall in the x-direction (ms^{-1})
t	Time (s)
Δ	Oscillation amplitude (m)
ω	Oscillation frequency (s^{-1})
$a(t)$	Unsteady function at potential flow
σ	Strohal number
α	Constant related to free stream acceleration
D	Unsteadiness parameter
k	Blowing parameter

$v_0(t)$

Unsteady vertical velocity at the surface

$u_0(t)$

Unsteady horizontal velocity at the surface



Chapter 1

Introduction

1.1: Motivation and Objectives:

1.1.1: Motivation

In the history of fluid dynamics, more and more interest has been given to the research on the field of non-steady stagnation point flows because of its wide range of applications in industry and aerodynamics. Stagnation point flows can be three dimensional or two-dimensional, time-dependent or independent, viscous or inviscid, orthogonal or inclined, and forward or reverse. The stagnation point flow solutions fundamentally deal with the flow motion in vicinity of stagnation field of a body surface transferring in the fluid or kept in a transferring fluid. A stagnation point flow with several physical meanings has a bigger physical importance, such as the prediction of the skin friction, decrease the effect of the aerodynamic drag, the mass transfer in vicinity of stagnation fields of bodies in high-speed flows, transpiration cooling, design of thrust bearings and radial diffusers.

The problem of the current study is a generalization of the problem discussed by Blyth and Hall (2003). The mathematical model based on our assumption can be used any unsteady function either at the initial or at the boundary conditions.

Two-dimensional oscillatory orthogonal stagnation-point flow towards a plane wall is investigated, the flow for two-dimensional case for arbitrary values of amplitude and frequency parameters was computed using a couple of unsteady oscillating functions, one an oscillating blowing at the wall. The second, an oscillating unsteady function at the potential flow. In this work, both oscillating flows we supposed to oscillate at the same oscillation frequency, the potential flow function includes the effect of the unsteadiness of the far field stream while the mass transfer function governing the flow through the wall is modulated by a dimensionless constant represents the blowing parameter.

1.1.2: Study Objectives

There are two fundamental objectives of this study:

- 1- Generalization of the problem of Blyth And Hall (2003) by creating a mathematical model in which could use any unsteady function at the initial or boundary conditions is applicable.
- 2- Finding the similarity solution to the problem of unsteady stagnation point flow using a new assumption didn't talked before in the previous studies.

1.2: Stagnation Point Flows (Literature Review)

Stagnation point flows occur when a flow becomes closed to adjacent boundary of a wall. This kind of flow behavior is of significant importance in engineering and aerodynamics since it exists whenever a fluid Collides with a solid body. Such flows have several applications such as, oscillating cylinder subjected to a flow or an airplane wing. A stagnation point is created in these flows, about which the flow stream-lines locally similar those about a saddle point.

Hiemenz (1911) was the first who addressed two-dimensional stagnation point flows travelling to a vertical non-moving surface. A similarity solution of the Navier Stokes equations was presented, due to non-satisfaction of no slip condition at the surface. The similarity solution makes the solution is obtainable at any point of the flow field, satisfying the flow velocity on the surface to that of the potential flow.

As the flow reaches a solid body, its stream lines resembled about the stagnation point which created at the origin.

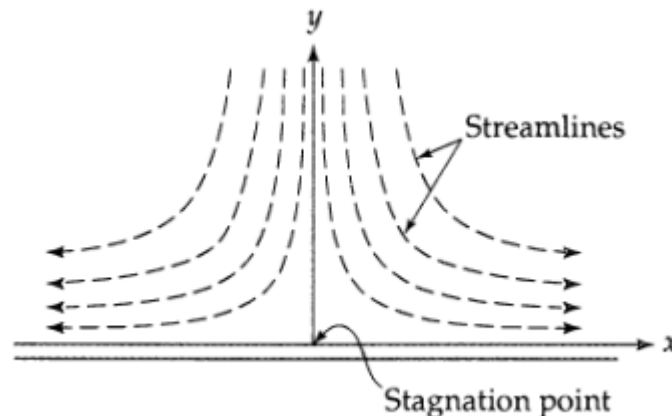


Figure (1.1): Stagnation Point Flow (Hiemens 1911)

Riley (1965) and Stuart (1966) analyzed a non-stationary stagnation point flow transferring perpendicularly towards a vertical fixed flat-plate. The potential stream-function was supposed to be totally in oscillation motion and dependent upon a dimensionless amplitude parameter and an oscillation frequency. No slip conditions at the free stream not being satisfied on the body surface, so it is important to obtain a solution in the form of a similarity solution in vicinity of the body surface. In the large-frequency limit, the solution shows two types of flow behavior. Two layer-structures created. The first, is Stokes-layer occurs in the region adjacent to the surface, within this layer the non-stationary terms become the same of components of viscous effect in the equations characterize the flow. As a result of a mean velocity component continuing to the roof of this layer, it isn't possible the Stokes-layer to make matching to the potential flow. To make this matching to happen, the introduction of a steady streaming-layer between the Stokes-layer and potential flow is needed. The steady streaming-layer thickness is on the order of the dimensionless oscillation frequency parameter, times the thickness of the Stokes-layer.

Riley and Vasantha (1989) focused on this phenomenon, where the free-stream in the far field is totally in oscillation state and found the solution numerically, this solution is unable to find the solution for all values of the oscillation frequency parameter, the equations blow-up at a finite-time singularity. They connect this with the horizontal flow motion to the Centre of coordinates, which leads to the release of flow particles from the borders of viscous region.

The inclusion of a mean flow component at far field flow was interested by Pedley (1972) and Grosch and Salwen (1982), where the mean component is large compared to the oscillatory component and oscillations frequency is high. As mentioned before, a Stokes-layer occurs in the region closed to the surface of body, which have to match to a layer that has a thickness on the order of the square root of the dimensionless oscillation frequency parameter, multiply by the Stokes layer thickness.

Because of the absence of a main flow at the far field region, the size of stokes-layer layer is considerably smaller than the problem discussed by Riley (1965) mentioned previously.

Merchant and Davis (1989) concluded the study of Pedley (1972) and Grosch and Salwen (1982), developing it to address the problem when the dimensionless frequency parameter value is high enough and the oscillatory component is much larger than the mean component. When the amplitude parameter is at a high critical value, the flow becomes reversal during a specific interval of the time. Thus, it is possible to compare this problem with the problem of Riley(1965), since the potential flow can be considered as totally in oscillating mode, then, flow is similar. Merchant and Davis considered the case of Synchronization of the two outer layers and concluded that for a specific oscillation dimensionless frequency, there exists a critical amplitude, above which, no solutions were found.

Hall and Papageorgiou's (1999) problem was the non-stationary incompressible stagnation point flow induced in an infinite channel, surfaces are moved with respect to space coordinates in an oscillating behavior. Corresponding to the oscillation frequency and the relative amplitude of the surface oscillating motion, the presence of totally periodic, semi-periodic and unstable flow solutions was numerically investigated. In the small amplitude and high Reynolds number limit they showed that the flow structure passes through two time stages with chaotic flow existing on the longer time-stage. The chaos is shown because of the non-stationary break-down of a stationary flow stream, figure (1.2).

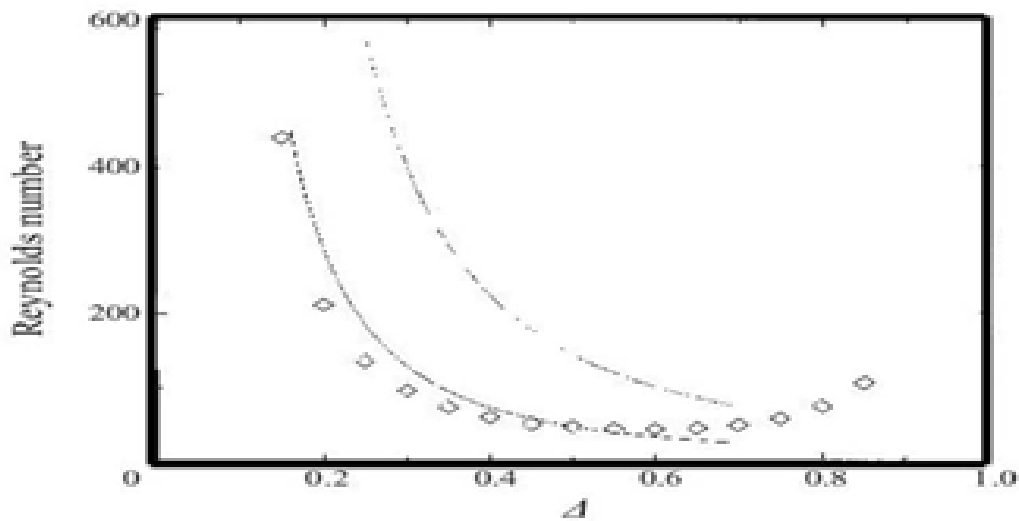


Figure (1.2): Stable and Unstable Flow Parameters in the Problem of (P. Hall and D. T. Papageorgiou 1999)

Blyth and Hall (2003) studied the problem of oscillatory stagnation point flows for both a large and a small oscillation frequency. They concluded that, in the case of a large oscillation frequency, if the relative amplitude increased to a critical value, the equations break-down at a finite-time singularity. also, they observed the behavior of the solutions in vicinity of the blowing-up time. For the small-frequency limit, they found that the leading order solution is semi-steady. When the dimensionless amplitude is at a critical large value, at the time where equations break-down at a finite-time singularity. They examined that, for any value of the relative amplitude, there exists a threshold frequency figure (1.2) under which the flow is regular and periodic, with the same period as the modulation factor, and beneath which the solution terminates in a finite time singularity. The dividing line in parameter space between these two possibilities is identified and favorably compared with the predictions of asymptotic analyses in the small and large frequency limits.

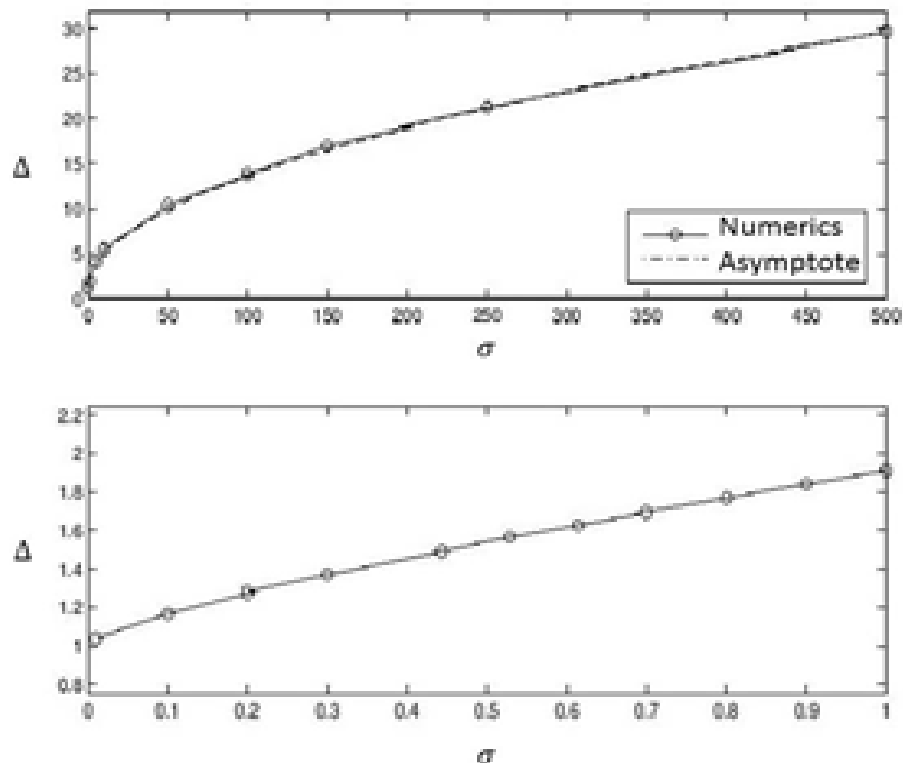


Figure (1.3): Stable and Unstable Flow Parameters in the Problem of (Blyth & Hall 2003)

The mentioned studies have been stagnation-point flows which moving towards fixed walls. In the following part, the case of approaching stagnation point flows to an oscillatory vertical flat-plate will be focused. This case can be supposed similar to the case mentioned above considering a horizontal oscillatory motion at the far-field moving to a fixed vertical flat-plate. Rott (1956) studied this problem if the surface made oscillatory motion in its own plane, with a stationary orthogonal flow at the potential region.

A similarity solution is presented including two functions, one consists a steadiness behavior and the other consists aperiodic behavior. This problem was examined in terms of a small and large frequency limiting cases. This problem was examined also by Glauert (1956).

The cylinder oscillates horizontally in a flow field is an application of Glauert problem. Compared to the earlier study on oscillatory vertical flat plates discussed previously, they considered the problem in the reference system, where the stagnation point is fixed. In the potential flow, the flow is consists of a time-dependent stagnation point flow including a mean component coincided with an oscillatory component. in addition to that is a oscillating horizontal motion, has the same oscillation frequency as the orthogonal stagnation point flow. This flow travelling towards a wall has an oscillating motion with the same oscillation frequency as the potential flow. They examined the problem where the mean component is dominant over the oscillating motion component and in the large frequency limit, the solution obtained showed a double layer structure at the wall which was talked above by Pedley (1972). Hazel and Pedley interested this problem, when the amplitude parameter was selected such that the flow non-reversed. they obtained the shear stress at the wall and the mean wall shear stress was examined for all the limiting cases. For the large frequency case, the oscillation of the wall was found that, it hasn't any effect on the mean shear stress of the wall and is only depends on the orthogonal flow. They considered this due to the viscous forces effect on the Stokes layer resisting any influence done by the oscillating wall.

Stuart (1959) examined the flow consisting a time-independent orthogonal stagnation point flow, a shear flow with constant vorticity and a uniform stream. the flow

characterized in terms of a stream function. A similarity solution is created because, this stream function in the potential flow does not in matching to the velocity on the wall.

After that, Drazin and Riley (2006) generalized the lasted work, to contain a free parameter at free-stream, which relates to the strength of the uniform stream in the potential flow. Stuart (2012) considered the viscous flow in the zone adjacent to a stagnation point when the external flow has uniform vorticity.

Upon increasing the free parameter, the shear velocity profile creates a region of reversed flow in the zone adjacent to the wall. They summarized their analysis with a discussion of the gradient of the resembled stream-line closed to the vertical surface, with the same results to that of Dorrepaal (1986). Particularly, it was shown that the ratio of the resembling stream-line rate of change near the surfacel, to that of the rate of change in the potential flow field is not a function of the flow vorticity.

Unsteady three-dimensional stagnation-point flow which, as in the steady case, embraces both the two-dimensional and axisymmetric flows. Such a flow has been considered by Cheng, Ozisik and Williams (1971). As for the steady case it is convenient to adopt a slight change of notation with x, y as co-ordinates in the plane and z perpendicular to it.

1.3: Problem of Current Study:

The flow in vicinity of a stagnation point on a plane wall is described by the classical Hiemenz solution (2011). When this stream is modulated in time by a periodic multiplicative factor on an infinite stream function, the solution describes the local dynamic responses in the region closed to the deceleration point on a vertical surface in an oscillation state. Similarly, the body can be considered fixed, while the flow in the far field changes periodically in time. Steady flow motion, created by Reynolds stresses associated with the vibrational motion Stuart (1966), is a considerable advantage of such time periodic flows. As a kind of such influence which occurs around a transversely oscillating circular cylinder Schlichting(1932),. When the amplitude of far-field fluctuations is small, the modified Hiemenz stream can be used to simulate local perturbation effects, such as acoustic noise incident on the boundary layer around the translational bluff body. In our study, we are interested in behavior in vicinity of the stagnation point of the bluff body, where the front surface of the body can be locally supposed vertical flat plate. According to this consideration, we allow variations of arbitrary amplitude and frequency.

Other studies related to this modified problem of Hiemenz are studies by Grosch and Salwen (1982) and Merchant and Davis (1989),; There are a set of previous studies on small fluctuations in free flow, the investigated flow with perturbations are high and low frequencies. It is worth mentioning here, those by Matunobu (1977), Pedley(1972), and Ishigaki (1970); see also Lighthill (1954).

The studies mentioned showed that, at low frequencies, there is simply a quasi-stationary version of the classical Hiemenz solution, and at high frequencies, there is a double boundary layer structure analogous to the structure first described by Riley (1965) and Stuart (1966) for such flows. Merchant and Davis solved the same unstable problem of Hiemenz, but also investigated the flow structure when the average component of free flow is much smaller than the vibrational surface.

The structure of the double boundary layer also found, although the authors showed that no solutions exist when the average component of the free flow falls below a certain cut-off point. This does not mean that solutions with a different asymptotic form do not exist for smaller mean values of the free flow.

Our interest in the problem was prompted by Blyth and Hall (2003). They considered a non-stationary version of the classical Hiemenz solution describing an incompressible two-dimensional flow of the deceleration point on a solid wall, especially considering the response near the wall, when the solution at infinity is modulated in time by a periodic factor of a given amplitude and frequency. Although this problem has already been solved in the literature for the total frequency in cases where the amplitude of the time periodic factor is either large or small, they calculated the flow for arbitrary values of both these parameters. They investigated that, for any given amplitude, there exists a threshold frequency above which the flow is regular and periodic, with the same period as the modulation factor, and beneath which the solution terminates in a finite time singularity. The dividing line in parameter space between these two possibilities is identified and favorably compared with the predictions of asymptotic analyses in the small and large frequency limits. Their aim was to investigate the possibility of such varied dynamics for a periodically forced stagnation point flow in a semi-infinite domain.

The aim was to investigate the possibility of such varied dynamics for a periodically forced stagnation point flow in a semi-infinite domain.

In conclusion, we can compare the progress of my studies with those of previous studies. While Chang studied the problem of three-dimensional stagnation point flow assuming the potential flow velocity components varies with time as we mention in the previous section:

$$U_e = \frac{A}{1 + \alpha t},$$

Using this assumption, he can transfer Navier Stoke's equations, which are 4 differential equations in the case of incompressible flow to 2 ordinary differential equations. In fact these function only satisfies this transformation, so we can't use other time function, either at initial or boundary positions.

similarity solution, which employed by Chang and followed by the majority of authors who study stagnation point flows is called (ODE solution), where ODE refers to ordinary differential equations.

Blyth & Hall use (PDE Solution) which is Partial differential equation solution, for two-dimensional flow, they added an oscillatory motion to the potential flow and resulted two

regions of oscillation, periodic and random, according to a limited values of oscillation frequency and amplitude.

They were satisfied with this important result and did not study the effect on the characteristics of boundary layer.

The problem of our study is a generalization of the problem discussed by Blyth and Hall. The mathematical model based on our assumption can be use any unsteady function either at the initial or at the boundary conditions, the development which created by our assumptions is showed in table (1.2).

Two-dimensional oscillatory orthogonal stagnation-point flow towards a plane wall is investigated, we compute the flow for two-dimensional case for arbitrary values of amplitude and frequency parameters using an oscillating blowing at the wall $v_e(0)$. The following function was selected to express the blowing velocity:

$$v_e(t) = \Delta \cos \omega t$$

As well as the effect of unsteady function at the potential flow $U_e = Axa(t)$. We assume the following function to express the horizontal velocity component of the potential flow:

$$a(t) = \frac{1}{1 + \frac{\alpha}{\omega} \sin \omega t}$$

Table (1.1): Generalization of the Previous Studies

(ODE) solution	$U_e(t) = Axa(t),$ $V_e(t) = -Aya(t)$ $a(t) = \frac{A}{1 + \alpha t}$	$u = Ax f_\eta(\eta, t)$ $v = -\sqrt{Av} f(\eta, t),$ $f(0) = f_\eta(0) = 0$ $\eta \rightarrow \infty, f_\eta \rightarrow 1$
BLYTH& Hall (2D) (PDE)	$U = (x/l)U_x a(t),$ $V = -(y/l)U_x a(t)$ $a(t) = 1 + \Delta \cos(\omega t)$	$u = (x/l)U_x f_\eta(\eta, t)$ $v = -(y/l)U_x \sqrt{\text{Re}},$ $\text{Re} = \frac{U_x l}{\nu}$ $f(0, t) = f_\eta(0, t) = 0$ $\eta \rightarrow \infty, f_\eta \rightarrow a(t)$
MY WORK (2D) (PDE)	$U_e(t) = Axa(t),$ $a(t) = \frac{A}{1 + \frac{\alpha}{\omega} \sin \omega t}$	$u = Ax f_\eta(\eta, t)$ $v = -\sqrt{Av} f(\eta, t),$ $f(0, t) = -\sqrt{\frac{1}{Av}} v_0(t),$ $f_\eta(0, t) = \frac{u_0(t)}{Ax},$ $\eta \rightarrow \infty, f_\eta \rightarrow a(t)$

1.4: Order of Thesis:

Having summarized the work which have done in this section, the analysis which will follow in the following chapters was outlined. The start of analysis on stagnation point flows in chapter (3) by considering the unsteady two-dimensional laminar incompressible stagnation point flow approaching an interspersed vertical surface with an oscillating mass transfer. As previously talked by **Blyth and Hall** (2003). In addition, we have made a generalization of their case at the boundary conditions. the problem formulation have done by reducing the non-linear partial differential equations of Navier Stoke's for two dimensional stagnation point flow to one partial similarity equation using similarity transformations. This equation has solved numerically using the implicit scheme of the finite difference method.

In chapter 4, our solver was investigated by comparing our results with CFD solver. The results of (ODE) solution of Chang (1970) was compared with our (PDE) solution for the same problem of Chang, hence the results were identical.

The stagnation point flow boundary layer characteristics were observed under the effect of flow parameters. For each combination of blowing parameter k , oscillation frequency ω and unsteadiness parameter D , the behavior of vertical and horizontal velocity profiles was observed, in addition to the shear stress distribution at the surface and within the boundary layer. It was found a border line separated between sets of parameters lead to periodic flow and sets of parameters lead to unstable flow, each set is a pair of (blowing parameter k , oscillation frequency ω), this line has determined according to a specific value of unsteadiness parameter D .

In the same context, it was found a border-line separates two regions of flow parameters, region of parameters lead to a reversed flow at a definite time at the surface and the other region of parameters lead to a non-reversed flow at a definite time at the surface.

Finally, chapter 5 introduced the most important conclusions from each chapter.

Chapter 2

Background knowledge of thesis

2.1: Similarity Transformations

Similarity solutions are a specifically small group of exact solutions to the boundary layer equations. In some flows, can be considered that, the velocity and enthalpy profiles differ only from several scale factors corresponding to the positions of the surface. This similarity property is very important in the boundary layer equations. The similarity method particularly used in transforming partial differential equations into ordinary differential equations. Converting the system to a set of ordinary differential equations can be applied by using appropriate dependent and independent variables in dimensionless form called similarity variables using methods of transformations defined as similarity transformations. However, the application of similarity transformations to time-dependent flows or three-dimensional flows of the boundary layer can't be, all the time ensure the system converting to the state of ordinary differential equations from the state of partial differential equations. The Falkner-Skan equations governing the flow of a similar velocity-profiles, MHD Falkner Skan and the related heat-transfer equations, the velocity equations and the thermal boundary layer in the incompressible stagnation test were provided as a result of employing similarity transformations on particular boundary-layer equations.

Similarity solutions are necessary for understanding the flow of a non-linear viscous flows. The similarity transformation converts the Navier-Stokes equations to a group of non-linear ordinary differential equations which make the solution is obtainable at all points of flow region to obtain universal curves.

2.1.1: Two-Dimensional Similarity Solutions: The Falkner-Skan Equation

Start with a brief mathematical derivation of the Falkner-Skan equation, in addition to addressing the physical significance related with a set of geometries and pressure gradients.

The Falkner-Skan equation contains an unique pressure gradient parameter β . For specific values of β , the stream-wise velocity profile solution provides some thoughtful features such as overshoot and back-flow. The possible physical significance for the

various ranges of β is discussed. The Falkner-Skan equation is well known, but it is worthwhile to discuss it here in some detail because there are many analogies between the two dimensional and three-dimensional cases

Derivation of the Falkner-Skan Equation

Consider the two-dimensional bluff body. Boundary layer arises from the stagnation-point and serves to reduce the far-field external velocity to zero at the surface of the body. The velocity distribution within the viscous region depends on the body shape and in reality, behaves in a complex way. but it can be considered, that region of the surface near the point of stagnation as a flat wall.

It can to be supposed a self-similar velocity-profile in this limited area, and it is here, for example, that the Falkner-Skan equation (Which will be derived later) applicable. Consider the two-dimensional plane body of the bluff-body shown in the figure (2.1). range. We can assume a self-similar velocity profile in this region, and in such situation that the Falkner-Skan equation is applied.

The dimensionless form of the boundary layer equations for two dimensional, incompressible, steady flow are:

$$\text{x-momentum: } u \frac{\partial u}{\partial x} + v \frac{\partial u}{\partial y} = U_e \frac{\partial U_e}{\partial x} + \frac{\partial^2 u}{\partial y^2} \quad (2.1)$$

$$\text{continuity: } \frac{\partial u}{\partial x} + \frac{\partial v}{\partial y} = 0 \quad (2.2)$$

Here y and v are modulated by $\text{Re}^{1/2}$, $y = y^* \text{Re}^{1/2}$, $v = v^* \text{Re}^{1/2}$, where : y^* and v^* are the actual normal coordinate and velocity respectively. In the scaled coordinates y and v are $O(1)$ in the boundary layer.

The boundary conditions are:

$$\begin{array}{lll} u = 0, v = 0 & \text{at} & y = 0, \\ u \rightarrow U_e(x) & \text{as} & y \rightarrow \infty, \end{array} \quad (2.3)$$

Where $U_e(x)$ denotes the mainstream velocity. Define:

$$\eta = \frac{y}{\delta(x)} \quad (2.4)$$

Where: $\delta(x)$ is a function proportional to the boundary-layer thickness which is to be found.

Define:
$$u = U_e(x)f_\eta(\eta) \quad (2.5)$$

Here η is a similarity variable and the interest is in self-similar solutions for which the dependence of the velocity profile on x and y can be collapsed into one variable, η .

The boundary conditions transform to:

$$\begin{aligned} f &= 0 & \text{at} & \eta = 0, \\ f_\eta &\rightarrow 1 & \text{as} & \eta \rightarrow \infty, \end{aligned} \quad (2.6)$$

From the continuity equation, a stream function ψ ; may be defined by:

$$u = \frac{\partial \psi}{\partial y}, \quad v = -\frac{\partial \psi}{\partial x} \quad (2.7)$$

From the definition of u , we obtain:

$$\frac{\partial \psi}{\partial y} = U_e(x)f_\eta(\eta)$$

by integration:

$$\psi = U_e(x)\delta(x)f_\eta(\eta) + \psi_0(x) \quad (2.8)$$

Here $\psi_0(x)$ at this step is an arbitrary function of integration.

By Differentiation with respect to x , equation (2.8) becomes:

$$v = -[U_{e,x}(x)\delta(x) + U_e(x)\delta_x(x)]f_\eta(\eta) - \psi_{0,x}(x) \quad (2.9)$$

The chain rule is used to find: $\frac{\partial u}{\partial x}$, $\frac{\partial u}{\partial y}$, $\frac{\partial v}{\partial y}$ and $\frac{\partial^2 u}{\partial y^2}$ in terms of η . Because, similarity

solutions have to be provided, it was supposed that $f = f(\eta)$. The final similarity transformations are:

$$\frac{\partial u}{\partial x} = U_{e,x}f_\eta - \eta \frac{\delta_x}{\delta} U_e f_{\eta\eta} \quad (2.10)$$

$$\frac{\partial u}{\partial y} = \frac{1}{\delta} U_e f_{\eta\eta}$$

(2.11)

$$\frac{\partial v}{\partial y} = -U_{e,x} f_{\eta} + \eta \frac{\delta_x}{\delta} U_e f_{\eta\eta}$$

(2.12)

$$\frac{\partial^2 u}{\partial y^2} = \frac{1}{\delta^2} U_e f_{\eta\eta\eta}$$

(2.13)

After substitution and simplification of the equations, the following result is obtained:

$$f_{\eta\eta\eta} + \delta(U_e \delta)_x f_{\eta\eta} + \delta^2 U_{e,x} (1 - f_{\eta}^2) + \psi_{0,x} \delta f_{\eta\eta} = 0$$

(2.14)

The only way (2.14) can be an ordinary differential equation IS if the coefficients are not functions of x. Therefore, defining:

$$\alpha = \delta(U_e \delta)_x = \text{cons.}$$

(2.15)

$$\beta = \delta^2 U_{e,x} = \text{cons.}$$

(2.16)

$$\gamma = \psi_{0,x} \delta = \text{cons.}$$

(2.17)

therefore equation (2.14) becomes:

$$f_{\eta\eta\eta} + \alpha f_{\eta\eta} + \beta(1 - f_{\eta}^2) + \gamma f_{\eta\eta} = 0$$

(2.18)

Generally, a solid wall is assumed so that γ vanishes. A constant value for $\alpha = 1$ may be chosen since the value of α : affects only the scale for η .

The solution of equation (2.18) depends only on the parameter β which is a measure of the stream-wise pressure gradient. Where upon equation (2.18) becomes:

$$f_{\eta\eta\eta} + f_{\eta\eta} + \beta(1 - f_{\eta}^2) = 0$$

(2.19)

for which ($\alpha = 1$). The boundary conditions are:

$$\begin{aligned} f = f_{\eta} = 0 & \quad \text{at} \quad \eta = 0, \\ f_{\eta} \rightarrow 1 & \quad \text{as} \quad \eta \rightarrow \infty, \end{aligned}$$

(2.20)

Table (2.1): Flow Structures Corresponding to the Measure of the Stream-Wise Pressure Gradient Parameter β .

1	$\beta = 0$	(Blasius solution for horizontal flat-plate).
2	$0 \leq \beta \leq 2$	Flow travelling towards a wedge of half angle
3	$\beta = 1$	For stagnation point flows
4	$\beta = 2$	Flow turned around an angle of wedge
5	$\beta \rightarrow \infty$	Flow travelling towards a point sink.
6	$-2 \leq \beta \leq 0$	Flow around an expansion corner of turning angle
7	$\beta = -2$	Flow around the edge of a thin flat-plate.
8	$\beta = -1$	Flow around a right-angle corner.

2.1.2: Three-Dimensional Similarity Solutions

Considered generalized orthogonal coordinates x, y, z . The lines of constant x and y form a network on the body surface, and z increases orthogonally from the body surface.

The increment of distance between coordinate lines x and $x + dx$ is $q_1 dx$; corresponding increments are $q_2 dy$ and $q_3 dz$. For thin boundary layers we can assume that the metric coefficients satisfy:

$$q_1 = q_1(x, y) \quad , \quad q_2 = q_2(x, y) \quad , \quad q_3 = 1$$

The velocity components in the x, y , and z directions are called u, v , and w . The corresponding surface velocities of the inviscid flow are:

$$U_e = U_e(x, y) \quad , \quad V_e = V_e(x, y) \quad , \quad W_e = 0$$

Derivation of the Governing Equations:

A stream-line coordinate system was chosen with ξ and ζ according to the stream-wise and cross-stream directions respectively; z is perpendicular to both x and y . The boundary layer equations in a general streamline orthogonal coordinate system are:

$$\frac{\partial u}{\partial t} + \frac{u}{q_1} \frac{\partial u}{\partial x} + \frac{v}{q_2} \frac{\partial u}{\partial y} + w \frac{\partial u}{\partial z} + \frac{uv}{q_1 q_2} \frac{\partial q_1}{\partial y} - \frac{v^2}{q_1 q_2} \frac{\partial q_2}{\partial x} = -\frac{1}{\rho q_1} \frac{\partial P}{\partial x} + \nu \frac{\partial^2 u}{\partial y^2} \quad (2.21)$$

$$\begin{aligned} \frac{\partial u}{\partial t} + \frac{u}{q_1} \frac{\partial u}{\partial x} + \frac{v}{q_2} \frac{\partial u}{\partial y} + w \frac{\partial u}{\partial z} + \frac{uv}{q_1 q_2} \frac{\partial q_1}{\partial y} - \frac{v^2}{q_1 q_2} \frac{\partial q_2}{\partial x} = \\ -\frac{1}{\rho q_1} \frac{\partial P}{\partial x} + \nu \frac{\partial^2 u}{\partial y^2} \end{aligned} \quad (2.22)$$

$$\frac{\partial v}{\partial t} + \frac{u}{q_1} \frac{\partial v}{\partial x} + \frac{v}{q_2} \frac{\partial v}{\partial y} + w \frac{\partial v}{\partial z} - \frac{u^2}{q_1 q_2} \frac{\partial q_1}{\partial y} + \frac{uv}{q_1 q_2} \frac{\partial q_1}{\partial x} = -\frac{1}{\rho q_2} \frac{\partial P}{\partial y} + \nu \frac{\partial^2 v}{\partial y^2} \quad (2.23)$$

The falkner transformation:

For discussions of exact self-similar solutions and for the formulation of systematic methods of calculation of more general boundary layer flows, it is helpful to transform variables in some manner which accounts roughly for the anticipated magnitudes of boundary-layer thickness and velocity components. Many such transformations are available.

We choose, rather arbitrarily, that associated with the name of Falkner. We call:

$$\xi = \frac{x}{L}, \quad \zeta = \frac{y}{L}, \quad z = \eta \sqrt{\frac{U_e(x, y)}{x\nu}}$$

where L is a characteristic body dimension and \mathcal{G} is the kinematic viscosity.

Thus:

$$\begin{aligned} \frac{\partial \xi}{\partial x} &= \frac{\partial \zeta}{\partial y} = \frac{1}{L} \\ \frac{\partial \xi}{\partial y} &= \frac{\partial \xi}{\partial z} = \frac{\partial \zeta}{\partial x} = \frac{\partial \zeta}{\partial z} = 0 \end{aligned}$$

$$\frac{\partial \eta}{\partial x} = \left(\frac{m-1}{2}\right) \frac{\eta}{\xi L}, \quad \frac{\partial \eta}{\partial y} = \left(\frac{2}{2}\right) \frac{\eta}{\zeta L}, \quad \frac{\partial \eta}{\partial z} = \sqrt{\frac{U_e}{\nu L \xi}}$$

Where:

$$m(\xi, \zeta) \equiv \frac{\partial[\ln U_e]}{\partial[\ln \xi]}, \quad n(\xi, \zeta) \equiv \frac{\partial[\ln U_e]}{\partial[\ln \zeta]}$$

The choice of u rather than v and of x rather than y in the normalization of z implies only that x increases in a more-or-less down-stream direction, and that $u \neq 0$ except at singular points or lines.

Our dependent variables are written as:

$$u \equiv U_e(\xi, \zeta) \frac{\partial}{\partial \eta} f(\xi, \zeta, \eta) = U_e f_\eta$$

which we designate simply $u = U_e f_\eta$. At this point the prime of f does **not** imply that f depends only upon η , but is simply a shorthand. We shall write out $\frac{\partial f}{\partial \xi}$ and $\frac{\partial f}{\partial \zeta}$ fully.

Similarly, we write:

$$v \equiv V_e(\xi, \zeta) \frac{\partial}{\partial \eta} g(\xi, \zeta, \eta) = V_e g_\eta$$

Using the continuity equation, with, we find, for the simple case of an impervious wall,

$$w = -\frac{1}{q_1 q_2} \sqrt{\frac{\nu \xi}{U_e L}} \left\{ \frac{U_e}{q_1 \xi} \left[\left(\frac{m+1}{2} \right) f + \left(\frac{m-1}{2} \right) \eta f_\eta + \xi \frac{\partial f}{\partial \xi} \right] + \frac{V_e}{q_2 \zeta} \left[\left(s - \frac{n}{2} + \lambda \right) g + \frac{n}{2\eta} g_\eta + \zeta \frac{\partial g}{\partial \zeta} \right] \right\} \quad (2.24)$$

where we have introduced our final shorthand notation:

$$\chi \equiv \frac{\partial[\ln q_2]}{\partial[\ln \xi]}, \quad \lambda \equiv \frac{\partial[\ln q_1]}{\partial[\ln \zeta]}$$

If u , v , and w are to vanish at $z = 0$, we see that boundary conditions on f and g are:

$$f(\xi, \zeta, 0) = g(\xi, \zeta, 0) = f_\eta(\xi, \zeta, 0) = g_\eta(\xi, \zeta, 0) = 0$$

While:

$$f_\eta(\xi, \zeta, \infty) = g_\eta(\xi, \zeta, \infty) = 1$$

The transformed component momentum equations, in which the pressure gradients have been eliminated in favor of inviscid-flow velocity gradients, etc., become:

$$\begin{aligned}
f_{\eta\eta\eta} + \frac{1}{q_1} \left(\frac{m+1}{2} + \chi \right) f f_{\eta\eta} + \frac{m}{q_1} (1 - f_\eta^2) + \frac{V_e \xi}{U_e \zeta} \frac{1}{q_2} \left[\left(s - \frac{n}{2} + \lambda \right) g f_{\eta\eta} + \right. \\
\left. (n + \lambda)(1 - g_\eta f_\eta) \right] - \left(\frac{V_e}{U_e} \right)^2 \frac{\chi}{q_1} (1 - g_\eta^2) = \\
+ \xi \left\{ \frac{1}{q_1} \left(f_\eta \frac{\partial f_\eta}{\partial \xi} - f_{\eta\eta} \frac{\partial f}{\partial \xi} \right) + \frac{V_e}{U_e} \left(\frac{1}{q_2} \right) \left(g_\eta \frac{\partial f_\eta}{\partial \zeta} + f_{\eta\eta} \frac{\partial g}{\partial \zeta} \right) \right\}
\end{aligned} \tag{1.25}$$

$$\begin{aligned}
g_{\eta\eta\eta} + \frac{1}{q_1} \left(\frac{m+1}{2} + \chi \right) f g_{\eta\eta} + \frac{1}{q_1} (r + \chi)(1 - f_\eta g_\eta) + \frac{V_e \xi}{U_e \zeta} \frac{1}{q_2} \left[\left(s - \frac{n}{2} + \lambda \right) g g_{\eta\eta} + \right. \\
\left. s(1 - g_\eta^2) \right] - \frac{U_e \xi}{V_e \zeta} \frac{\lambda}{q_2} (1 - f_\eta^2) = \\
+ \xi \left\{ \frac{1}{q_1} \left(f_\eta \frac{\partial g_\eta}{\partial \xi} - g_{\eta\eta} \frac{\partial f}{\partial \xi} \right) + \frac{V_e}{U_e} \left(\frac{1}{q_2} \right) \left(g_\eta \frac{\partial g_\eta}{\partial \zeta} - g_{\eta\eta} \frac{\partial g}{\partial \zeta} \right) \right\}
\end{aligned} \tag{2.26}$$

For stagnation point flow, suppose we deal with a "rounded" body, to which the flow from up-stream "attaches" at some point P, which we take as the origin of coordinates.

In the immediate vicinity of P we can expand the surface metric coefficients in power series in ξ and ζ , e.g.,

$$q_1(x, y) = q_1(0,0) + \left(\frac{\partial q_1}{\partial \xi} \right)_{(0,0)} \xi + \left(\frac{\partial q_1}{\partial \zeta} \right)_{(0,0)} \zeta + \dots$$

In particular, we choose a system of coordinates that is locally rectangular at the origin, so that:

$$q_1(0,0) = q_2(0,0) = 1$$

Since $\left(\frac{\partial q_1}{\partial \xi} \right)_{0,0}$ and the similar derivatives are finite, we have, in the vicinity of the origin,

$$\chi = \lambda = 0$$

Furthermore, if the approaching upstream flow is irrotational, it can be shown that there is an orientation of the x and y axis for which, in the vicinity of the origin,

$$U_e = Ax + \dots, \quad V_e = By + \dots$$

The desired orientation of the x and y axes is along the principal directions of curvature of the surface. To be specific, we may take the x axis along the direction of maximum (convex outward) curvature.

Then we shall have $A > 0$, and $A > B$.

If B is positive, we speak of a nodal attachment point; if it is negative, we designate it as a saddle point of attachment.

We see that the given correspond to

$$m = s = 1, \quad n = r = 0$$

If we assume a constant: $C = \frac{B}{A} = \frac{V_e x}{U_e y}$

Where is the constant related with the three dimensional body geometry.

We can then expect to use similarity transformations to find similar solutions for f and g,

for which $\frac{\partial f}{\partial x} = \frac{\partial g}{\partial x} = 0$. The governing equations reduce to:

$$f_{\eta\eta\eta} + (f + Cg)f_{\eta\eta} - f_{\eta}^2 + 1 = 0 \quad (2.27)$$

$$g_{\eta\eta\eta} + (f + Cg)g_{\eta\eta} + C(1 - g_{\eta}^2) = 0 \quad (2.28)$$

These equations have been solved numerically by Howarth (1951) for $0 \leq C \leq 1$, and by Davey (1961) for $-1 \leq C \leq 0$.

2.2: General Review of Steady Stagnation Point Flows

2.2.1: The Classical Hiemenz (1911) Solution

When a steady stream of a viscous fluid approaches a rigid stationary cylinder, the stream is brought to rest at the surface of the body and divides about it. Although the fluid is at rest, at each point of the surface of the cylinder, by analogy with the flow of an inviscid fluid, we identify stagnation points as those points on the surface at which the stream attaches to, or separates from, the cylinder. The flow in the neighborhood of a stagnation point of attachment may be modeled by the flow towards an infinite rigid flat plate. Now, for an inviscid fluid, the ir-rotational flow against the flat plate $y = 0$ is well known to be :

$$U = Ax, \quad V = -Ay$$

The constant A is not directly relevant to the flow pattern close to the stagnation point and is proportional to the free-stream speed about the cylinder. The inviscid stream function is:

$$\psi = -Axy$$

In his study of the flow of a viscous fluid at a stagnation point it would appear to have been natural for Hiemenz (1911) to have assumed $\psi(x, y) = xF(y)$. If we introduce dimensionless variables, noting that there is no natural length scale in this problem, then:

$$\psi = (\nu A)^{1/2} xf(\eta), \quad (2.29)$$

where:

$$\eta = \left(\frac{A}{\nu}\right)^{1/2} y$$

$$f_{\eta\eta\eta} + ff_{\eta\eta} - (f_{\eta})^2 + 1 = 0 \quad (2.30)$$

$$\begin{aligned} f(0) = f_{\eta}(0) = 0, \\ f_{\eta}(\infty) = 1 \end{aligned} \quad (2.31)$$

$$\frac{P_0 - P}{\rho} = \frac{1}{2} A^2 x^2 + \frac{1}{2} \nu A f^2 + \nu A f_{\eta} \quad (2.32)$$

where P_0 is a constant. This solution describes a flow in which linear diffusion of vorticity is balanced by *non-linear* convection of vorticity. The solution of (2.30), subject to the conditions (2.31), has been calculated numerically by Hiemenz (1911) and by Howarth (1934).

Rott (1956) extended the solution of Hiemenz to include the situation in which the plane boundary slides in its own plane in the x -direction. This provides, for example, a model of the flow in the neighborhood of the stagnation point of a rotating circular cylinder placed in a uniform stream. In place of (2.29) we have:

$$\psi = (\nu A)^{1/2} xf(\eta) + u_w \left(\frac{\nu}{A}\right)^{1/2} \int_0^{\eta} g d\eta \quad (2.33)$$

where u_w is the speed of the translating plate. With P unchanged as in (2.32), equation (2.30) then yields, as equation for g ,

$$g_{\eta\eta} + fg_{\eta} - f_{\eta}g = 0, \quad g(0) = 1, \quad g(\infty) = 0 \quad (2.34)$$

2.2.2: Oblique Stagnation-Point Flows

In section 2.3.1 above, the dividing, or stagnation, streamline intersects the plane boundary $y = 0$ orthogonally. There is, however, a class of stagnation point flows for which the dividing streamline intersects the boundary at an arbitrary angle. Consider first an inviscid fluid and the stream function:

$$\psi = Axy + \frac{1}{2}\zeta_0 y^2$$

which combines both the classical stagnation-point flow and a cross flow of uniform shear, that is of constant vorticity $-\zeta_0$. This stream function satisfies both the Euler equations and the Navier–Stokes equations, though not the viscous condition of no slip at $y = 0$. Taking $y = 0$ as the boundary again the dividing streamline is now

$$y = -2(A/\zeta_0)x.$$

This form of stagnation-point flow has been developed by Stuart (1959), Tamada (1979) and Dorrepaal (1986) for a viscous fluid as follows. With a superposed cross flow present it is natural, the stream function as:

$$\psi = (\nu A)^{1/2} xf(\eta) + \zeta_0 \left(\frac{\nu}{A}\right) \int_0^{\eta} g d\eta$$

where again $\eta = (\nu A)^{1/2} y$, finally, similarity equation for g and initial conditions are :

$$\begin{aligned} g_{\eta\eta} + fg_{\eta} - f_{\eta}g &= \text{constant} \\ g(0) &= 0, \quad g_{\eta}(\infty) = 1 \end{aligned} \quad (2.35)$$

2.2.3: Two-Fluid Stagnation-Point Flow

The classical Hiemenz stagnation-point flow is that of a stream against a solid boundary. Wang (1985a) has extended this to the flow against the interface with a second fluid. The interface is assumed planar so that we may expect the surface tension to be

large, or the density of the lower fluid to be much greater than the density of the upper fluid.

The similarity of the Hiemenz flow is preserved so that in the upper fluid the stream function is expressed as in (2.29), with $f(\eta)$ again satisfying equation (2.30). However the no-slip condition is violated in this case and we have $f_\eta(0) = \lambda$, where λ is determined only following a consideration of the flow in the second fluid in $y < 0$. In the second fluid, which we assume has density ρ and viscosity ν , we write

$$\eta = -(\bar{\nu}A\lambda)^{1/2} x f(\eta), \quad \text{where now} \quad \eta = -\left(\frac{A\lambda}{\bar{\nu}}\right)^{1/2} y$$

Since we require, where a prime again denotes differentiation with respect to the independent variable, the equation for f is:

$$\begin{aligned} f_{\eta\eta\eta} + f f_{\eta\eta} - (f_\eta)^2 &= 0, \\ f(0) = 0, \quad f_\eta(0) = 1, \quad f_\eta(\infty) &= 0 \end{aligned} \tag{2.36}$$

Where the conditions at $\bar{\eta} = 0$ ensure continuity of velocity at the interface.

2.2.4: The Classical Homann Solution

This case is a special case of the three-dimensional stagnation point flow, but we include it here for completeness. In our formulation we allow the plate to slide in its own plane with constant velocity, and also allow for transpiration across it when porous; both of these features have been examined by Libby (1974, 1976) in the more general context of a three-dimensional stagnation point, whilst Wang (1973) has considered axisymmetric flow against a sliding plane.

The boundary is taken as $z = 0$, and with no natural length scale in the problem a self-similar solution with velocity components

$$v_r = Arf_\eta(\eta) + u_w \cos \theta g(\eta), \quad v_\theta = -u_w \sin \theta g(\eta), \quad v_z = -2(\nu A)^{1/2} f(\eta)$$

$$\eta = \left(\frac{A}{\nu}\right)^{1/2} z$$

And pressure:

$$\frac{P - P_0}{\rho} = -\frac{1}{2} A^2 r^2 - 2A\nu(f^2 + f_\eta),$$

Leads to using equations (2.19), (2.20), to the following equations for f and g ,

$$\begin{aligned} f_{\eta\eta\eta} + 2ff_{\eta\eta} - f_{\eta}^2 + 1 &= 0, \\ g_{\eta\eta} + 2fg_{\eta} - f_{\eta}g &= 0, \end{aligned} \quad (2.37)$$

With boundary conditions:

$$\begin{aligned} f(0) = \lambda, \quad f_{\eta}(0) = 0, \quad f_{\eta}(\infty) = 1, \\ g(0) = 1, \quad g(\infty) = 0 \end{aligned} \quad (2.38)$$

With $\Omega = u_w = 0$ we recover the classical stagnation-point flow of Homann (1936). With

$u_w \neq 0$ we have, without any loss of generality, the boundary

sliding in its own plane with constant speed in the direction $\theta = 0$; this corresponds to the case addressed by Libby (1974) at a three-dimensional stagnation point, and by Wang (1973). For $\Omega \neq 0$ the boundary is assumed to be porous with transpiration across it, again a case considered by Libby (1976) (in fact, for a compressible fluid) at a three-dimensional stagnation point. For $\Omega < 0$ we have injection, perhaps the more interesting case. As the injection rate increases the position η_0 , where $f(\eta, 0) = 0$, increases, with viscous effects

increasingly unimportant for $\eta < \eta_0$. For $\eta < \eta_0$ there is again, relatively speaking, a lack of structure in the solution with a fairly rapid change taking place in the neighborhood of $\eta = \eta_0$.

2.3: General Review of Unsteady Stagnation Point Flows:

Introduction:

The importance of studying the unsteady boundary layers is the fact that the majority of boundary layers that actually occur are unsteady. One or some of the following conditions may exist: either the time elapsed after the start of the movement is not significant, or there are fluctuations in prevailing velocity (which may itself have a mean of zero), or the boundary layer is unstable. Non-stationary flows occur in a variety of real life such as the pulsing flow of the arteries, the flow over fish fins and the wings of volatile birds, flow in the heart, some important technological applications, such as in gas turbine engines. In the latter case, periodic motions.

Unsteady stagnation point flow has been studied on a range of different movements over decades because of its importance in many engineering applications such as thermal cooling processes and industrial manufacturing processes. Although many studies have been conducted on the unsteady flow in the vicinity of the stagnation point on a moving body, most of them investigated the flow on the plane associated with oscillations or with motion in the direction parallel to the plane itself as discussed above and little work has been reported on such an unsteady flow on a body moving along the impinging flow direction.

In section 2.2 we examined steady stagnation-point flows on an infinite flat plate in different situations, as a model for the flow in the neighborhood of the stagnation point on a bluff body. Several authors have examined unsteady effects on such flows with a motivation, in part, prompted by aerodynamic flutter problems, and these we now consider.

2.3.1: Orthogonal Oscillations

In contrast to the flow in section 2.3 above we now consider the situation in which the steady stagnation-point flow is modified by the infinite plane performing harmonic fluctuations in its position along a normal direction. It is convenient, without loss of generality, to deal with the case in which the boundary is fixed with the far-field stagnation-point flow modulated by harmonic fluctuations of arbitrary amplitude and frequency. The study finds application to describe the local dynamics around a stagnation point on an oscillating body, or to model the local effects of disturbances at the stagnation point of a translating bluff body.

The problem has received the attention of Grosch and Salwen (1982), Riley and Vasantha (1988), Merchant and Davis (1989) and Blyth and Hall (2003), where the most recent of these investigations is the most comprehensive.

Where,

$$\eta = \left(\frac{A}{\nu}\right)^{1/2} y$$

Far from the plane boundary $y = 0$ the modulated stagnation-point flow has the form:

$$\begin{aligned} u &= Ax(1 + \Delta \cos \omega t) \\ v &= -Ay(1 + \Delta \cos \omega t) \end{aligned} \tag{2.39}$$

and so we write, in place of (2.29),

$$\psi = (\nu A)^{1/2} x f(\eta, \tau) \quad (2.40)$$

where:

$$\eta = \left(\frac{A}{\nu}\right)^{1/2} y, \quad \tau = \omega t$$

With the pressure now given by :

$$\frac{P_0 - P}{\rho} = \frac{1}{2} A^2 x^2 a^2(\tau) + \frac{1}{2} \omega A x^2 a'(\tau) + \frac{1}{2} \nu A f^2 + \nu A f_{\eta\eta} - \omega \nu \int_0^{\eta} f_{\tau} d\eta \quad (2.41)$$

$$a(\tau) = 1 + \Delta \cos \omega t \quad (2.42)$$

Using similarity transformation, the following similarity equation was got:

$$a f_{\eta,\tau} = f_{\eta\eta\eta} + f f_{\eta\eta} - f_{\eta}^2 + \sigma a' + a^2 \quad (2.43)$$

Together with:

$$f(0, \tau) = f_{\eta}(0, \tau); \quad f_{\eta}(\infty, \tau) = a(\tau) \quad (2.44)$$

It may be noted that is $\sigma = \frac{\omega}{A}$ the Strouhal number

2.3.2: The Homann Flow Against an Oscillating Plate

Weidman and Mahalingham (1997) consider the axisymmetric stagnation-point flow against a porous plane boundary at which the transpiration velocity is a constant, equal to $-W_0$, and which performs periodic oscillations in its own plane, in the x -direction, with frequency ω . With rectangular co-ordinates (x, y, z) the velocity components may be written as:

$$\begin{aligned} u &= A x f_{\eta}(\eta) + U_0 g(\eta) e^{i\omega t}, & v &= A y f_{\eta}(\eta), \\ w &= -2(\nu A)^{1/2} f(\eta) - W_0, & \eta &= \left(\frac{A}{\nu}\right)^{1/2} z \end{aligned} \quad (2.45)$$

and the pressure as :

$$\begin{aligned} \frac{P-P_0}{\rho} = & -\frac{1}{2}A^2(x^2+y^2) - 2\nu A[f_\eta(\eta) \\ & + f^2(\eta)] + \frac{1}{2}\nu A(f+g)^2 - 2(\nu A)^{1/2}W_0 \end{aligned} \quad (2.46)$$

A is again the constant strain rate with $\frac{U_e}{\omega}$ the amplitude of the plate oscillations.

Applying Navier stoke's equations:

$$\begin{aligned} f_{\eta\eta\eta} + 2ff_\eta + Sf_{\eta\eta} - f_\eta^2 + 1 = \\ g_{\eta\eta} + fg_\eta + Sg_\eta - f_\eta g + i\Omega g = 0 \end{aligned} \quad (2.47)$$

where: $S = \frac{W_0}{(A\nu)^{1/2}}$ and $\Omega = \frac{\omega}{A}$. The boundary conditions require:

$$\begin{aligned} f(0) = f_\eta(0) = 0, \quad f_\eta(\infty) = 1 \\ g(0) = 1, \quad g(\infty) = 0 \end{aligned} \quad (2.48)$$

There are special cases: (a) $U_e = S = 0$, which corresponds to the classical steady, axisymmetric stagnation-point flow of Homann (1936), (b) $\Omega = S = 0$, which represents the case of a flat plate moving transversely at uniform speed U_e beneath the axisymmetric stagnation-point flow as considered by and (c) $S = 0$, representing the stagnation-point flow towards an impermeable plate performing transverse oscillations.

2.3.3: Three-Dimensional Stagnation-Point Flow

Three-dimensional stagnation-point flow which, as in the steady case, embraces both the two-dimensional and axisymmetric flows. Such a flow has been considered by Cheng, Ozisik and Williams (1971). As for the steady case it is convenient to adopt a slight change of notation with x, y as co-ordinates in the plane and z perpendicular to it. Cheng *et al.* assume that far from the boundary the x and y components of velocity are given by

$$U_e = \frac{Ax}{1 - \alpha\omega t} \quad (2.49)$$

$$V_e = \frac{By}{1 - \alpha\omega t} \quad (2.50)$$

where A, B, α and ω are constants, and introduce a self-similar solution as :

$$u = \frac{Ax}{1 - \alpha\tau} f_\eta(\eta) \quad (2.51)$$

$$v = \frac{By}{1 - \alpha\tau} g_\eta(\eta) \quad (2.52)$$

$$w = -\sqrt{\frac{\nu}{A(1 - \alpha\tau)}} [Af(\eta) + Bg(\eta)] \quad (2.53)$$

$$\eta = \left[\frac{A}{\nu(1 - \alpha\tau)} \right]^{1/2} z \quad (2.54)$$

$$\tau = \omega t \quad (2.55)$$

With $C = B/A$ and $\sigma = \frac{\alpha\omega}{A}$, using similarity transformations the following equations were yielded:

$$f_{\eta\eta\eta} + (f + Cg)f_{\eta\eta} + 1 - f_\eta^2 + D(f_\eta + \frac{1}{2}\eta f_{\eta\eta} - 1) = 0 \quad (2.56)$$

$$f(0) = f_\eta(0) = 0, \quad f_\eta(\infty) = 1$$

$$g_{\eta\eta\eta} + (f + Cg)g_{\eta\eta} + C - g_\eta^2 + D(g_\eta + \frac{1}{2}\eta g_{\eta\eta} - 1) = 0 \quad (2.57)$$

$$g(0) = g_\eta(0) = 0, \quad g_\eta(\infty) = 1$$

$$\frac{P_0 - P}{\rho} = \frac{1}{2(1 - \alpha\tau)^2} [A^2(1 - D)x^2 + B^2(1 - D)y^2] + \quad (2.58)$$

$$\frac{\nu k}{2(1 - \alpha\tau)} [2(f_\eta + g_\eta) + (f + g)^2 + D\eta(f + g)] = 0$$

Numerical solutions of the equations for f and g are presented by Cheng (1971) for a range of values of C and D , although the analogues of the dual solutions of Davey and Schofield (1967) and Schofield and Davey (1967) do not appear to have been explored. As for the steady case, values of $C > 0$ and $C < 0$ correspond, respectively, to nodal and saddle points of attachment; values of $D > 0$ and $D < 0$ correspond to decelerating and accelerating flows respectively.

Chapter 3

Similarity Transformation and Numerical Solution

3.1: Similarity Transformations:

The problem under consideration is that of two-dimensional version of Blyth and Hall (2003) flow approaching a vertical flat plate. Referring to a set of Cartesian axes (x, y) , the flat plate occupies $-\infty < x < \infty, y = 0$.

The velocity components are expressed as $u(x, y, t), v(x, y, t)$ in the x, y directions, respectively, governing equations which describe the fluid motion in this case are the two-dimensional unsteady Navier-Stokes equations.

In some simplified cases, such as a fluid travels through a rigid body (e.g., missile, sports ball, automobile, spaceflight vehicle), or in oil recovery industry crude oil that can be extracted from an oil field is achieved by gas injection, or equivalently, an external flow impinges on a stationary point called stagnation-point that is on the surface of a submerged body in a flow, of which the velocity at the surface of the submerged object is zero. A stagnation point flow develops, and the streamline is perpendicular to the surface of the rigid body. The flow in the vicinity of this stagnation point is characterized by Navier-Stokes equations. By introducing coordinate variable transformation, the number of independent variables is reduced by one or more.

The governing equations can be simplified to the non-linear ordinary differential equations and are analytic solvable

Navier-Stokes Equations

The full Navier-Stokes equations are difficult or impossible to obtain an exact solution in almost every real situation because of the analytic difficulties associated with the nonlinearity due to convective acceleration. The existence of exact solutions are fundamental not only in their own right as solutions of particular flows, but also are agreeable in accuracy checks for numerical solutions.

The Navier-Stokes equations are a system of non-linear, coupled partial differential equations (PDEs) which are derived from the principles of mass and momentum conservation.

The equation of mass conservation, or continuity equation, can be written as:

$$u_x + v_y = 0 \quad (3.1)$$

The equations of momentum conservation for a fluid are obtained from the application of the force-momentum principle, and can be written:

x- momentum:

$$u_t + uu_x + vv_y = -\frac{1}{\rho} P_x + \nu[u_{xx} + u_{yy}] \quad (3.2)$$

y- momentum:

$$v_t + uv_x + vv_y = -\frac{1}{\rho} P_y + \nu[v_{xx} + v_{yy}] \quad (3.3)$$

with the parameters, kinematic viscosity ν , pressure P and density ρ .

The boundary conditions are taken as:

$$\begin{aligned} u = 0, \quad v = v_0(t) & \quad \text{at} \quad y = 0 \\ u \rightarrow U_e(t) & \quad \text{at} \quad y \rightarrow \infty \end{aligned} \quad (3.4)$$

Where $u, &v$ the velocity components of the flow through the boundary layer are, $v_0(t)$ is the velocity of blowing\suction through the wall, $U_e(t)$ is unsteady potential velocity component.

near the surface, because of the no slip condition not being satisfied, a similarity solution is employed. We defined dimensionless similarity variables as ξ, η since:

$$\xi = Ax \quad (3.5)$$

$$\eta = \sqrt{\frac{A}{\nu}} * y \quad (3.6)$$

Where, A is a constant related with the body geometry, where $A > 0$.

The velocity components u and v of the boundary-layer flow are assumed to have solutions of the following form:

$$u = \xi * f_\eta(\eta, t) \quad (3.7)$$

Then, the y-direction velocity component v of the potential flow is immediately determined from the continuity equation (3.1), by substituting the foregoing velocity components u and v .

$$v = -\sqrt{\nu A} f(\eta, t) \quad (3.8)$$

Consider the unsteady periodic motion of an incompressible viscous fluid in the vicinity of the stagnation point at $x = y = 0$ on a blunt body. The potential flow approaches the body in the negative y-direction, impinges on the surface normally at the stagnation point flows away radially in all directions along the surface, and is assumed to have unsteady velocity components:

$$U_e = \xi a(t) \quad (3.9)$$

Where $a(t)$ is an arbitrary time-dependent function, as a case study it was chosen $a(t)$ as:

$$a(t) = \frac{1}{1 + \frac{\alpha}{\omega} \sin \omega t}, \quad (3.10)$$

Where, α is a constant related to free stream acceleration and ω is the potential flow frequency.

When $\alpha = 0$, the problem reduces to the steady case, that means $U_e \rightarrow Ax$.

Corresponding to α & A , we can define the unsteadiness parameter D as:

$$D = \frac{\alpha}{A}$$

The equations of motion [3.1 to 3.3] for the two-dimensional unsteady flow of incompressible viscous fluid in the vicinity of a forward stagnation point are reduced to two partial differential equations for a potential flow field chosen to vary periodically as a function of time, using the following procedure.

At first, we consider a general form of chain rule: let us assume $r(s)$ to the first derivative with respect to transformation variables ξ, η .

$$r_s = r_\xi \xi_{s_s} + r_\eta \eta_s \quad (3.11)$$

let us apply this rule, so that we can transform each term of the equation (3.2),

separately:

Term1: By differentiating u in eq (3.7) with respect to the time, we got:

$$u_t = Ax f_{\eta,t}(\eta, t) \quad (3.12)$$

Term2: applying the rule (3.11)

$$u_x = u_\xi \xi_x + u_\eta \eta_x$$

By differentiating u in eq (3.7) with respect to the $\xi : u_\xi = f_\eta(\eta, t)$

Then, with respect to $\eta : u_\eta = A x f_{\eta\eta}(\eta, t), \eta_x = 0, \xi_x = A$

By substitution, $u_x = A f_\eta(\eta, t) + 0,$

Therefore, $u_x = A x f_\eta(\eta, t).$

By multiplying $u u_x = A x f_\eta(\eta, t) * A f_\eta(\eta, t),$

Finally,

$$u u_x = A^2 x f_\eta^2(\eta, t) \tag{3.13}$$

Term3: applying rule (3.11) to find $u_y :$

$$u_y = u_\xi \xi_y + u_\eta \eta_y$$

By differentiating:

$$u_\xi = f_\eta(\eta, t), \xi_y = 0, u_\eta = A x f_{\eta\eta}(\eta, t), \eta_y = \sqrt{\frac{A}{\nu}} h$$

Therefore:

$$u_y = A x \sqrt{\frac{A}{\nu}} f_{\eta\eta}(\eta, t) \tag{3.14}$$

By multiplying ν from eq. (3.8) by $u_y,$ we get:

$$\nu u_y = -A^2 x f(\eta, t) f_{\eta\eta}(\eta, t) \tag{3.15}$$

Term4: applying the acceleration equation at the far-field flow:

$$-\frac{1}{\rho} P_x = (U_e)_t + U_e (U_e)_x + V_e (U_e)_y \tag{3.16}$$

Where, $(U_e)_t$ is the rate of change of velocity with respect to time at a given point in a flow field which called as (the local acceleration or Temporal acceleration).

And $U_e(U_e)_x$ is the rate of change of velocity due to the change of position of fluid particles in a fluid flow which called as (the convective acceleration).

From eq (3.9) : $U_e = Axa(t)$

By differentiating U_e with respect to t, x, y we get:

$$(U_e)_t = Axa_t(t), \quad (U_e)_x = Aa(t), \quad (U_e)_y = 0$$

By substitution in eq. (3.20), we get:

$$-\frac{1}{\rho} P_x = Axa_t(t) + A^2x[a(t)]^2 \quad (3.17)$$

Term5: by considering eq. (3.14), let $\zeta = u_y$

$$\zeta = Ax\sqrt{\frac{A}{\nu}} f_{\eta\eta}(\eta, t) = \vartheta f_{\eta\eta}(\eta, t) \text{ j}$$

Applying rule (3.11) to ζ :

$$\zeta_y = \zeta_{\vartheta} \vartheta_y + \zeta_{\eta} \eta_y$$

By differentiating, we get:

$$\zeta_{\vartheta} = f_{\eta\eta}(\eta, t), \quad \vartheta_y = 0, \quad \zeta_{\eta} = Ax\sqrt{\frac{A}{\nu}} f_{\eta\eta\eta}(\eta, t), \quad \eta_y = \sqrt{\frac{A}{\nu}}$$

By substituting in ζ_y :

$$\zeta_y = \frac{A^2}{\nu} x f_{\eta\eta\eta}(\eta, t)$$

Finally, we get:

$$u_{yy} = \frac{A^2}{\nu} x f_{\eta\eta\eta}(\eta, t) \quad (3.18)$$

by substituting in eq (3.2), by relations (3.12, 3.13, 3.15, 3.17, (3.18), we get the final similarity equation describes the stream-wise flow in stagnation point flow boundary layer:

$$\left(\frac{1}{A}\right) f_{\eta,t} + (f_{\eta})^2 - f f_{\eta\eta} = \left(\frac{1}{A}\right) a_t(t) + [a(t)]^2 + f_{\eta\eta\eta} \quad (3.19)$$

Initial and Boundary Conditions:

Boundary conditions for the differential equation are expressed as follows:

$$\begin{aligned} f_{\eta}(0, \eta) &= \frac{u_0(t)}{Ax}, & f(0, t) &= -\sqrt{\frac{1}{Av}} v_0(t), \\ \eta \rightarrow \infty, & & f_{\eta} &\rightarrow a(t) \end{aligned} \quad (3.20)$$

To satisfy the interspersed wall boundary conditions and to match to the outer potential solution.

Our study aim was create a mathematical model can generalize the flow boundary conditions, and studying the effect of flow parameters change on the characteristics of boundary layer, for different values of the fluctuation amplitude Δ , the oscillation frequency ω and the unsteadiness parameter D .

The boundary conditions in eq.(3.21) in a generalized form and our assumptions were applied to achieve a special case which under the effect of flow parameters' changing.

For that, the boundary conditions are reformed according to our case study as:

$$\begin{aligned} f_{\eta}(0, \eta) &= 0, & f(0, t) &= -\sqrt{\frac{1}{Av}} v_0(t), \\ \eta \rightarrow \infty, & & f_{\eta} &\rightarrow a(t) \end{aligned} \quad (3.21)$$

$v_0(t)$ was chosen as:

$$v_0(t) = \Delta \cos \omega t \quad (3.22)$$

Where Δ is the amplitude of the oscillating flow due to blowing/suction at the wall, and ω is the oscillation frequency.

By substituting by eq. (3.21) in eq. (3.20), we get:

$$f(0,t) = -\sqrt{\frac{1}{A\nu}} \Delta \cos \omega t, \text{ hence, } A,\nu,\Delta \text{ are constants, we can introduce, } k = -\sqrt{\frac{1}{A\nu}} \Delta,$$

and named it as “blowing parameter”.

3.2: Numerical Procedure to Solve (PDE) Similarity Equations:

To solve equations (3.19) numerically, A fully implicit finite difference based PDE solver is used (Implicit Euler)

Grid points:

To find a numerical solution with finite difference methods, we first need to define a set of grid points in a limited domain as follows: Choose a state step size $\Delta\eta$ and a time step size Δt , draw a set of horizontal and vertical lines across the domain, and get all intersection points (i,n) as shown in figure(3. 1) ,

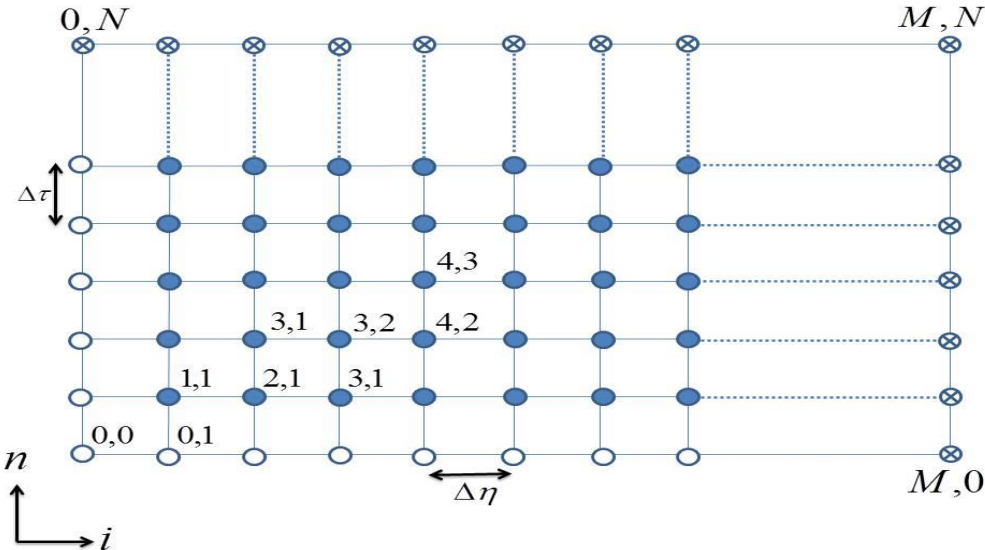


Figure (3.1): Grid Points

Implicit & Explicit Scheme:

When the data at the next time level is obtained from an explicit formula involving data from the previous time levels, this called an explicit scheme. In the case of explicit scheme, the situation leads to a stability restriction on the maximum allowable time step.

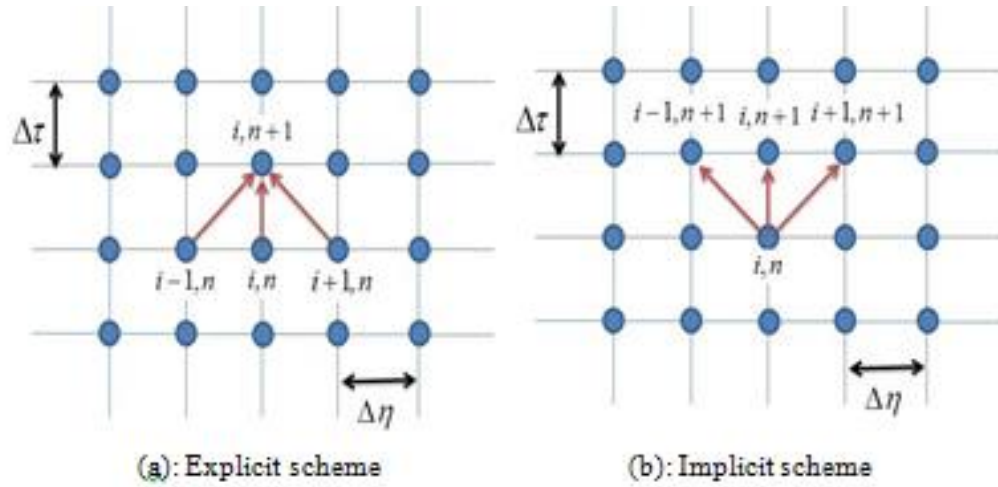


Figure (3.2): Explicit and Implicit Schemes

Numerical Solution Procedure:

To solve equations (3.19) numerically, the following procedure is applied:

1- Assume:

$$Q_i = f_{\eta,t}, \quad Q = f_{\eta} \rightarrow Q_{\eta} = f_{\eta\eta} \rightarrow Q_{\eta\eta} = f_{\eta\eta\eta}$$

By substitution the- Qs variables instead of the-fs variables in equation (3.19)

$$Q_t + AQ^2 - AfQ_{\eta} = a_t + Aa^2 + AQ_{\eta\eta} \quad (3.23)$$

2- Use implicit scheme as:

$$Q_t = \frac{Q_i^{n+1} - Q_i^n}{\Delta t}, \quad Q^2 = Q_i^n Q_i^{n+1}, \quad Q_{\eta} = \frac{Q_{i+1}^{n+1} - Q_{i-1}^{n+1}}{2\Delta\eta} \quad (3.24)$$

$$Q_{\eta\eta} = \frac{Q_{i+1}^{n+1} - 2Q_i^{n+1} + Q_{i-1}^{n+1}}{(\Delta\eta)^2}$$

3- By substituting (3.25) in (3.24)

$$\frac{Q_i^{n+1} - Q_i^n}{\Delta t} + A Q_i^n Q_i^{n+1} - A f^n \left(\frac{Q_{i+1}^{n+1} - Q_{i-1}^{n+1}}{2\Delta\eta} \right) = (a_t)^n + A(a^2)^n + A \left(\frac{Q_{i+1}^{n+1} - 2Q_i^{n+1} + Q_{i-1}^{n+1}}{(\Delta\eta)^2} \right)$$

4- By multiplication by (Δt)

$$\begin{aligned} & Q_i^{n+1} - Q_i^n + A\Delta t Q_i^n Q_i^{n+1} - A \frac{\Delta t}{2\Delta\eta} f^n (Q_{i+1}^{n+1} - Q_{i-1}^{n+1}) \\ &= (a_t)^n \Delta t + A(a^2)^n \Delta t + A \frac{\Delta t}{(\Delta\eta)^2} (Q_{i+1}^{n+1} - 2Q_i^{n+1} + Q_{i-1}^{n+1}) \end{aligned}$$

Let: $\beta_1 = A \frac{\Delta t}{2\Delta\eta} \quad \beta_2 = A \frac{\Delta t}{(\Delta\eta)^2}$

Then the last equation becomes:

$$\begin{aligned} & Q_i^{n+1} - Q_i^n + A\Delta t Q_i^n Q_i^{n+1} - \beta_1 f^n (Q_{i+1}^{n+1} - Q_{i-1}^{n+1}) \\ &= (a_t)^n \Delta t + A(a^2)^n \Delta t + \beta_2 (Q_{i+1}^{n+1} - 2Q_i^{n+1} + Q_{i-1}^{n+1}) \end{aligned}$$

Rearrange the equation to be the next time step variables in the left side

and the current time step variables in the right side:

$$\begin{aligned} & Q_i^{n+1} + A\Delta t Q_i^n Q_i^{n+1} - \beta_1 f^n Q_{i+1}^{n+1} + \beta_1 f^n Q_{i-1}^{n+1} - \beta_3 Q_{i+1}^{n+1} \\ & \quad + 2\beta_3 Q_i^{n+1} - \beta_3 Q_{i-1}^{n+1} \\ &= Q_i^n + (a_t)^n \Delta t + A(a^2)^n \Delta t \end{aligned}$$

Finally, we get:

$$\begin{aligned} & Q_i^{n+1} [1 + A\Delta t Q_i^n] - Q_{i+1}^{n+1} [\beta_1 f^n - \beta_2 g^n] + Q_{i-1}^{n+1} [\beta_1 f^n - \beta_2 g^n] \\ &= Q_i^n + \Delta t [(a_t)^n + A(a^2)^n] \end{aligned} \quad (3.25)$$

This equation is solved using Thomas algorithm because the system is tridiagonal.

Chapter 4

Results and Discussion

4.1: Results Investigation

Since there is no experimental data published, it was not possible to compare the present results. Instead, the available analytical/numerical results in literature were used for comparison.

4.1.1: Comparison PDE Solution with ODE Solution

Similarity solutions exist for flows which show specific symmetries and group properties, such that a similarity transformation reforms the Navier–Stokes equations into a set of ordinary differential equations. Such solution called (ordinary differential equation solution), in our case the (partial differential equation solution) because of our study main object, where our aim was assume any unsteady function at the initial and the boundary conditions. This comparison between ODE solution in the literature and our PDE solution for the same assumptions used in the literature. The comparison shows a good matching using our solver as shown in figures (4.1), (4.2), that's what prompted us to go ahead achieving our objectives.

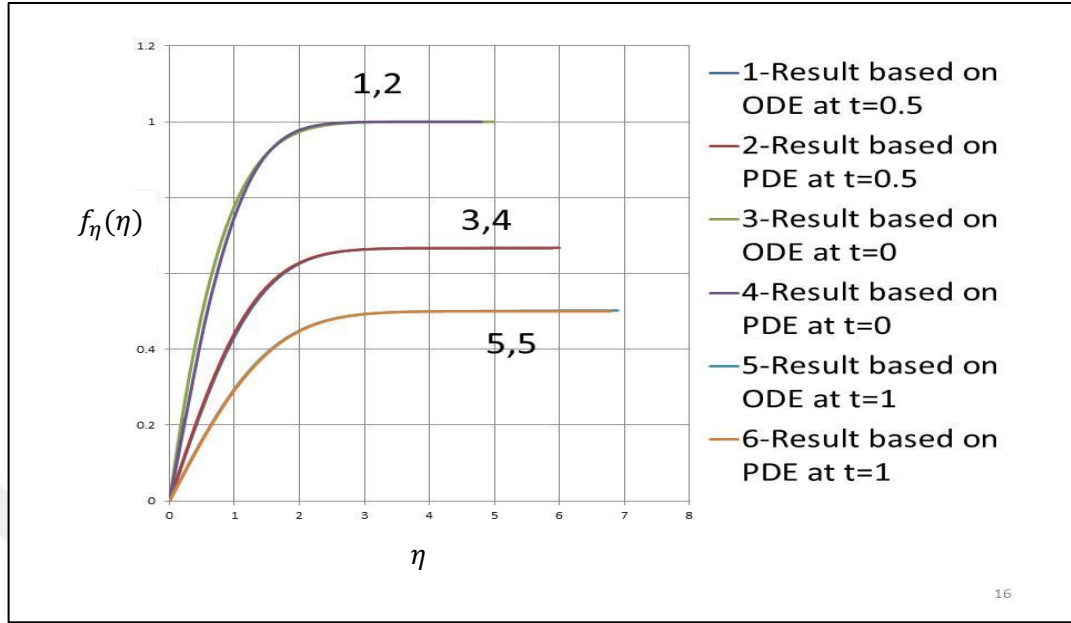


Figure (4.1): Compression PDE Solution With ODE Solution for Horizontal Velocity Profile

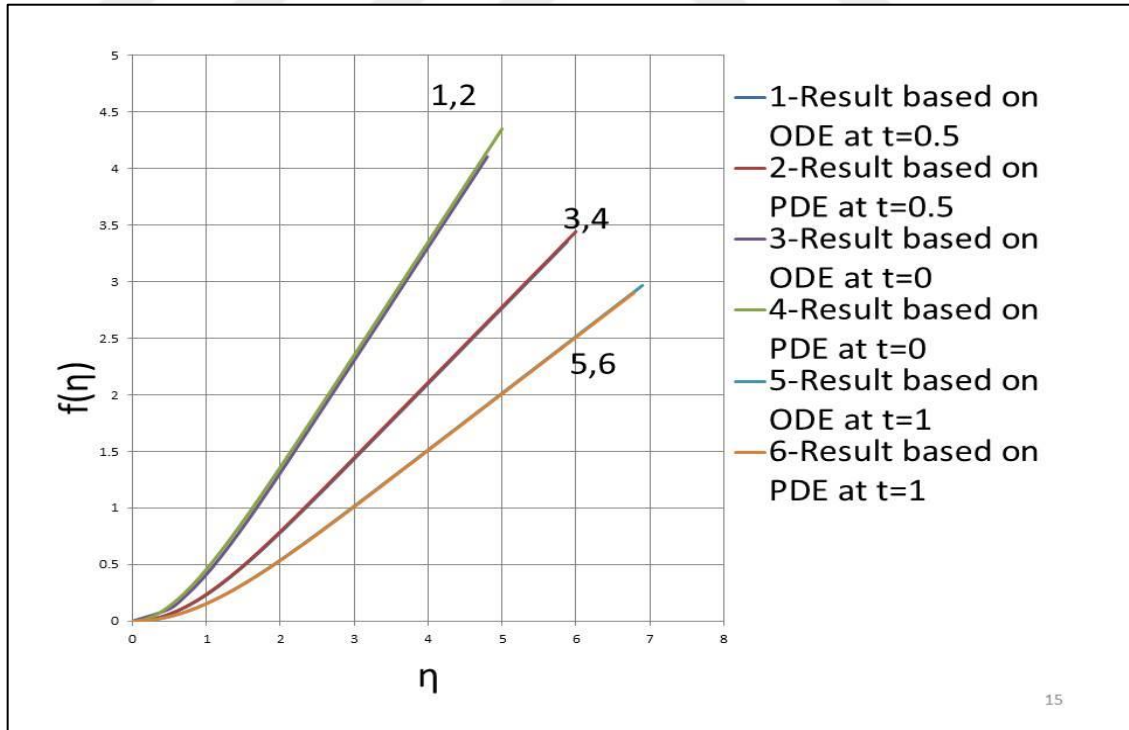


Figure (4.2): Compression PDE Solution with ODE Solution for Vertical Velocity profile

4.1.2: Comparison Between Similarity Solution (PDE) and CFD Code:

SU2 is an open-source CFD (computational fluid dynamics) software written in C++ using object-oriented programming to solve the partial differential equations (PDEs) and PDE-constrained optimization problems on unstructured meshes. Through the initiative of users and developers around the world, SU2 is now a well-established tool in the computational sciences with wide applicability to aeronautical, automotive, naval, and renewable energy industries. SU2 is used to validate the computer code developed in this thesis work. The steady-state flow over a vertical plate is solved using both the present method and SU2. The mesh employed in SU2 has 7396 rectangular elements with 7569 nodes, Figure (4.3). The solution by SU2 requires more than an hour of wall clock time on a 64-bit Windows 8 running personal computer with two 2.5-Ghz CPUs and 8-GB memory. The developed computer code is also run on the same computer which gives the ODE solution less than a second.

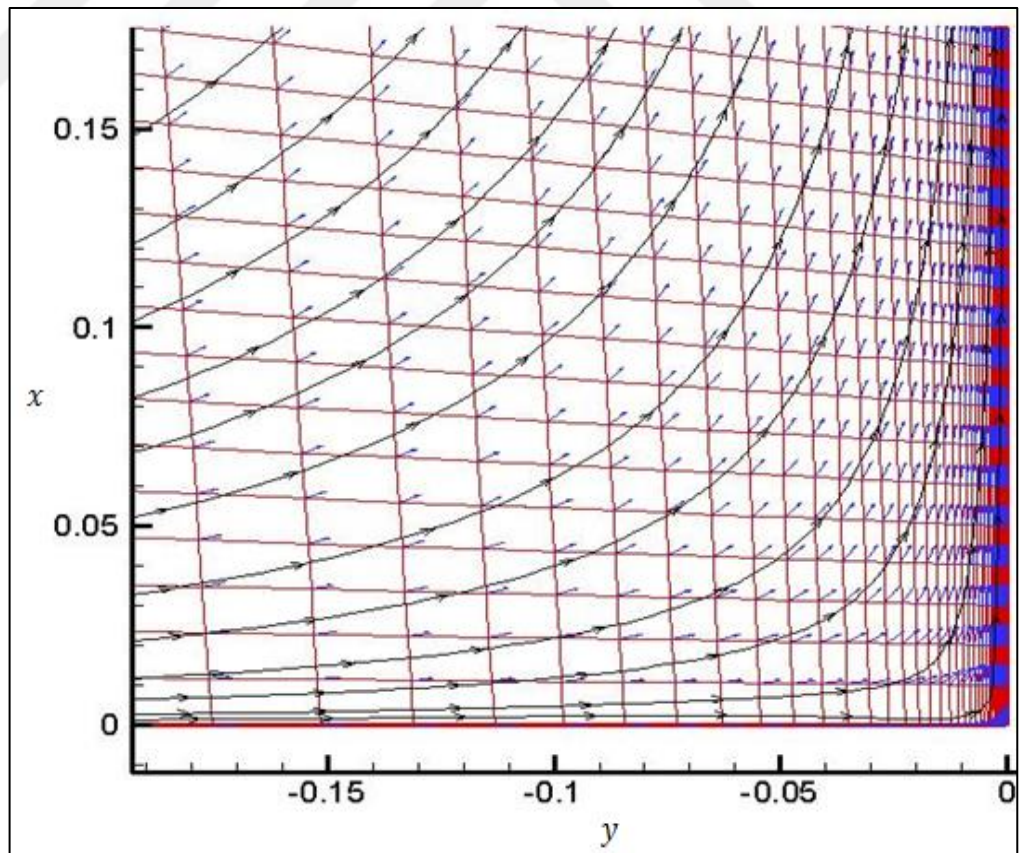


Figure (4.3): Velocity Field Stream Lines

The comparison between CFD solution and similarity solution was done as shown in figures (4.4), (4.5), the comparison shows a good matching.

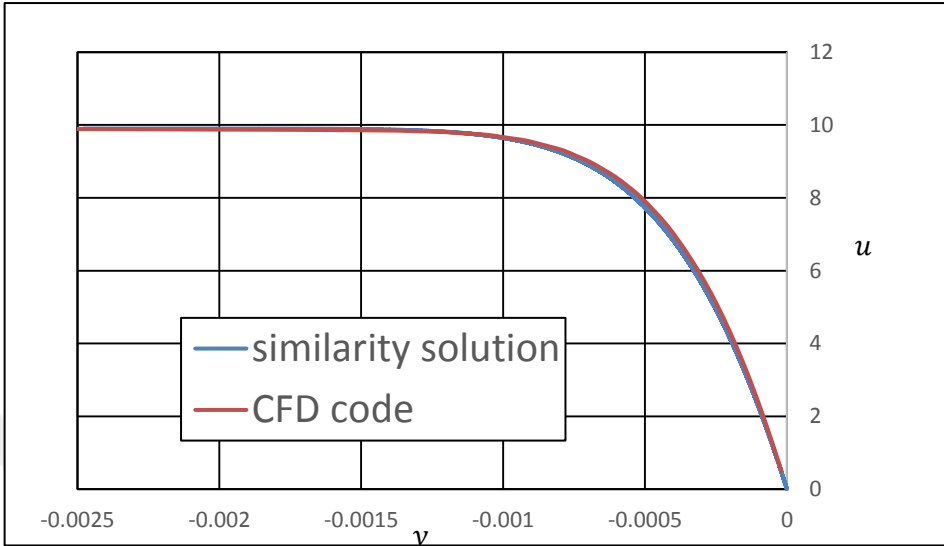


Figure (4.4): Variation of the Velocity Component Parallel to the Wall near the Stagnation Point

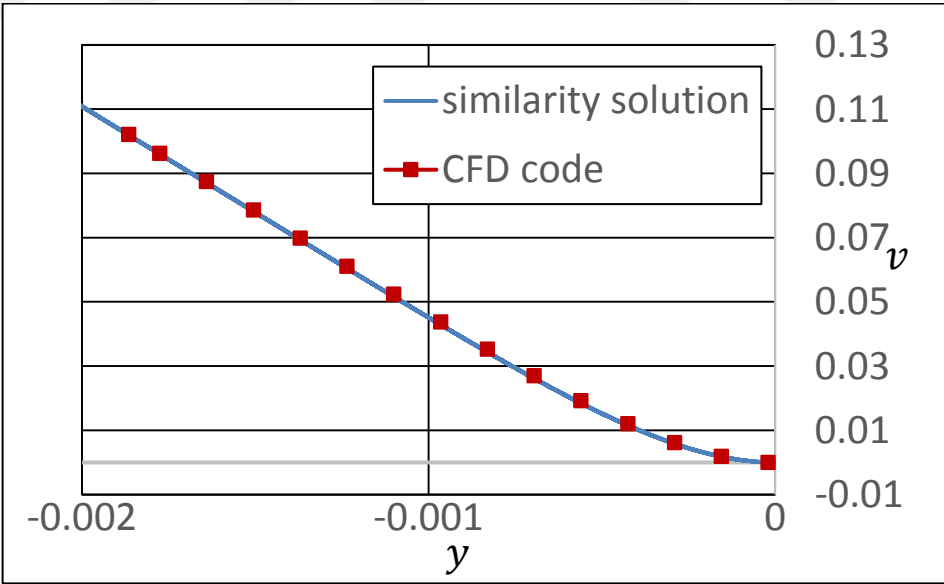


Figure (4.5): Variation of the Velocity Component Vertical to the Wall near the Stagnation Point

4.2: Flow Parameters and Regimes

The behavior of unsteady flow is affected by the conditions in which it exists in.

In our case, for an unsteady viscous incompressible laminar stagnation point flow and according to our assumed functions (chapter 3), the boundary layer characteristics were affected by three parameters, which are:

- D : *the steadiness parameter*

- k : *the blowing parameter*

- ω : *the oscillation frequency*

4.2.1: Regions of Stable and Unstable flow Parameters Regions

Regions of flow parameters are the regions formed by a combination of flow parameters (D, k, ω),

This combination makes the flow take a certain behavior dependent on time and position. At first, we could classify the flow parameters to two combinations:

- 1- Parameters' combination, lead to periodic oscillatory motion.
- 2- Parameters' combination, lead to unstable oscillatory motion.

We have focused our work in the first region, so we have rejected the flow Parameters' combinations, lead to irregular oscillatory motion because they lead to blowing-up at definite time from our calculations.

We have selected specific values of unsteadiness parameters and classified other parameters according to it. Table (4.1) shows this classification:

Table (4.1): Stable Periodic & Unstable Flow Parameters Regions

Unsteadiness parameter	Regular oscillation	Irregular oscillation
$D = 2$	$\omega \geq 2$	$\omega < 2$
$D = 4$	$\omega \geq 5$	$\omega < 5$
$D = 6$	$\omega \geq 8$	$\omega < 8$
$D = 10$	$\omega \geq 11$	$\omega < 11$

This can be further clarified by observing the following figure (4.6) where at each border line D there is a boundary between the regularity and irregularity of the oscillating flow, where we find the regular flow parameters region above the line and the irregular flow parameters region below it. The results were examined accurately and found to be valid at any η . Where ($0 \leq \eta \leq 10$).

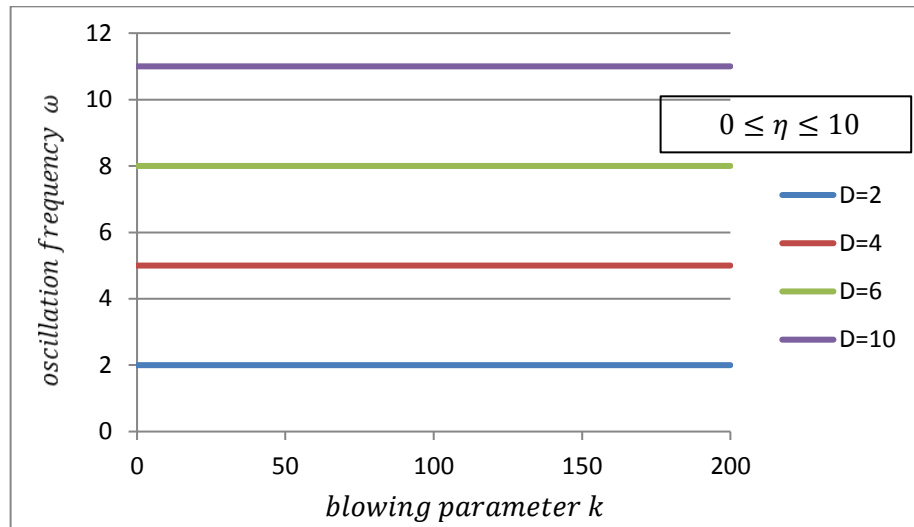


Figure (4.6): Stable Periodic & Unstable flow Parameters Regions

Periodic flow is a general expression describes the flow. In fact, this motion could be periodic or quasi-periodic. Such motions are shown for f , f_η & $f_{\eta\eta}$ profiles in figures (4.7), (4.8), (4.9) and (4.10), (4.11) respectively.

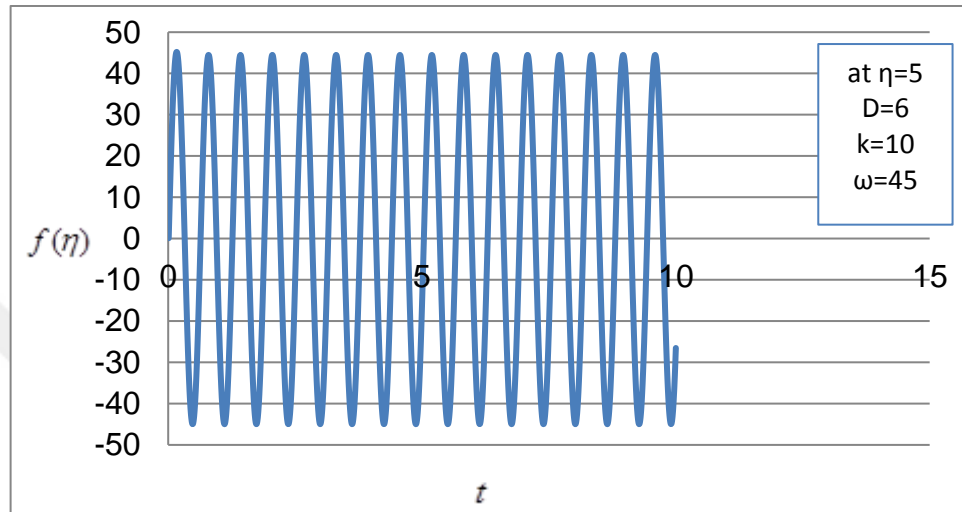


Figure (4.7): Regular Periodic Structure for f – profile

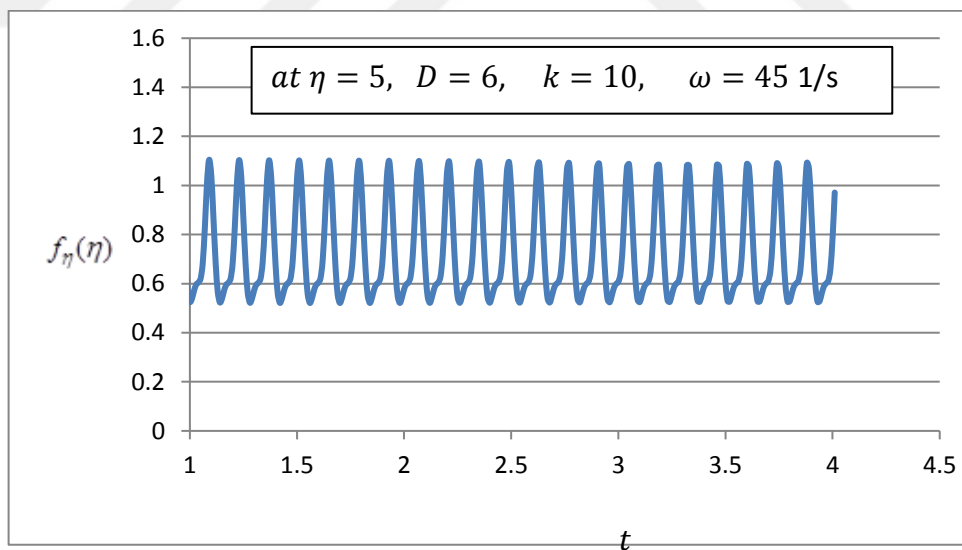


Figure (3.8): Regular Periodic Structure for f_η – profile (example1)

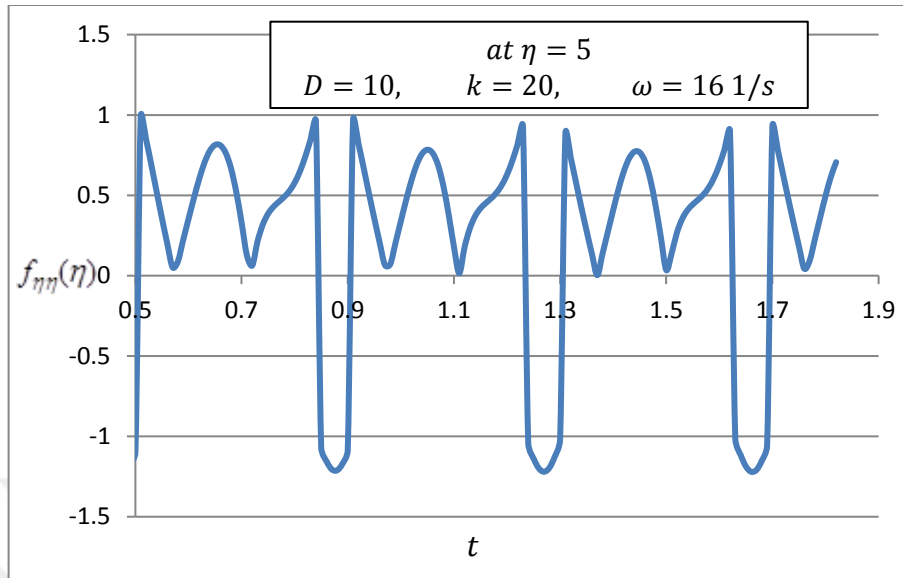


Figure (4.9): Regular Periodic Structure for $f_{\eta} - profile$ (example2)

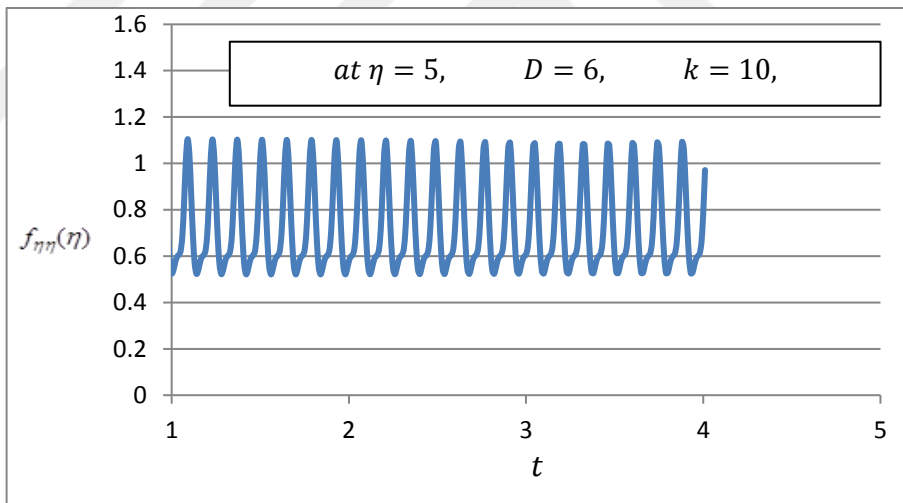


Figure (4.10): Regular Periodic Structure for $f_{\eta\eta} - profile$ (example1)

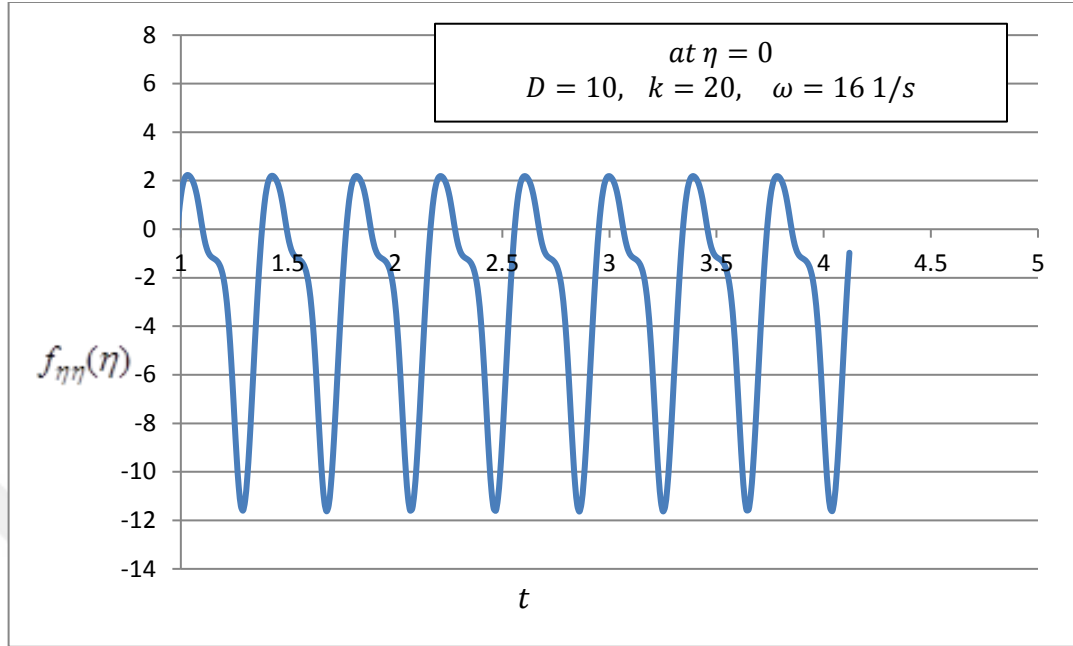


Figure (4.11): Regular Quasi-Periodic Structure for $f_{\eta\eta}$ – profile (example2)

4.2.2: Regions of Reversed and Non-Reversed flows at: $\eta = 0$

In this section the classification of the combinations of flow parameters based on the reversibility.

The flow velocity is inversely proportional dependent of pressure therefore, if the pressure gradient has a positive sign along flow direction that means the velocity decreases (reversed flow), and if it has a negative sign, that means the velocity increases (non-reversed flow)

It is known from the previous studies dealing with unsteady stagnation point flows that the unsteadiness parameter D effects on the pressure gradient, that as a result of an unsteady function for the potential flow velocity U_e .

The pressure gradient sign is dependent of the value of unsteadiness parameter. Table (4.2), summarize this relation:

Table (4.2): Regions of Reversed & Non-Reversed Flows (ODE solution)

	$\frac{\partial P}{\partial x}$	$\frac{\partial u}{\partial x}$	Flow type
$D < 1$	-	+	Non-reversed
$D > 1$	+	-	Reversed

Most of studies were concerned with (ODE solution) ordinary differential equations solution solving the governing equations describing the unsteady stagnation point flows. This solution was investigated by the solution we presented in this study.

PDE solution enabled us to assume any unsteady function either at the surface or at the potential flow, in our study as mentioned chapter 3, our supposed unsteady function was:

$$U_e = \frac{A}{1 + \frac{\alpha}{\omega} \sin \omega t}$$

This supposed oscillation function was applied, the behavior of flow could be observed under the effect of change of k, ω , at $D < 1$, and found that, for any arbitrary values of k, ω , the flow at $\eta = 0$ is always non-reversed all the time, which is the same flow behavior in (ODE solution) case (table4.2). But there is an interesting behavior observed in our results due to our new assumed unsteady function, it was the existing of a non-reversed during the interval ($0 \leq t \leq 10$) flow even the unsteadiness parameter exceeds a unity.

When ($D > 1$) at a t higher values of oscillating frequency ω , It could be found at each ($D \& k$) parameter values, a corresponding value of ω which we distinguished as ω^* , where ω^* is a searched highest value of oscillation frequency at the border of irreversibility.

When: $\omega < \omega^*$:

- It was observed the possibility of existence of reversed flow at a definite time, as shown later in section (4.6)

Here was the point of excellence that, our assumptions have created. So we could modify table (4.3) to take the following form:

Table (4.3): Regions of Reversed & Non-Reversed flows (due to our assumptions)

	Frequency ω	$\frac{\partial P}{\partial x}$	$\frac{\partial u}{\partial x}$	Flow type
$D < 1$	any	-	+	Non-reversed
$D > 1$	$\omega > \omega^*$	-	+	Non-reversed
	$\omega < \omega^*$	+	-	Reversed

As an important benefit of our work was finding a general map shows two regions of flow parameters. So, it was possible to find a borderline formed by ω^*

- Values which were found under different flow conditions. The border line separates two regions, where the area above the borderline represents to parameters' values related with flow irreversibility parameters, and the area under represents to the variable's values related with flow reversibility parameters. k -values were selected to vary from 5 to 700, and the selected D values were [$D = 2, D = 4, D = 6$]

The indicator representing the $u - component$ velocity direction at $\eta = 0$ is $f_{\eta\eta}(0)$. Where if: $f_{\eta\eta}(0) > 0$ non-reversed flow (at $t: 0 \leq t \leq 10$)

$$f_{\eta\eta}(0) < 0 \quad \text{reversed flow (at definite time)}$$

The flow under the effect of combination of flow parameters was observed accurately, the following values have been got and inserted in the following table.

Table (4.4): Values of ω^* at which the Point Separates Reversed and Non- Reversed Regions of Parameters at the Wall (reversed flow at the wall exists at definite time)

k	ω^*		
	at $D = 2$	at $D = 4$	at $D = 6$
5	9	24	38
10	25	47	65
30	75	101	117
50	96	120	131
70	103	126	137
100	107	130	140
200	105	126	139
300	103	120	131
400	101	119	127
500	99	117	126
600	97	116	124
700	96	117	124

According to this table, the following can be commented:

- At values of $k < 5$, $f_{\eta\eta}(0) \rightarrow \infty$
- After $k \approx 500$, ω^* has a small variation and can be considered as constantly changes with k .
- Reversibility of flow may be occur at any time, so ω^* values were searched corresponding to $f_{\eta\eta}(0)^*$, where $f_{\eta\eta}(0)^*$ is the value of $f_{\eta\eta}(0)$ when inflected from negative to positive value.

The results in table (4.4) was plotted in figure (4.12)

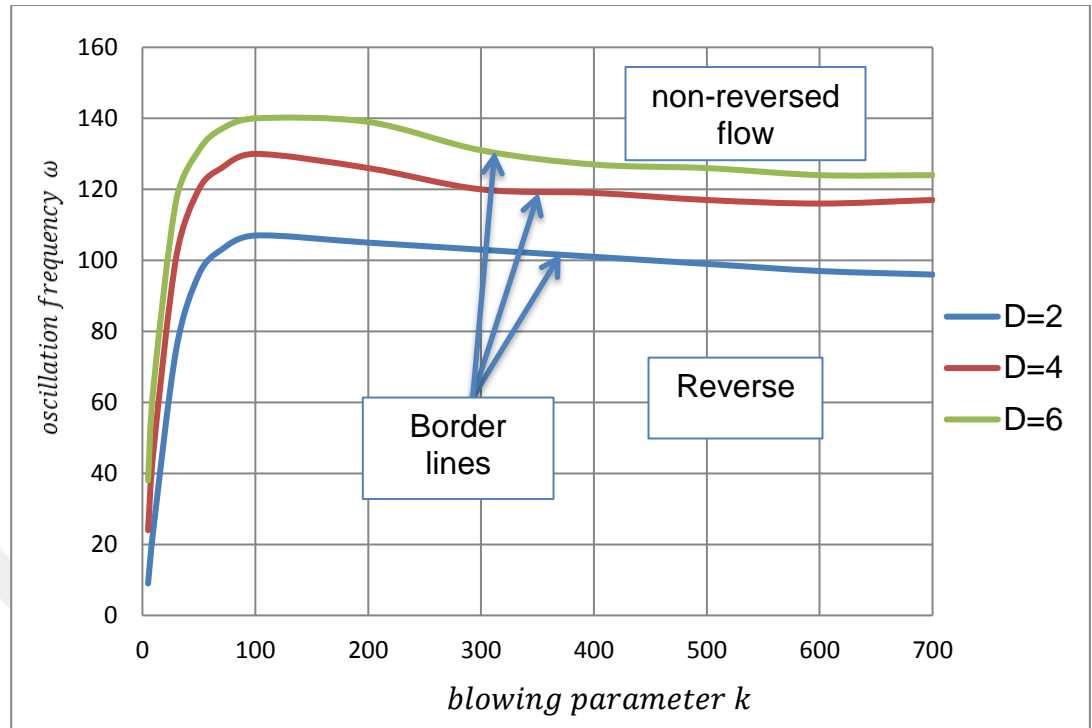


Figure (4.12): Reversed and Non-Reversed Regions of Parameters at the Wall (reversed flow at the wall exists at definite time)

4.2.3: Matching Regions of Stable Periodic and Unstable flow Parameters with Regions of Reversed and Non-Reversed flow Parameters

We found it necessary to be more efficient and accurate to study the effect of flow parameters on the characteristics of the boundary layer starting by determining the limits of those parameters to be applied.

In the following figure, figures (4.6) & (4.12) were combined in one figure, the figure shows at $D = 4$ three regions of flow parameters as following:

- 1- Unstable oscillating flow parameters region: This region has been excluded from this work because the combination of parameters involved in this region leads to a blow-up at a definite time.
- 2- Regular & reversed oscillating flow parameters region, this region valid at $\eta = 0$.
- 3- Regular & non-reversed oscillating flow parameters region, this region valid at $\eta = 0$.

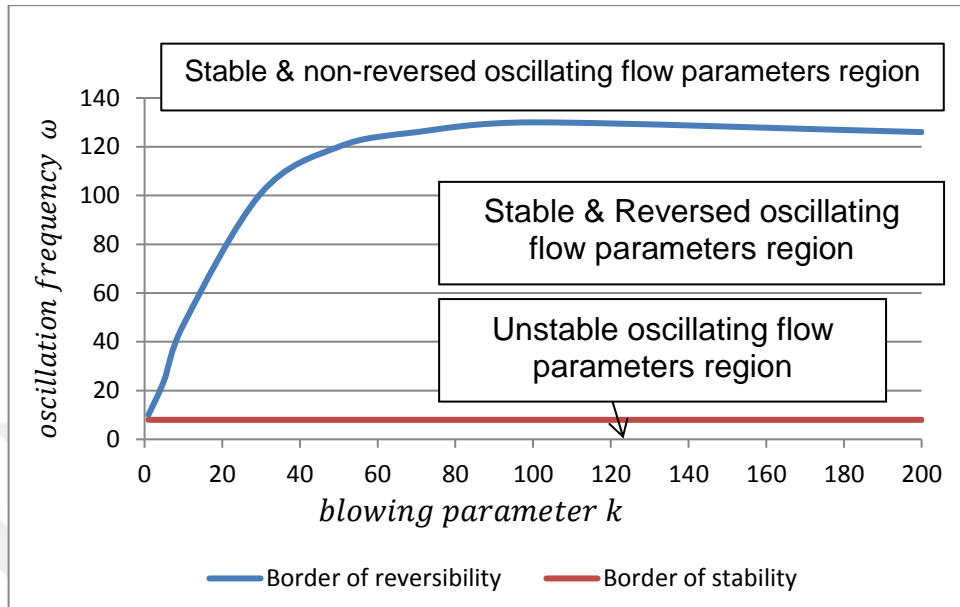


Figure (4.13): Matching Regions of Stable Periodic and Unstable Flow Parameters with Regions of Reversed and Non-Reversed Flow Parameters at the Wall

Figure (4.13): Matching regions of stable periodic and unstable flow parameters with regions of reversed and non-reversed flow parameters at ($D = 2$)

At each point of the regions of flow parameters showed in figure (4.13), the flow behaves differently in terms of $f_{\eta\eta}(0)_{max-rev}$ and the period of time in which it occurred.

For a specific case, at $D = 2$, $k = 100$, the flow was accurately observed to enclosure the flow behavior during the first period of time motion where the reversed flow occurs & its maximum value. At the mentioned case, it was found the starting and ending time of reversed flow, in addition to the maximum value referred to the maximum reversed shear stresses at the wall.

Table (4.5): Intervals of Reversed Flow & $f_{\eta\eta}(0)_{max-rev}$ at the 1st Period of Oscillation

ω	t (at starting reversed flow period)	t (at ending reversed flow period)	$f_{\eta\eta}(0)_{max-rev}$
2	2.63	3.5	-9.448683
5	1.06	1.4	-2.7437
10	0.54	0.72	-1.62
25	0.22	0.3	-0.66759
40	0.16	0.19	-0.26
70	0.1	0.11	-4.02E-02

from table (4.5), it could be commented that:

- As ω increases, as the starting of reverd flow interval becomes eirlier.
- As ω increases, as the reverd flow interval becomes shorter. Where at $\omega = 2 \text{ 1/s}$, the reverd flow interval $\Delta t_{rev.} = 0.87s$ and at $\omega = 70 \text{ 1/s}$, the reverd flow interval $\Delta t_{rev.} = 0.01 s$
- As ω increases, as $f_{\eta\eta}(0)_{max-rev}$ becomes smaaller. So at high values of oscillation frequency ω , $f_{\eta\eta}(0)_{max-rev} \rightarrow 0$.

To clarify more, the data in the previous table was illustrated in figures (4.14), (4.15)

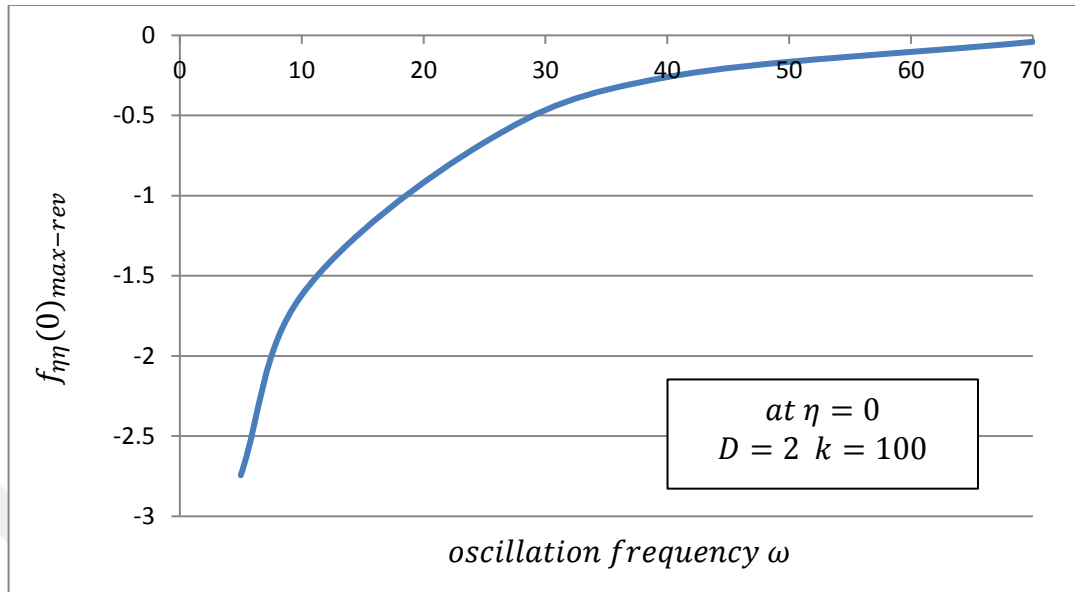


Figure (4.14): Maximum Reversal Wall Shear Stress vs. Oscillating Frequency Increasing (at $\eta=0$, unsteadiness parameter $D=2$, blowing parameter $k=100$)

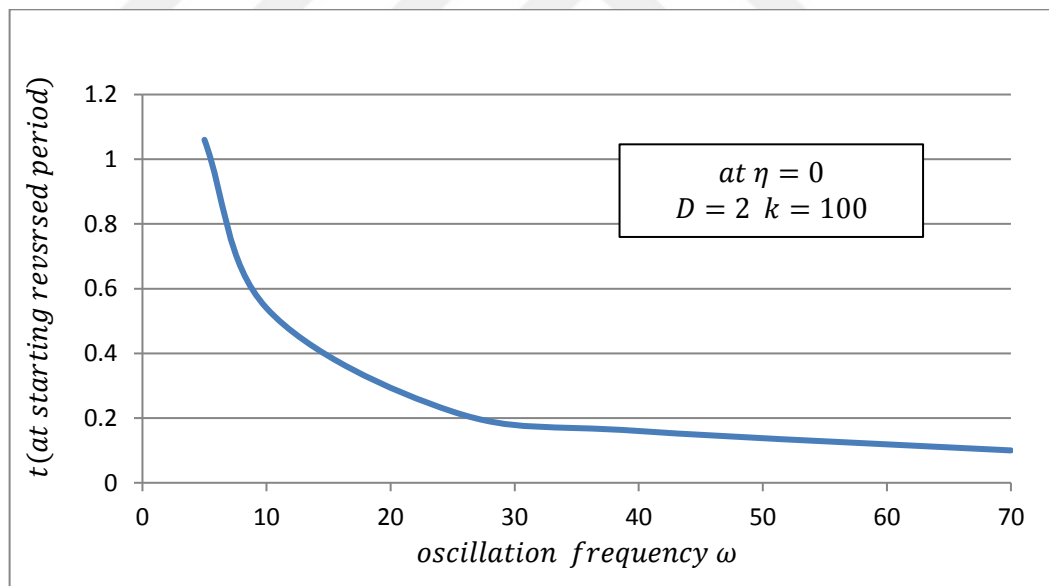


Figure (4.15): Reversal Flow Interval Starting Time vs. Oscillating Frequency (at $\eta=0$, unsteadiness parameter $D=2$, blowing parameter $k=100$)

4.3: The Effect of Flow Parameters On $f - profile$

4.3.1: The Effect of Blowing Parameter On $f - profile$

Figure(4.16) present the profiles of f , for values of k (from 0 & 10) for specific values of unsteadiness parameter D and oscillation frequency ω during a definite time from $t=5.81$ s to 5.85 s.

Figures show the effect of blowing parameter on $f(0)$ which increases as k be higher.

Since, the motion is sinusoidal, $f(0)$ moves alternatively within the interval of $[-k, k]$. If we consider $f - profile$ as a straight line, so we can consider the blowing parameter in terms of the slope of $f(\eta)$, a small period of time was focused on and the main slope for that period was calculated, where profiles' slope values during the considered time interval had a small differences between each other at the same flow parameters, therefore, it could be made a slope comparison at different values of k , it was found that, the main slope at ($k = 0, 10, 100, 500$) is as in the following figure :

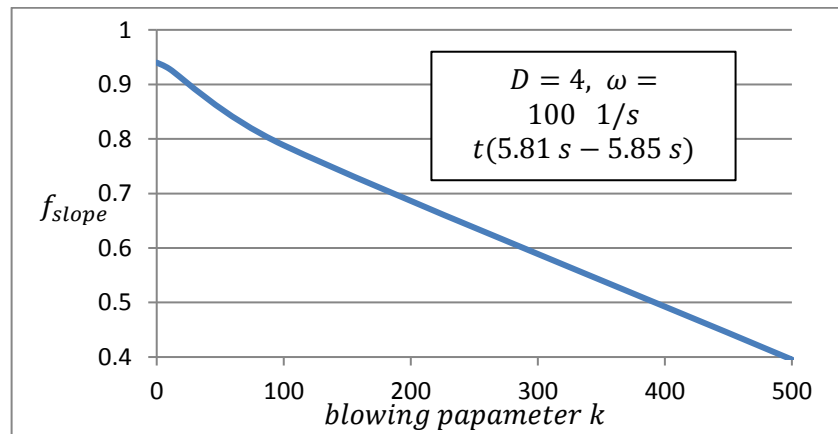


Figure (4.16): Slope of f -Profile vs. Blowing Parameter k (at unsteadiness parameter $D=4$, oscillation frequency $\omega=100$ 1/s) during the period $t = (5.81$ s – 5.85 s)

When no blowing effect, the initial velocity at the wall is independent of time, on the contrary of that when the blowing effect exists, the initial velocity at the wall changes with time, Figure (4.17).

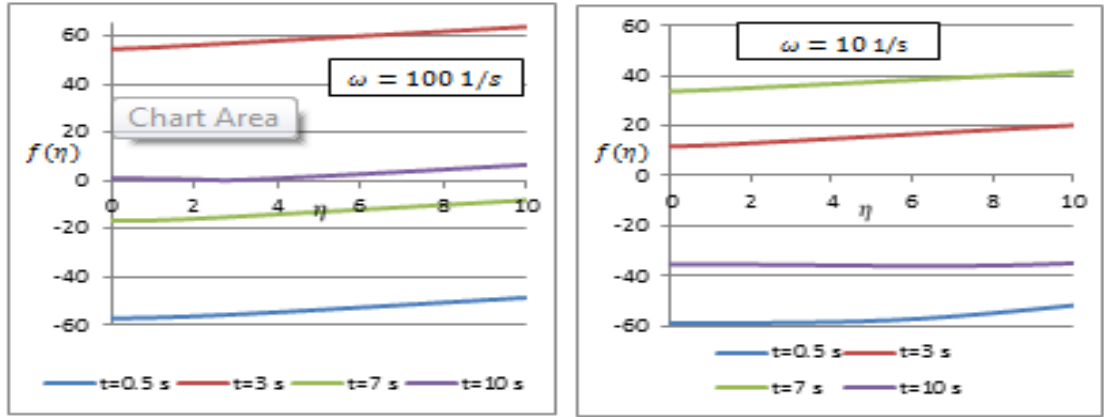


Figure (4.17): Structures of (f -velocity profile) during a definite period of time at(unsteadiness parameter $D=4$,oscillation frequency $\omega=100$ 1/s,blowing parameter $k=0,10$ respectively)

4.3.2: The Effect of Oscillation Frequency On f – profile

Applying different arbitrary values of oscillation frequency ω didn't show obvious effect on f – profile . We have reached this conclusion after observing the flow under the influence of the flow parameter, for example, at: $D = 4$ & $k = 60$, and, at ($t = 0.5s, t = 3s, t = 7s, 10s$) ,the oscillation frequency values applied were ($\omega = 10$ 1/s, $\omega = 100$ 1/s). The effect of these combinations of flow parameters is shown in figures (3.18).

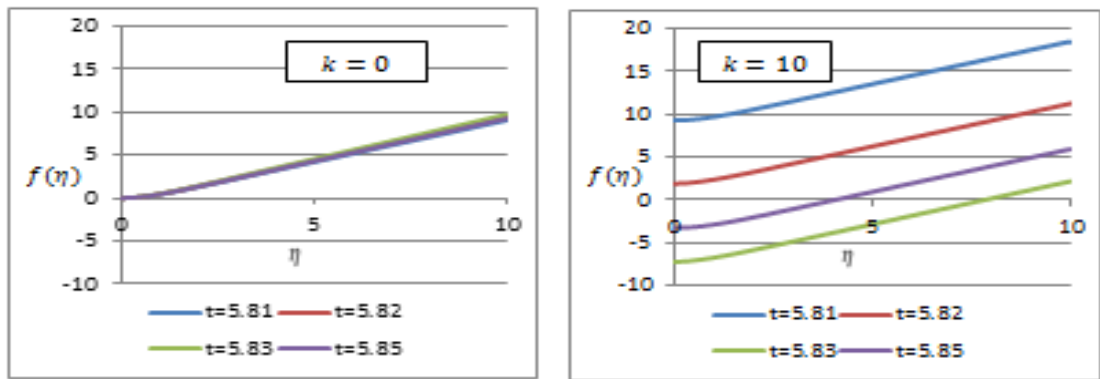


Figure (4.18): Structures of (f -profile) Under the Effect of (blowing parameter $k=60$,unsteadiness parameter $D=4$,oscillation frequency $\omega=10$ 1/s,100 1/s)respectively at different times

4.3.3: Effect of Unsteadiness Parameter On f Profiles (for specific k & ω)

By analyzing the effect of unsteadiness parameter D at specific blowing parameter $k = 30$ & oscillation frequency $\omega = 201/s$ at $t = 4.5s$ on f - profile . As shown in figure (3.24), the effect of unsteadiness parameter is very obvious at the same position η , as the unsteady parameter D is smaller, as $f(\eta)$ is greater.

Within the region closer to the wall, at the higher values of unsteadiness parameter, the flow is reversed at the specified time along the direction perpendicular to the wall.

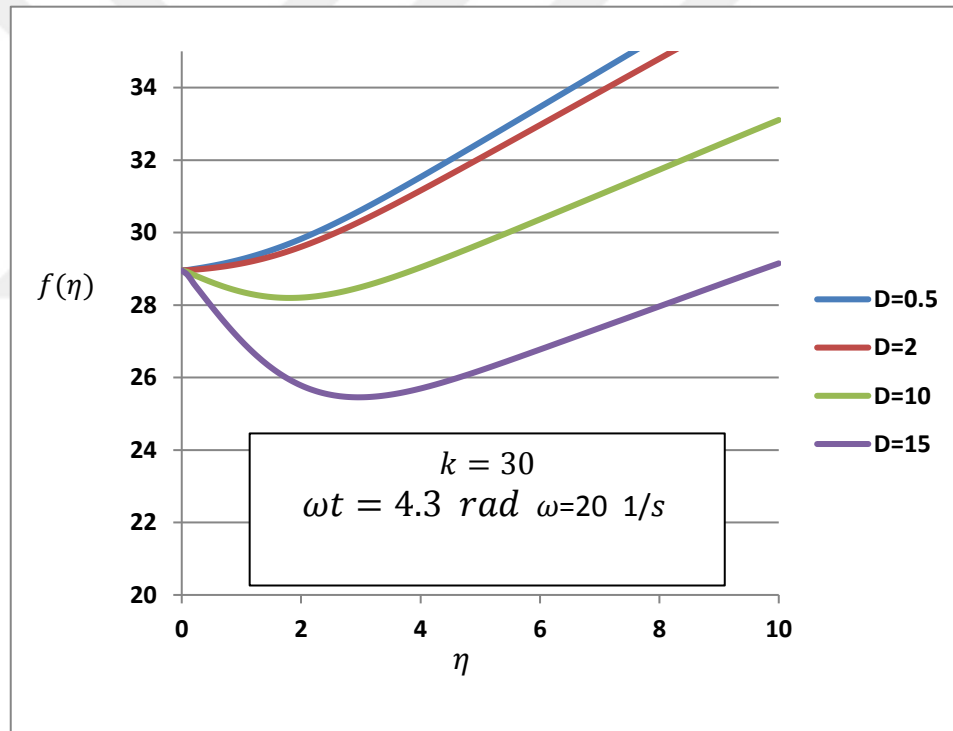


Figure (4.19): Changing of Unsteadiness Parameter D On f -Profile Structure at (blowing parameter $k=30$ oscillation frequency $\omega=20$ 1/s) at $\omega t=4.3$ rad

By comparing the effect of the oscillation frequency values at ($\omega = 20 \frac{1}{s}$ & $\omega = 50 \frac{1}{s}$, $\omega = 100 \frac{1}{s}$, $\omega = 300 \frac{1}{s}$) on $f - profile$, the following comments could be concluded:

- Flow reversibility disappears as the oscillation frequency increases. The existence of reversed flow was observed in figure (4.19) especially at $D=15$ but, as shown in figures (4.20) and (4.21) the flow is non-reversible at this case.
- The effect of unsteadiness parameter decreases as the oscillation frequency increases. This effect is very weak at ($\omega = 100 \frac{1}{s}$ & $\omega = 300 \frac{1}{s}$) as shown in figures (3.22), (3.23).

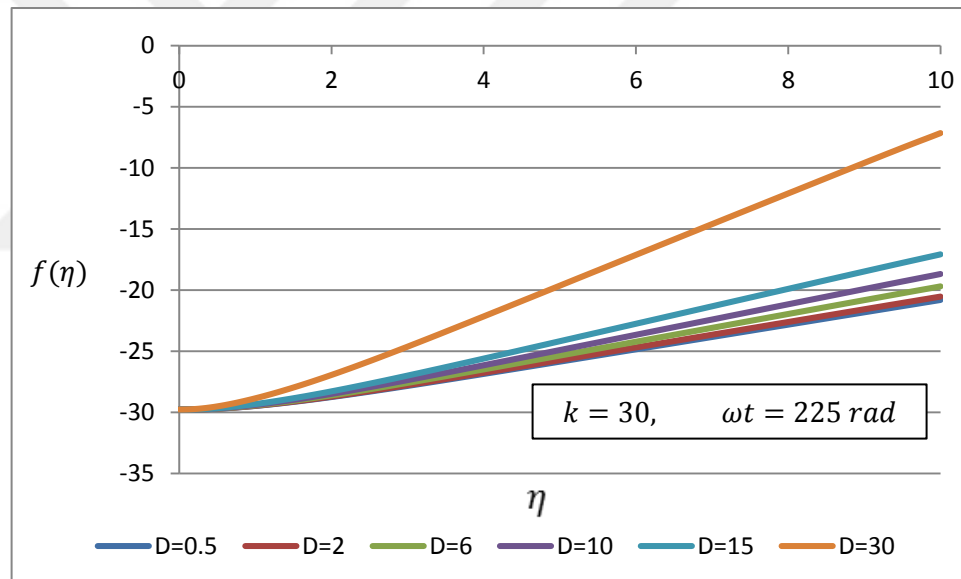


Figure (4.20): Changing of Unsteadiness Parameter D On f-Profile Structure at (blowing parameter $k=30$ oscillation frequency $\omega=50 \text{ 1/s}$) at $\omega t=5.8 \text{ rad}$

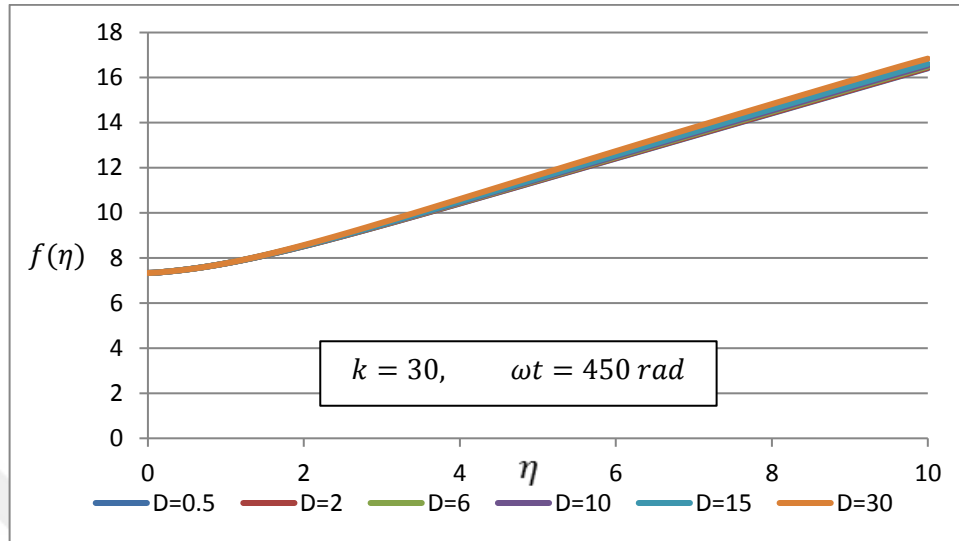


Figure (4.21): Changing of Unsteadiness Parameter D On f-Profile Structure at (blowing parameter $k=30$ scillation frequency $\omega=100$ 1/s) at $\omega t=1.62$ rad

4.4: The effect of flow parameters on f_{η} - profile

4.4.1: The effect of blowing parameter on f_{η} - profile :

What is noticeable in the case of f_{η} - profile (which refers to the velocity component along the stream-wise direction, and didn't observe in the case of f - profile (which refers to the velocity component along the vertical direction) is that sometimes under some flow parameter combinations, the existence of oscillating motion either at the surface ($\eta = 0$) or at the border of boundary layer ($\eta \rightarrow \infty$). The main parameter causes this phenomenon is the blowing parameter k .

As shown in figure (4.22), the unsteadiness parameter was selected as ($D = 4$) and the oscillation parameter ($\omega = 30$ 1/s) at a specific time ($\omega t = 4.7$ rad), an arbitrary values of blowing parameter were applied as ($k = 0, 10, 60, 160, 500$). We will discuss the effect of the blowing parameter on f_{η} - profile in two points as following:

According to our boundary conditions where at:

$$\eta \rightarrow \infty, \quad u \rightarrow a(t)$$

$$\text{where: } a(t) = \frac{A}{1 + \frac{\alpha}{\omega} \sin \omega t}$$

The velocity profile $f_\eta(\eta)$ matches the potential velocity at the edge of boundary layer. As shown in Figure (4.22), velocity profiles have different paths to match the potential flow, these paths were determined by blowing parameter under the current conditions.

It was observed that, $f_\eta(\eta)$ matches the potential flow at η further to the wall, as the blowing parameter was higher, that means the thickness of the viscous region adjacent to the wall (the boundary layer) must to be thicker.

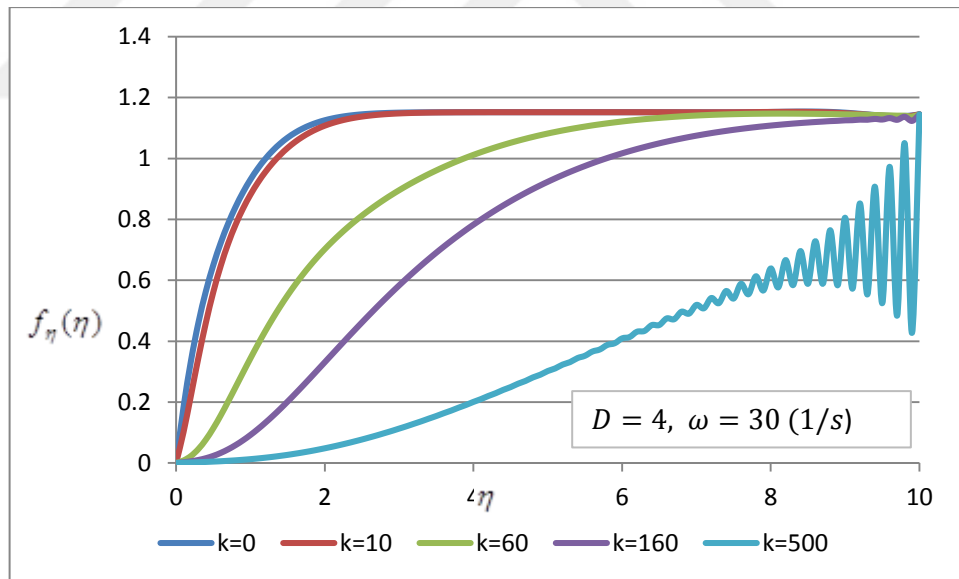


Figure (4.22): Changing of Blowing Parameter k Effect On f_η -Profile Structure at (unsteadiness parameter $D=4$, scillation frequency $\omega=30$ 1/s) at $\omega t=5.7$ rad

The existence of an oscillating motion near the wall or at the border of the viscous region in the current situation due to the increasing of the blowing parameter. As shown in figures (4.23), (4.24), (4.25) and (4.26), at time ($t = 0.5s, 3s, 7s, 10s$) for a different values k & $D = 4, \omega = 30$.

- At $k = 10$, it wasn't observed any oscillating motion. And the flow during the boundary layer matches the potential flow closer to the wall.
- At $k = 60$, small oscillations were observed near the wall (at sometimes). And the flow during the boundary layer matches the potential flow at η further than the previous case.
- At $k = 160$, higher oscillations might be observed near the wall (at sometimes).
- At $k = 500$, very high oscillations might be observed near the wall and sometimes), oscillations might be observed at the edge of boundary layer too.

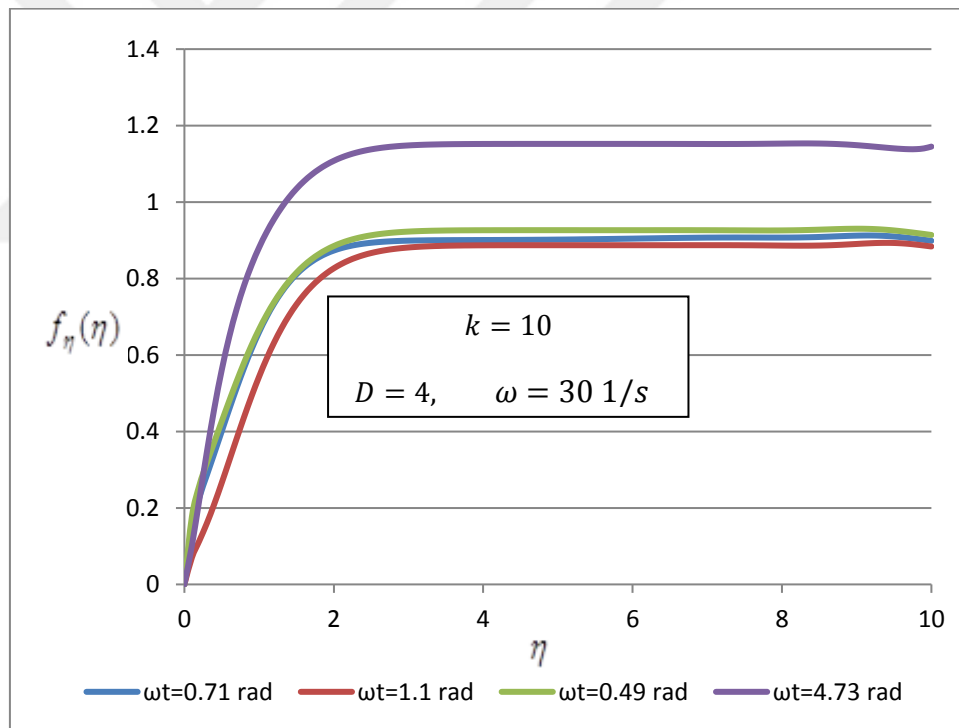


Figure (4.23): Structures of f_{η} -Profile at (blowing parameter $k=10$, unsteadiness parameter $D=4$) at different values of ωt

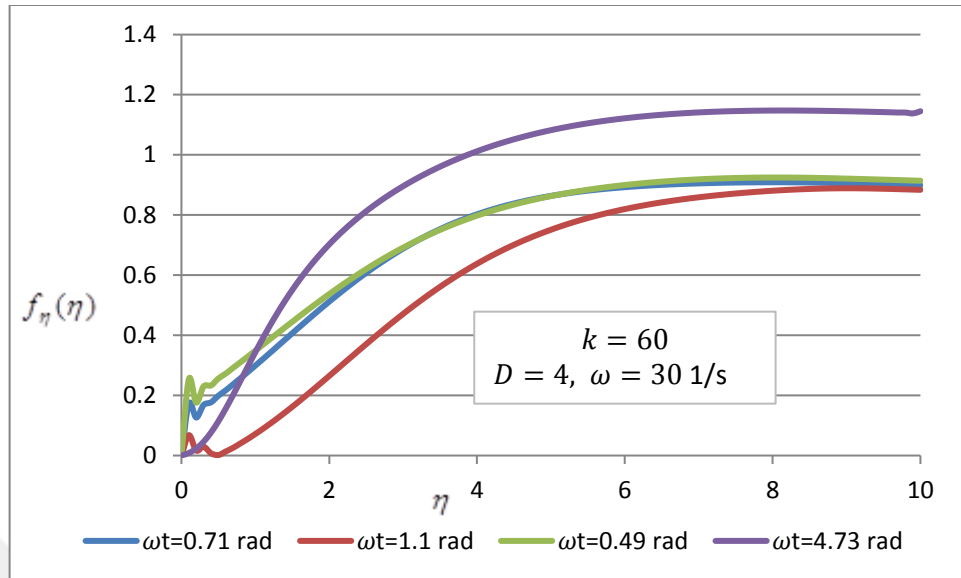


Figure (4.24): Structures of f_{η} -Profile at (blowing parameter $k=60$ unsteadiness parameter $D=4$) at different values of ωt

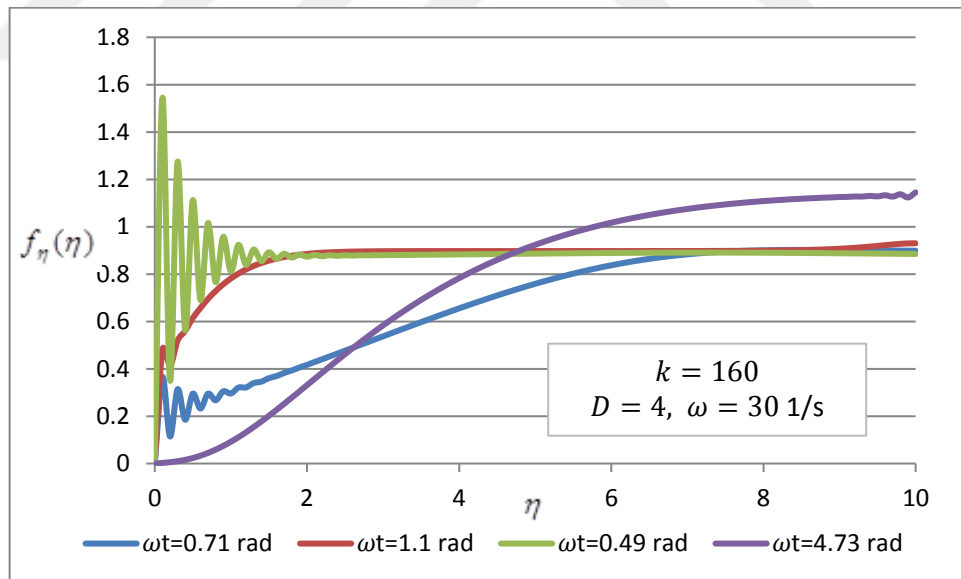


Figure (4.25): Structures of f_{η} -Profile at (blowing parameter $k=160$, unsteadiness parameter $D=4$) at different values of ωt

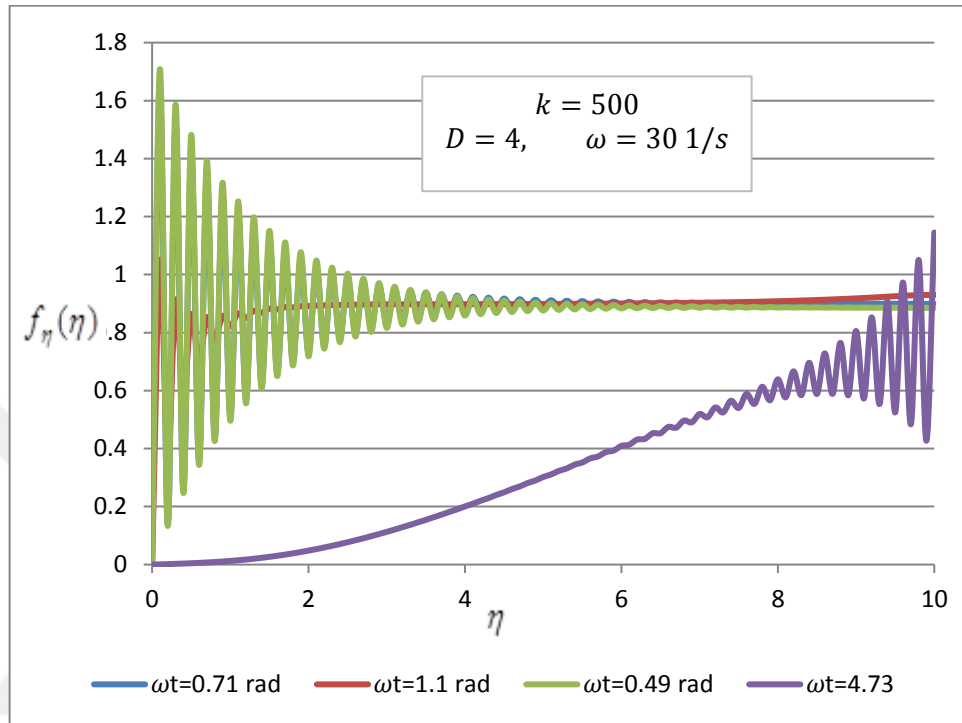


Figure (4.26): Structures of f_{η} -Profile at (blowing parameter $k=500$, unsteadiness parameter $D=4$) at different values of ωt

4.4.2: The Effect of Oscillation Frequency on f_{η} - profile :

Figure (4.27) shows the effect of oscillation frequency on f_{η} - profile for $D = 4$, $k = 60$ at different values of ωt , as shown f_{η} - profile has different structures, in general $f_{\eta}(\eta)$ takes the usual shape of f_{η} - profile sometimes, it was observed small oscillation (at flow parameters applied).

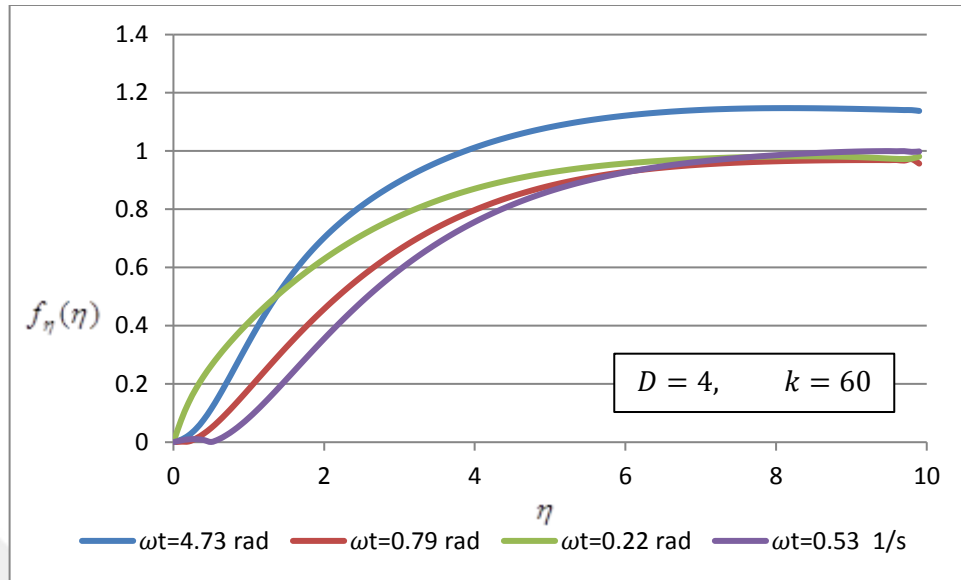


Figure (3.27): Structures of f_η -profile at (blowing parameter $k=60$, unsteadiness parameter $D=4$) at different values of ωt

In figures (4.28), (4.29), (4.30) and (4.31), it was shown some (f_η - profile) structures under the effect of changing the oscillation parameter at ($t = 0.5s, 3s, 7s, 10s$).

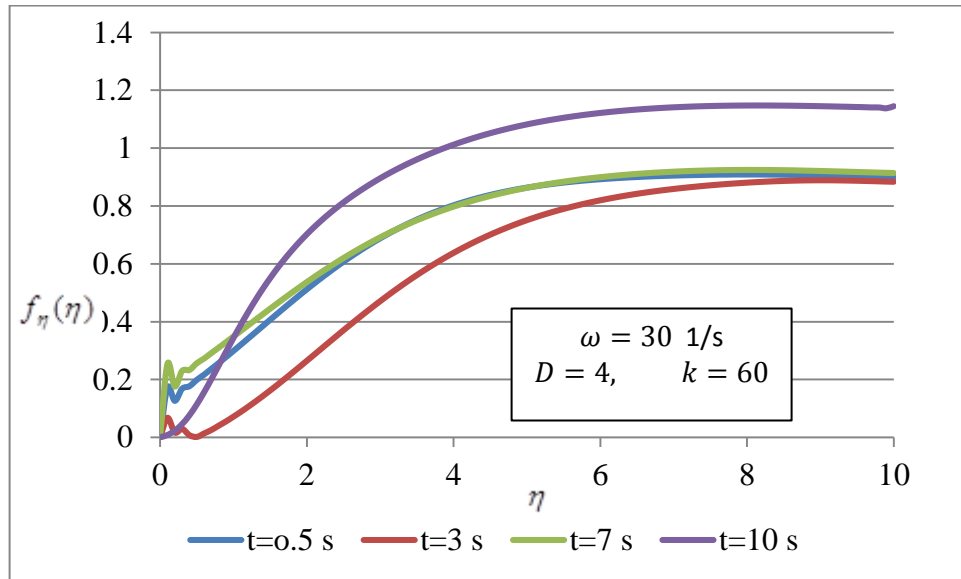


Figure (4.28): Structures of f_η -profile at (blowing parameter $k=60$, unsteadiness parameter $D=4$, oscillation frequency $\omega=30$ 1/s

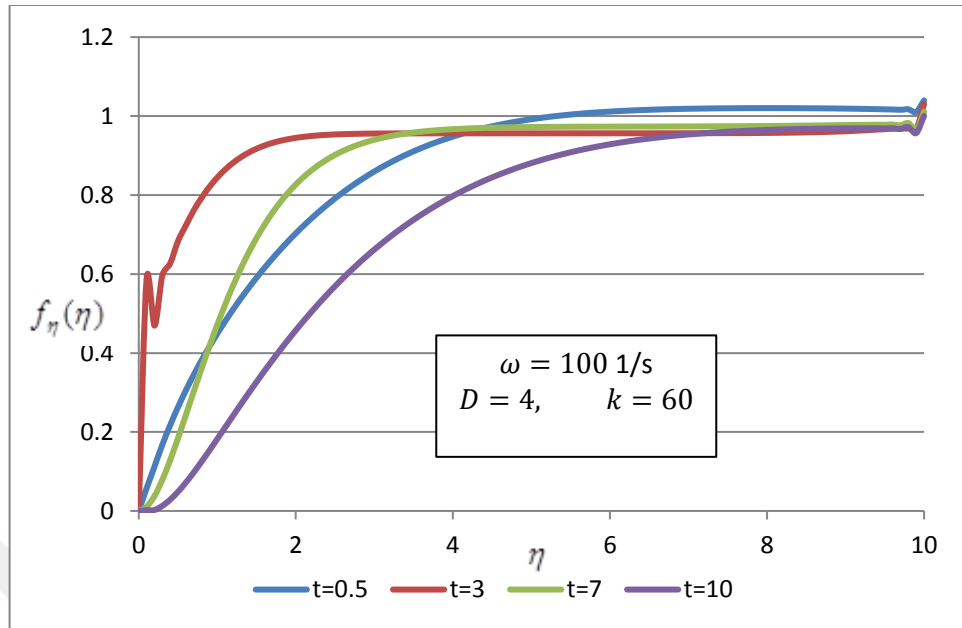


Figure (4.29): Structures of f_{η} -Profile at (blowing parameter $k=60$, unsteadiness parameter $D=4$, oscillation frequency $\omega=100$ 1/s)

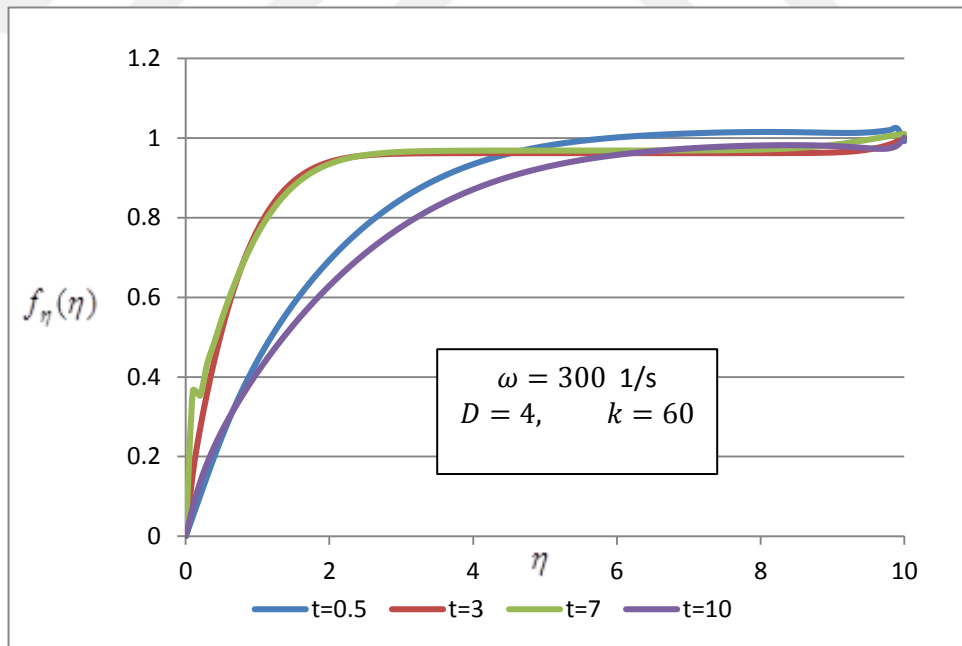


Figure (4.30): Structures of f_{η} -Profile at (blowing parameter $k=60$, unsteadiness parameter $D=4$, oscillation frequency $\omega=300$ 1/s)

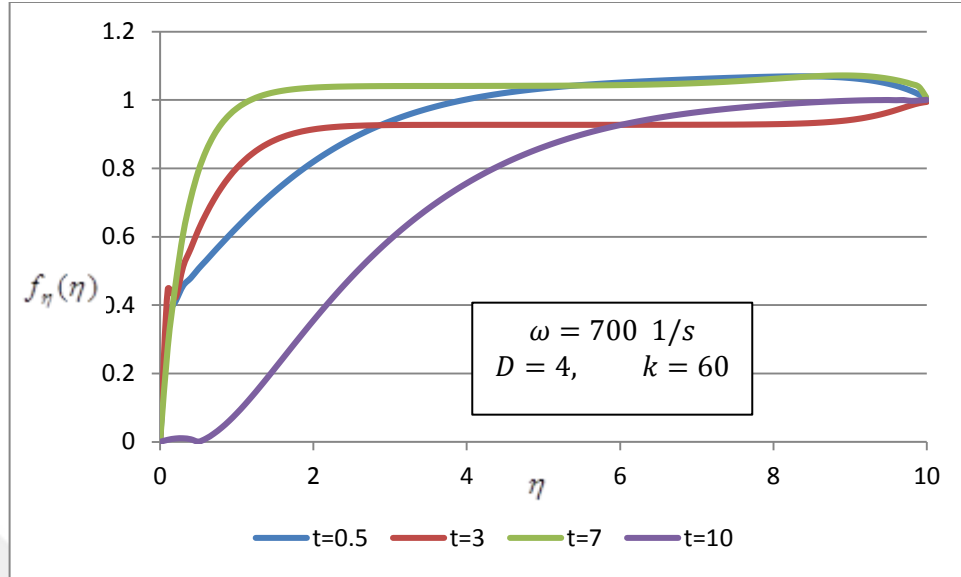


Figure (4.31): Structures of f_{η} -Profile at (blowing parameter $k=60$, unsteadiness parameter $D=4$, oscillation frequency $\omega=700$ 1/s)

4.4.3: The Effect of Unsteadiness Parameter on f_{η} - profile :

In contrast of f - profile case, the unsteadiness parameter D don't always effect on f_{η} - profile in our case of assumptions. An accurate observation was done by applying the unsteadiness parameter as ($D = 0.5, 2, 6, 10$) for $k = 60$ at different values of ωt .

Figures (4.32) and (4.33) show less effect of D on f_{η} - profile at different values of ωt . However, was to make sure that this is not always true.

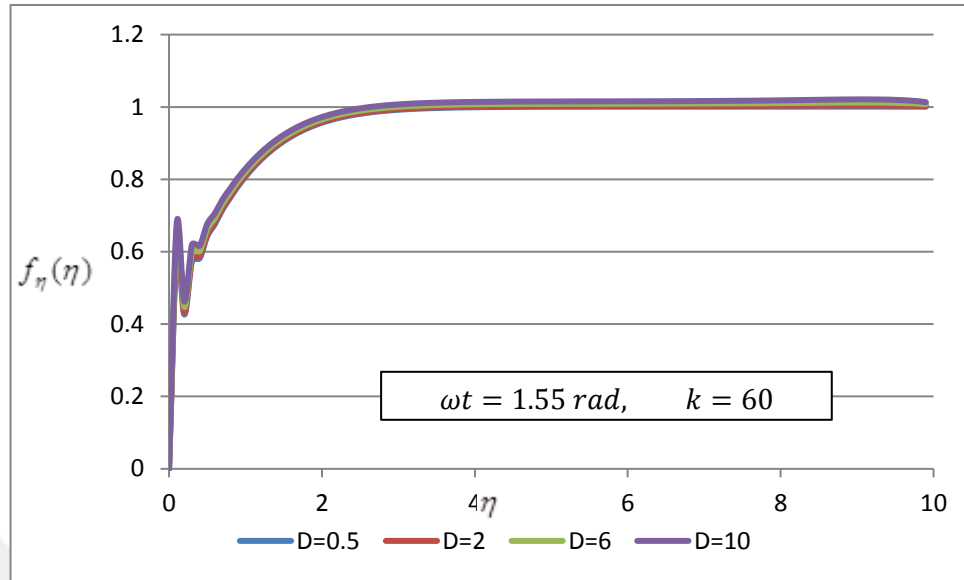


Figure (4.32): Structures of f_{η} -profile at ($\omega t=1.55 \text{ rad}$) and (blowing parameter $k=60$, oscillation frequency $\omega=160 \text{ 1/s}$) at different values of unsteadiness parameter D

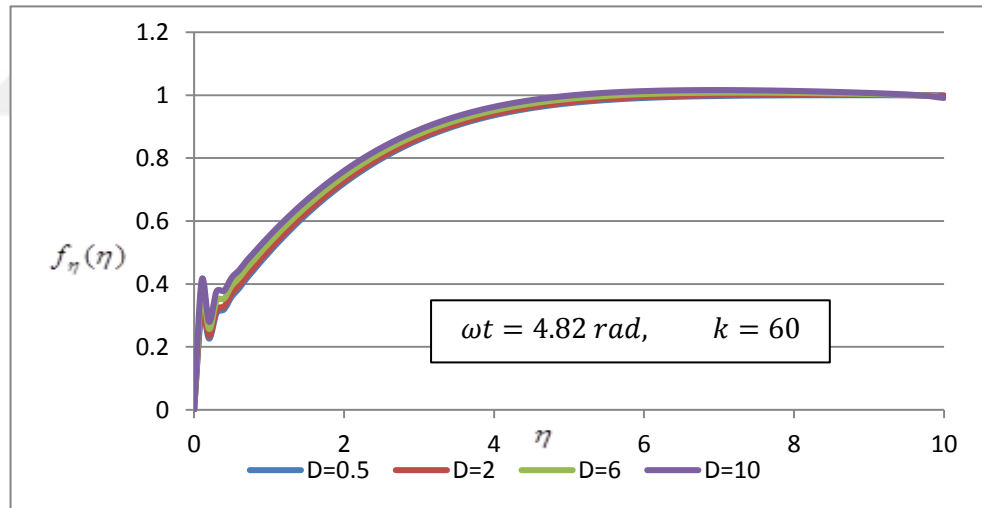


Figure (4.33): Structures of f_{η} -profile at ($\omega t=4.82 \text{ rad}$) and (blowing parameter $k=60$, oscillation frequency $\omega=160 \text{ 1/s}$) at different values of unsteadiness parameter D

Figures (4.34) and (4.35) show a different structure of f_{η} -profile at (blowing parameter $k=60$ oscillation frequency $\omega=160 \text{ 1/s}$) where, unsteadiness parameter at $D=0.5$ and $D=2$ respectively t different time scales.

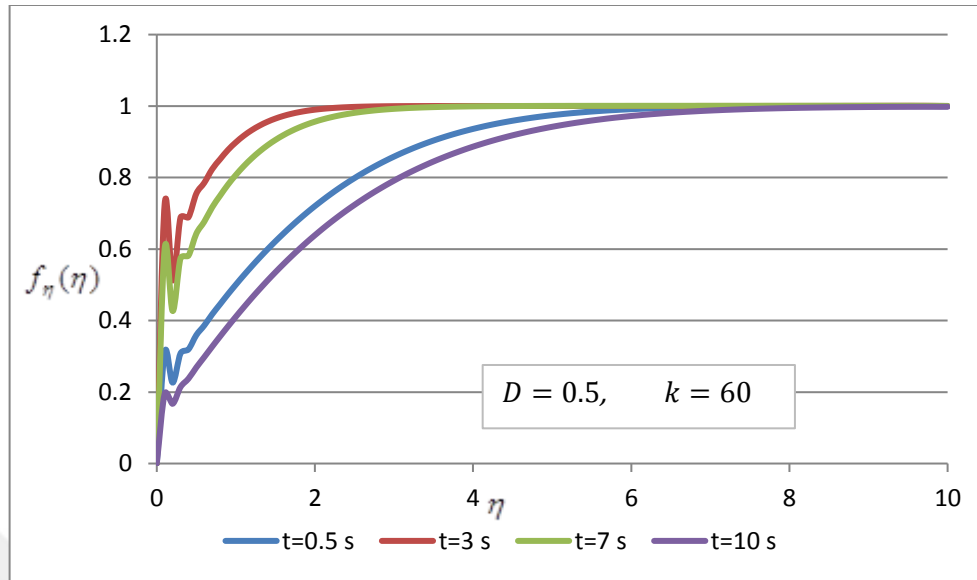


Figure (4.34): Structures of f_{η} -profile at (blowing parameter $k=60$, unsteadiness parameter $D=0.5$, oscillation frequency $\omega=160$ 1/s), at different times

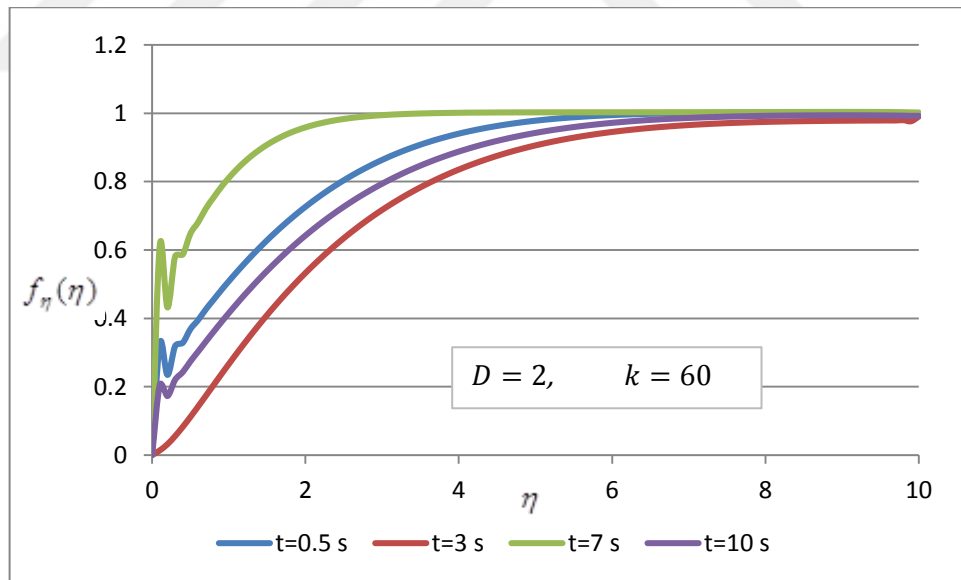


Figure (4.35): Structures of f_{η} -profile at (blowing parameter $k=60$, unsteadiness parameter $D=2$, oscillation frequency $\omega=160$ 1/s), at different times.

4.5: The Effect of Flow Parameters on $f_{\eta\eta}$ - profile

The importance of studying $f_{\eta\eta}$ - profile behavior relates to the fact that it represents the rate of change of f_{η} - profile which refers to stream-wise velocity component through the boundary layer.

The sign of $f_{\eta\eta}$ - profile at any η refers to the direction of u - velocity at that position. We talked about this issue in details in section (4.3).

The second benefit is that $f_{\eta\eta}$ - profile behavior refers to the shear stress distribution within the boundary layer.

In next sections, the effect of the flow parameters was discussed.

4.5.1: The Effect of Blowing Parameter on $f_{\eta\eta}$ - profile

The influence of blowing parameter was studied by applying the flow parameters at $t = 4.5$ s where, $\omega = 4$ & $\omega = 60$ 1/s .

Blowing parameter had the values of $k = 0, 20, 60, 120$. The observed results can be summarized as following:

- At the given time and parameters, shear stress is maximum at $k = 0$. And then, as k increases, $f_{\eta\eta}(\eta)_{max}$ goes inside the boundary layer. For example, as shown in figure (4.43).
- It is obvious from figure (4.36) that as blowing parameter k increases $f_{\eta\eta}(\eta)_{max}$ decreases.

These results led us to study the effect of blowing parameter at higher frequency, all parameters were maintained at the previous values unless oscillation frequency became as $\omega = 300$ 1/s. As shown in figure (4.36) maximum value of shear stress is very close to the wall. This contrasts with what was in the case of $\omega = 60$ 1/s.

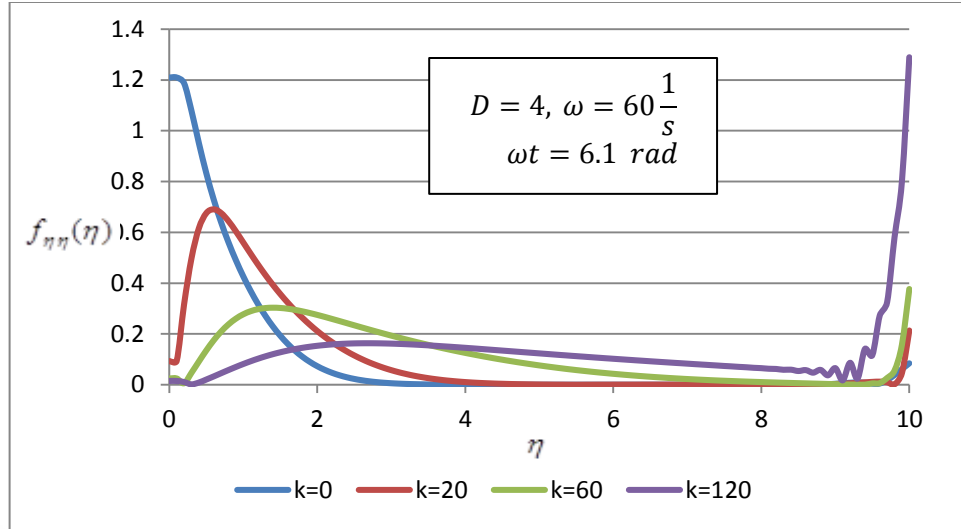


Figure (4.36): Structures of $f_{\eta\eta}$ -profile at (unsteadiness parameter $D=4$, oscillation frequency $\omega=60$ 1/s), at different values of blowing parameter.

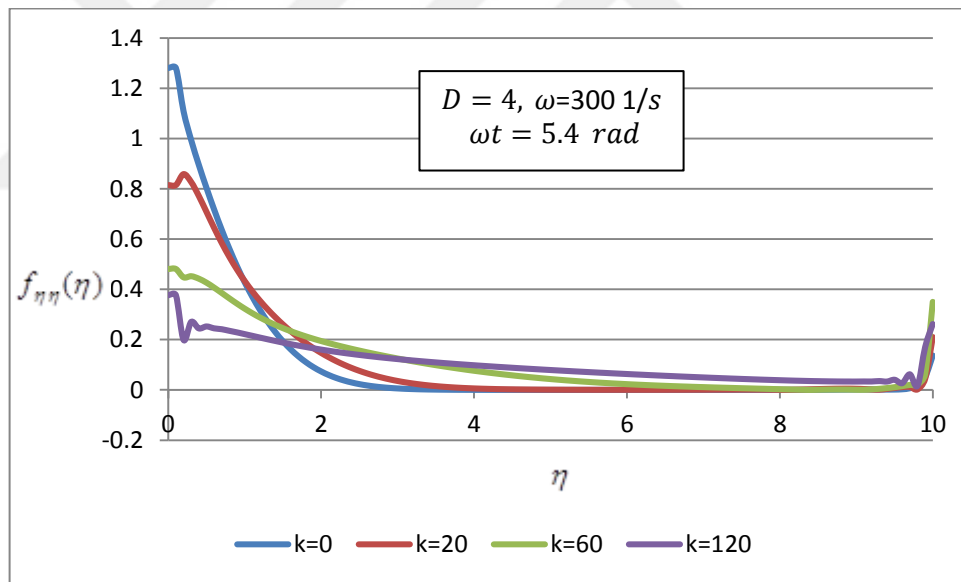


Figure (4.37): Structures of $f_{\eta\eta}$ -profile at (unsteadiness parameter $D=4$, oscillation frequency $\omega=300$ 1/s), at different values of blowing parameter.

By observing figures (4.36) and (4.37), it was observed that at low values of blowing parameter the flow during the boundary layer matches the potential flow closer to the wall which means that the boundary layer thickness is thinner as the blowing parameter is smaller. Figure (4.36) shows that at $k = 0, k = 20$ the flow matches during

the range of $\eta = 2$ to $\eta = 4$, at $k = 60$ the flow matches during the range of $\eta = 6$ to $\eta = 8$, and

it was interesting to observe the effect of applying a higher blowing parameter for example at $k = 300$ by applying the same flow parameters and at the same time.

Relatively, observed a higher oscillation comparing with the previous cases. These oscillations sometimes occur near the wall then transfers to the border or boundary layer.

As shown in figures (4.38) and (4.39) a $t = 4.5$ s, $k = 300$, $D = 4$ the maximum wall shear at ($\omega=30$), after that as (ω increases) as the oscillation amplitude becomes smaller. Figure (4.38) shows at $\omega = 10$ 1/s, the flow during the boundary layer matches the potential flow at $\eta = 2$, continued stable to $\eta = 10$. While at $\omega = 60$ 1/s, $f_{\eta\eta}(\eta) \approx 0$ during the interval $[0 \leq \eta \leq 8]$ and oscillated at $\eta > 8$.

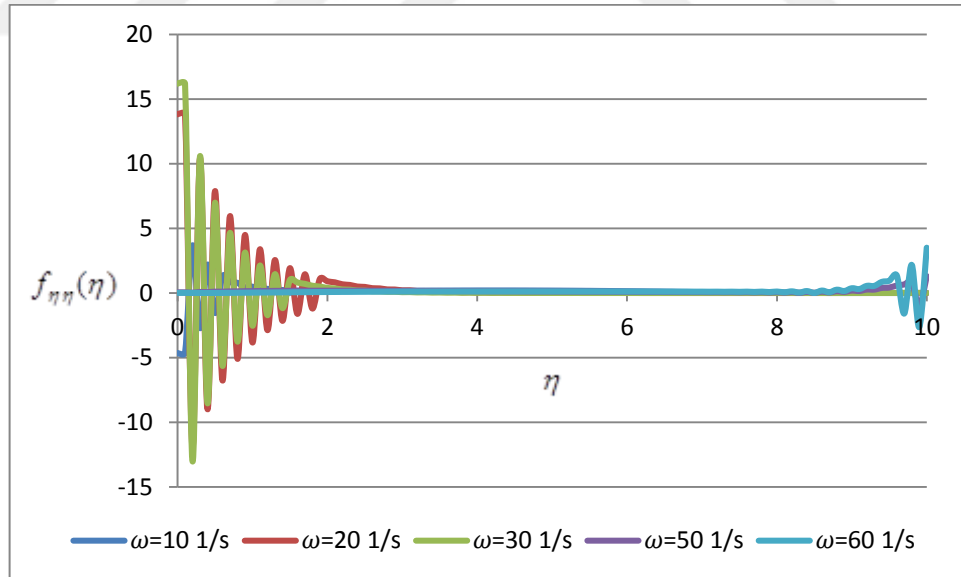


Figure (4.38): Structures of $f_{\eta\eta}$ -profile at (unsteadiness parameter $D=4$, blowing parameter=300, at different values of oscillation frequency ω).

Figure (4.39) shows at $\omega = 120$ 1/s and $\omega = 300$ 1/s, small oscillation with comparing with the previous cases, near the wall and at the potential flow.

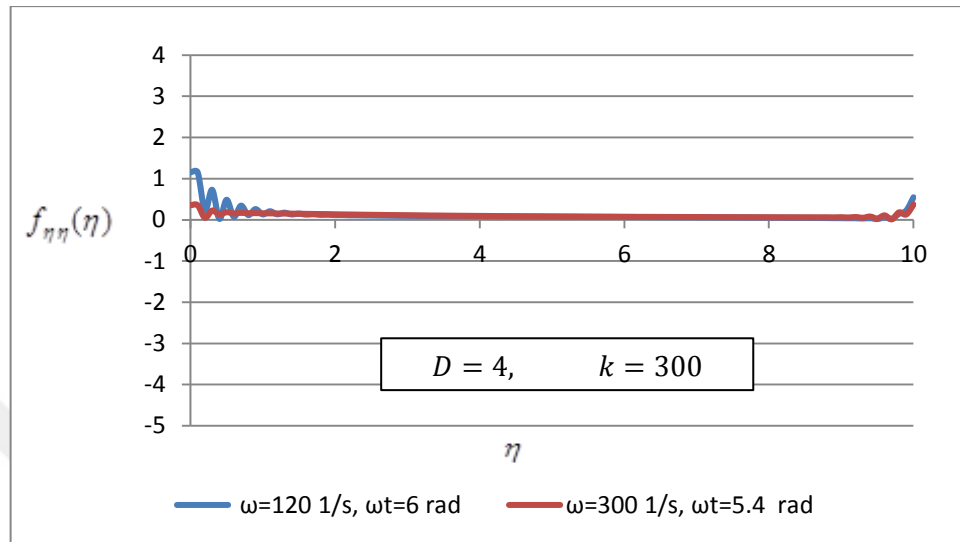


Figure (4.39): Structures of $f_{\eta\eta}$ -profile at (unsteadiness parameter $D=4$, oscillation frequency $\omega=300$ 1/s) , at different values of blowing parameter.

4.5.2: The Effect of Oscillation Frequency on $f_{\eta\eta}$ - profile

The influence of oscillation frequency ω were observed in the range of $\omega = (5 \text{ to } 200)$ 1/s at: $t = 4.5s$ for unsteadiness parameter $D = 4$ and blowing parameter $k = 60$.

From figures (4.40) and (4.41) the following could be deduced:

- At specific times, maximum shear stress can exist within the boundary layer, for example, as shown in figure (4.40).
- At $t = 4.5s$ it is obvious that maximum shear stress decreases and goes further inside the boundary layer as the oscillation frequency ω increases at the same unsteadiness and blowing parameters.
- On the other hand, at the same time, it was observed that the maximum shear stress has a maximum value at the wall for example, as shown in figures (4.41).

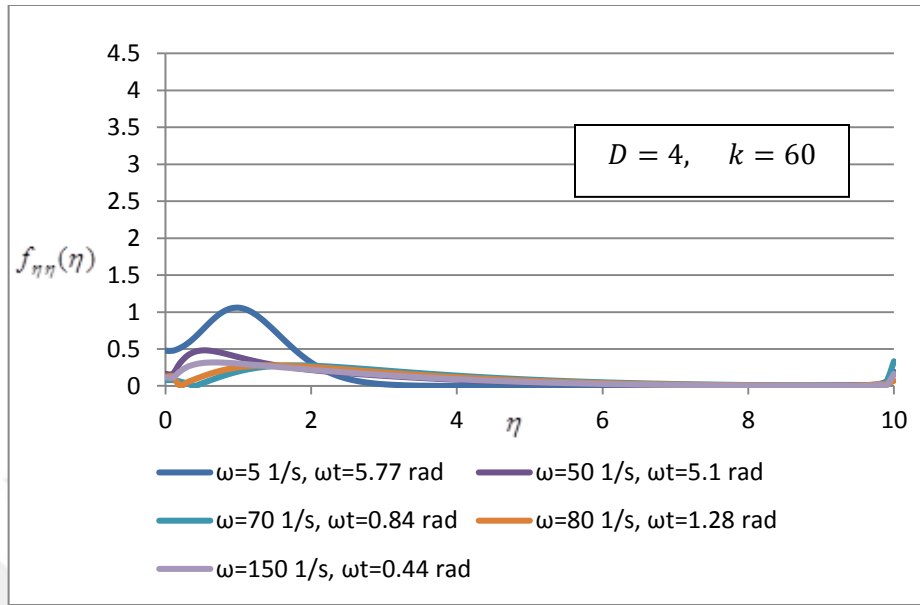


Figure (4.40): Structures of $f_{\eta\eta}$ -profile at (unsteadiness parameter $D=4$, blowing parameter $k=60$) at different values of oscillation frequency ($\omega=5,50,70,80,150$ 1/s)

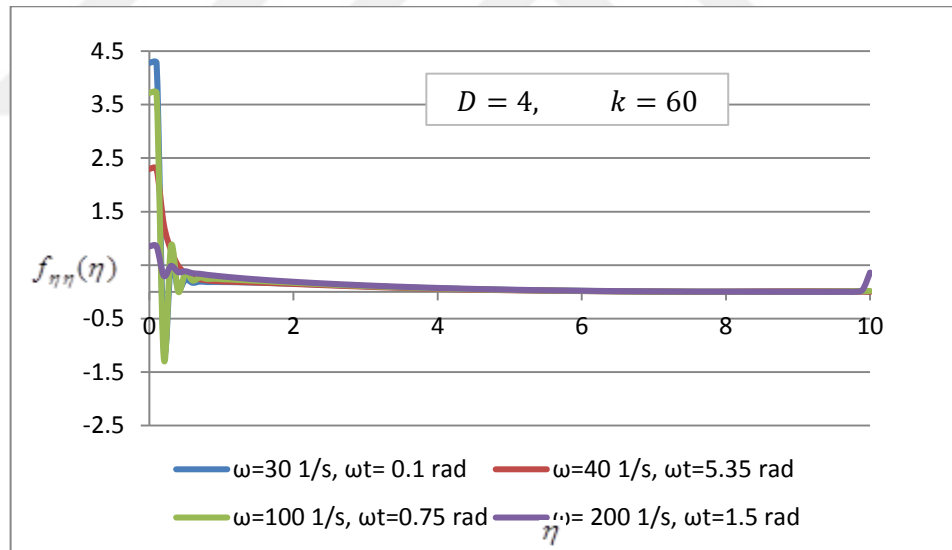


Figure (4.41): Structures of $f_{\eta\eta}$ -profile at (unsteadiness parameter $D=4$, blowing parameter $k=60$) at different values of oscillation frequency ($\omega=30,40,100,200$ 1/s)

4.5.3: The Effect of the Unsteadiness Parameter on $f_{\eta\eta}$ - profile

- At the lower values of ω , the maximum shear stress may be move inside the boundary layer at specific time.
- As the oscillation frequency increases, the maximum shear stress becomes closer to the wall.
- The effect of changing of unsteadiness parameter, is more obvious at low frequency values, as shown in figure (3.42), for $\omega = 50 \text{ 1/s}$, the effect of unsteadiness parameter change seems obvious in values of $f_{\eta\eta}(0)$ & $f_{\eta\eta}(\eta)_{\max}$. Before $\eta \approx 4$ the effect of unsteadiness parameter change can be seen.

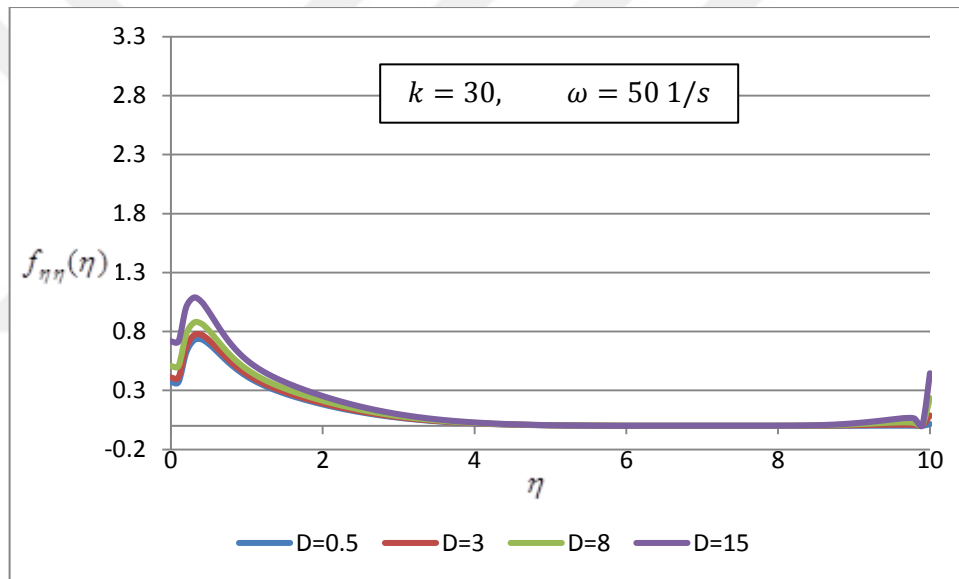


Figure (4.42): Structures of $f_{\eta\eta}$ -profile at (blowing parameter $k=60$, oscillation frequency $\omega=50 \text{ 1/s}$) at different values of unsteadiness parameter D

- For all the chosen values of ω , as shown in figures (4.43), (4.44) and (4.45), it is possible to say: from $\eta \approx 4$ to $\eta \approx 10 \rightarrow f_{\eta\eta}(\eta) \approx 0$, at $\eta \approx 10$ the flow was disturbed again.
- When the change of ω is in the range of $\omega \approx (100 - 260) \text{ 1/s}$, the effect of unsteadiness parameter change is almost nonexistent, this situation still exist for $\omega \geq 200 \text{ 1/s}$ unless at $\eta \approx 0$ where, as shown in figure(4.45), $f_{\eta\eta}(0)$ is dependent on the unsteadiness parameter D .

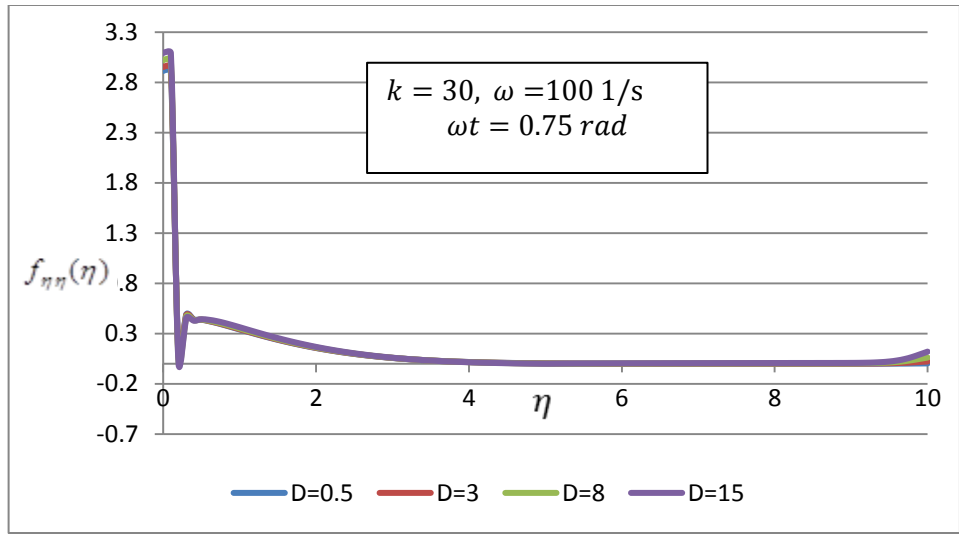


Figure (4.43): Structures of $f_{\eta\eta}$ -profile at (blowing parameter $k=60$, oscillation frequency $\omega=100$ 1/s) at different values of unsteadiness parameter D

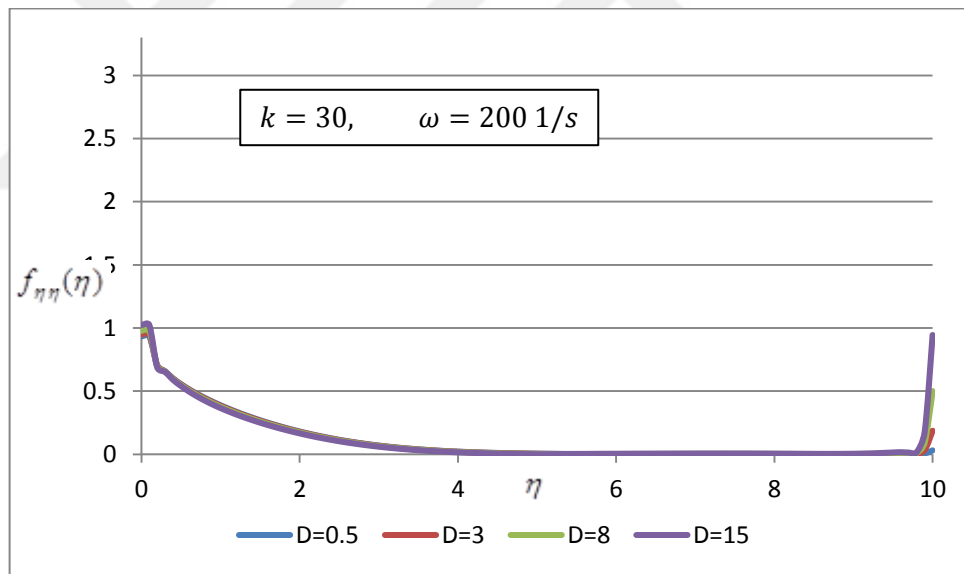


Figure (4.44): Structures of $f_{\eta\eta}$ -profile at (blowing parameter $k=60$, oscillation frequency $\omega=200$ 1/s) at different values of unsteadiness parameter D

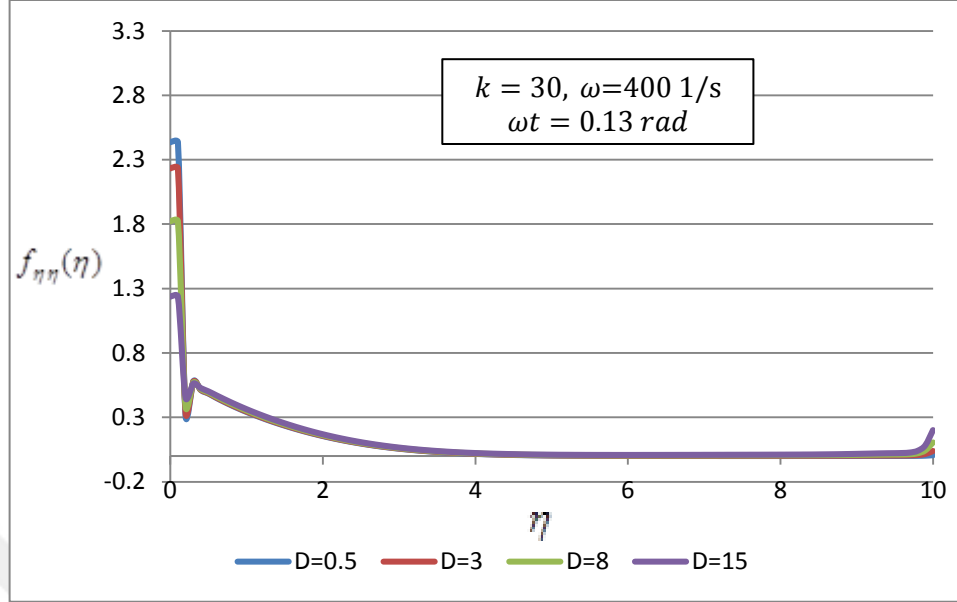


Figure (4.45): Structures of $f_{\eta\eta}$ -profile at (blowing parameter $k=30$, oscillation frequency $\omega=400$ 1/s) at different values of unsteadiness parameter D

4.6: Effect of Low Parameters on Wall Shear Stress τ_{wall}

According to our assumptions, $f_{\eta\eta}(\eta)$ is the similarity function refers to the shear stress distribution within the boundary layer, since:

$$\begin{aligned}\tau &= \mu \frac{\partial u}{\partial y} \\ &= \mu \left(\frac{\partial u}{\partial \eta} \right) \left(\frac{\partial \eta}{\partial y} \right)\end{aligned}$$

$$\begin{aligned}\text{from our assumptions: } \frac{\partial u}{\partial \eta} &= Ax f_{\eta}(\eta) \text{ \& } \frac{\partial \eta}{\partial y} = \sqrt{\frac{A}{\mu}} \\ \tau &\propto f_{\eta\eta}(\eta)\end{aligned}$$

In the following sections we will discuss the results considering the influence of flow parameters on shear stress within the boundary layer.

4.6.1: Effect of Blowing Parameter on the Wall Shear Stress

The following table includes the maximum values of $f_{\eta\eta}(\eta)$ which was found within a period of time don't exceed 0.6 second from the beginning of the unsteady

motion, in table (4.6) were included the time at which $f_{\eta\eta}(\eta)$ has a maximum value at ($D = 2, k = 10, 50, 100, 200$). As it was mentioned in sec (4.5), and shown in figures (4.36), (4.40), (3.42), the maximum shear stress may be exist inside the viscous boundary layer if k & ω don't exceed specific values. But for higher values maximum shear stress exist at the wall (at $\eta \approx 0$). These values were searched to correspond the value of $D = 2$, and various values of k & ω . These values were plotted in Figure (4.46). Associating to Figure (4.46), it could to be commented the following:

- Maximum $f_{\eta\eta}(\eta)$ increases with blowing parameter k .
- For each k value, $f_{\eta\eta}(\eta)$ increases rapidly to its maximum value, corresponds to a specific value of the oscillation parameter at $\omega = \omega$ where ω within the range of $[30 - 70] 1/s$.
- $f_{\eta\eta}(\eta)$ decreases during the range $\omega \approx [70 - 300] 1/s$, to goes almost constantly after $\omega \geq 300 1/s$.

Table (4.6): Maximum Values of $f_{\eta\eta} - profile$ Indicates Maximum Shear stress $f_{\eta\eta}(\eta)_{max}$. vs. oscillation frequency ω at different values of *BL*owing parameter k at unsteadiness parameter $D = 2$

ω ($1/s$)	$f_{\eta\eta}(\eta)_{max}$ at $D = 2$, within 0.6 s			
	(k=200)	(k=100)	(k=50)	(k=10)
1	9.258861	7.299397	8.337737	
5	14.12924	12.33942	10.30847	4.717446
10	15.61116	14.06375	11.86223	5.029949
20	16.77482	15.15149	12.77014	4.470926
30	17.20849	15.50646	12.72162	3.952873
40	17.41046	15.59892	12.29333	3.577264
70	17.42147	14.83062	10.56896	2.859268
100	16.72094	13.42369	8.950562	2.508152
200	13.28164	9.575809	5.944116	1.977901
300	7.475956	5.844906	4.210639	1.726169
400	7.604838	5.611407	3.692614	1.57697
500	7.696629	5.881554	4.027748	1.657984

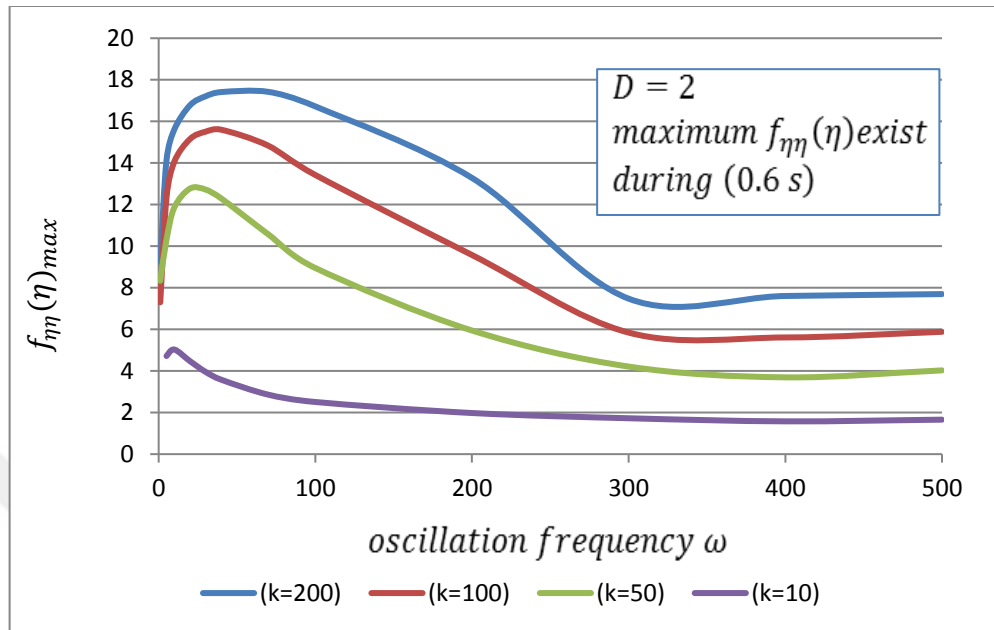


Figure (4.46): Maximum Values of $f_{\eta\eta}$ -profile Indicates Maximum Shear Stress $f_{\eta\eta}(\eta)_{max}$ vs. oscillation frequency ω at different values of blowing parameter k at unsteadiness parameter $D=2$

4.6.2: Effect of Unsteadiness Parameter on the Shear Stress

In the previous section, the effect of the blowing parameter on the shear stress was discussed, in this section we'll discuss the effect of the unsteadiness parameter on $f_{\eta\eta}(\eta)_{max}$, at $k = 100$.

Associating to table (4.7) and figure (4.47), it could to be comment the following:

- Maximum $f_{\eta\eta}(\eta)$ decreases with the increasing of the unsteadiness parameter D .
- For each D , $f_{\eta\eta}(\eta)$ increases rapidly to its maximum value, corresponds to a specific value of the oscillation parameter at $\omega = \omega$ where ω within the range of $[30 - 40] 1/s$.
- $f_{\eta\eta}(\eta)$ decreases during the range of $\omega \approx [40 - 300] 1/s$, to goes almost constantly after $\omega \geq 300 1/s$.

- $f_{\eta\eta}(\eta)_{max}$. is almost the same in the range of $\omega \approx [100 - 300]$ $1/s$, so the effect of D is absent.
- As shown in table (4.7), at values of $D \geq 8$, corresponding the values of $\omega \leq 10$ $1/s$, $f_{\eta\eta}(\eta)_{max} \rightarrow \infty$.

Table (4.7): Maximum Shear Stress $f_{\eta\eta}(\eta)_{max}$. vs. Oscillation Frequency ω , blowing parameter $k = 100$ at at different values of unsteadiness parameter D

ω ($1/s$)	$f_{\eta\eta}(\eta)_{max}$. at $k = 100$					
	D=0.5	D=2	D=4	D=6	D=8	D=10
1	11.57255	7.299397	5.174363	3.967744	diverge	diverge
5	15.14843	12.33942	10.58405	9.544457	diverge	diverge
10	15.86737	14.06375	12.62341	11.73697	11.10935	diverge
20	16.20153	15.15149	14.16732	13.50914	13.01286	12.66048
30	16.22204	15.50646	14.80039	14.23102	13.83276	13.44041
40	16.02257	15.59892	15.04938	14.63641	14.37666	14.11536
70	14.951	14.83062	14.66735	14.50092	14.33132	14.15852
100	13.4547	13.42369	13.38082	13.33619	13.28975	13.24147
200	9.537017	9.575809	9.629546	9.68594	9.745383	9.808267
300	5.97941	5.844906	5.677917	5.540308	5.389138	5.287292
400	5.830675	5.611407	5.317554	5.021995	4.72474	4.425796
500	6.104455	5.881554	5.584054	5.286202	4.98799	4.689408

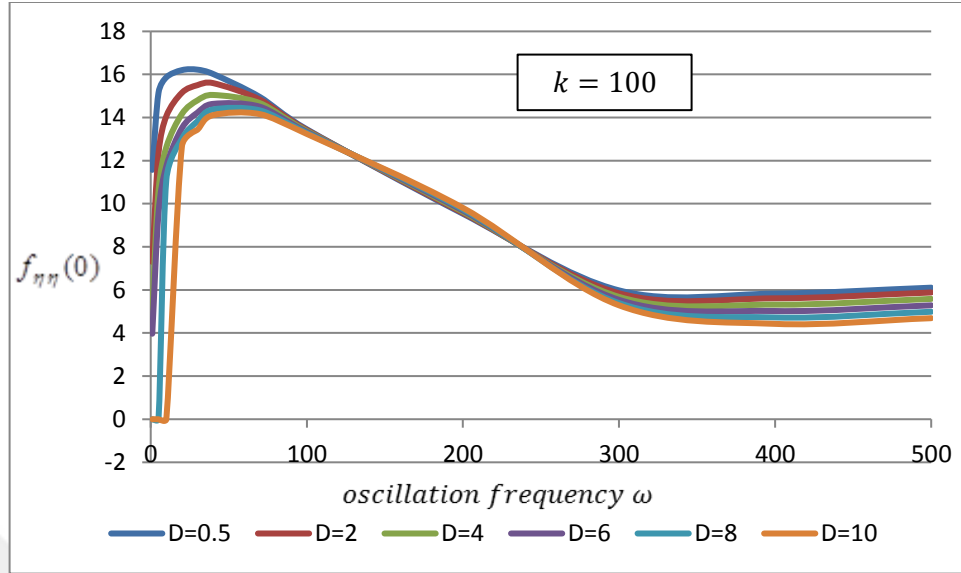


Figure (4.47): Maximum values of $f_{\eta\eta}$ -profile Indicates Maximum Shear Stress $F_{\eta\eta}(\eta)_{(max.)}$ vs. Oscillation Frequency ω , Blowing Parameter $k=100$ at at Different Values of Unsteadiness Parameter D

4.6.3: The Observation of the Time of Maximum Shear Stress

It was interesting to determine the time at which $f_{\eta\eta}(\eta)_{max.}$ occurs, this critical time changes according to flow parameters changing, so table (4.7) and figure (4.54) are valid only for the corresponding flow parameters' values. It was selected for $k = 100$, the unsteadiness parameter values as $(D = 0.5, 2, 6, 10)$ and $(from 5 to 700 \frac{1}{s})$. By analyzing the data installed in table (4.8), it could be comment that:

- The time at which $f_{\eta\eta}(\eta)_{max.}$ exists, occurs earlier if D was smaller.
- As the oscillation frequency becomes higher, $f_{\eta\eta}(\eta)_{max.}$ occurs earlier.
- For the considered range of ω values, the maximum time that $f_{\eta\eta}(\eta)$ can take to reach its highest value is $t = 0.6s$ at $\omega = 5 \frac{1}{s}, D = 2, k = 100$. Table (4.8): the time at which
- the previous results were illustrated in figure (4.48).

Table(4.8): $f_{\eta\eta}$ – profile Maximum Value Occurrence Time vs. Oscillation frequency ω , blowing parameter $k = 100$ at at Different Values of unsteadiness parameter D

oscillation frequency ω	time [$f_{\eta\eta}(\eta)_{max.}$] at $k = 100$			
	D=0.5	D=2	D=6	D=10
5	0.35	0.5	0.57	0.6
10	0.19	0.19	0.28	0.3
20	0.1	0.12	0.14	0.15
30	0.08	0.08	0.08	0.1
40	0.07	0.07	0.08	0.08
60	0.05	0.06	0.06	0.06
80	0.05	0.05	0.05	0.05
90	0.04	0.04	0.04	0.04
100	0.04	0.04	0.04	0.04
104	0.04	0.04	0.04	0.04
110	0.04	0.04	0.04	0.04
120	0.04	0.04	0.04	0.04
140	0.03	0.03	0.03	0.03
160	0.03	0.03	0.03	0.03
200	0.03	0.03	0.03	0.03

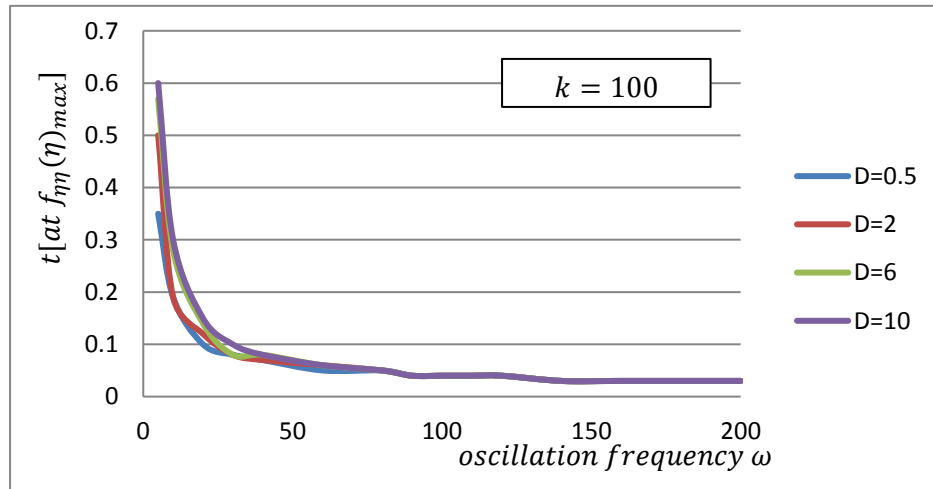


Figure (4.48): The Time at which $f_{\eta\eta}$ -profile Maximum Value Occurs vs. Oscillation Frequency ω , Blowing Parameter $k=100$ at at Different Values of Unsteadiness Parameter D

Chapter 5

Conclusion and Future Work

5.1 Concluding Remarks:

The study has interested on oscillatory stagnation point flows. The problem comprised an unsteady oscillating motion at the potential flow with a periodic flow motion through the wall surface. This problem was a generalization of the problem that previously addressed by Blyth and Hall (2003). The oscillatory stagnation point flows problem was analyzed by many researchers, such as Merchant and Davis (1989). They showed that for a high oscillation frequency value, it is found a critical oscillation dimensionless amplitude, above which equations can't be solved. The mentioned study promoted Blyth and Hall (2003) to address the problem and concluded that above the critical relative amplitude equations blow-up at a finite time singularity. In current study we assume a specific unsteady function at the far-field flow and an unsteady blowing/suction at the surface. It was interesting in analysis finding that the solutions below a critical value of oscillation parameter break down at a finite time. According to our assumptions, for each determined value of the unsteadiness parameter, the critical value of oscillation parameter approximately constant with changing of the blowing parameter. So, we could consider a border line separates to regions of flow parameters, the region above the line refers to the flow parameters leading to a regular or stable flow motion, while the region below the line refers to the flow parameters leading to unstable flow motion where the flow break down at a finite time.

In chapter 3, a mathematical model in a form of a non-linear partial similarity differential equation with boundary conditions was done, it was derived from Navier-Stoke's equations in a two-dimensional version.

The effect of change of flow parameters on the boundary layer characteristics was addressed in chapter 4.

It was observed that, the change of the blowing parameter k doesn't effect on flow stability or un-stability, while, for a specific blowing parameter and a specific unsteadiness parameter, there exists a critical oscillation dimensionless frequency, under which, no solutions was found.

the effect of the unsteadiness parameter and the oscillation frequency was as following:

At: $D = 2$ the flow profiles are periodic for $\omega \geq 2 \left(\frac{1}{5}\right)$

At: $D = 4$ the flow profiles are periodic for $\omega \geq 5 \left(\frac{1}{5}\right)$

At: $D = 6$ the flow profiles are periodic for $\omega \geq 8 \left(\frac{1}{5}\right)$

And so on, as the unsteadiness parameter increases, the oscillation frequency must increase to maintain the boundary layer profiles in a periodic structure.

At: $D \leq 1$, the boundary layer profiles always periodic regardless of the change of flow parameters.

It was observed that the flow at a specific value of the unsteadiness parameter where $D > 1$ can be non-reversed at the surface all the time if $\omega \geq \omega^*$. At $D > 1$ & $\omega \geq \omega^*$ the flow becomes reversed at definite period of time.

At the values of $D \leq 1$ the flow at the wall is non-reversed all the time regardless of the value of ω .

5.2 Further work

As mentioned, the purpose of this thesis is a generalization of the problem of Blyth and Hall (2003), the case considered was adding an unsteady motion to the potential flow with the presentence of periodic motion at the wall. In fact, our model allows adding any type of unsteady motion either through the wall or at the far-field stream. In addition, the problem can be developed to be three-dimensional case. So, we recommend the following researchers who interest the area of stagnation point flows, applying different assumptions for the same problem to compare the effect of flow parameters on the boundary layer characteristic discussed in our study.

References

Cheng, E.H.W., Ozisik, M.N. and Williams, J.C , (1971) Nonsteady three dimensional stagnation point flow, *J. Appl. Mech.*, 38, 282-287.

DAVEY, A. & SCHOFIELD, D. 1967 Three-dimensional flow near a two-dimensional stagnation point.

Dorrepaal, J. M. "An exact solution of the Navier–Stokes equation which describes non-orthogonal stagnation-point flow in two dimensions." *Journal of Fluid Mechanics* 163 (1986): 141–147.

Drazin, Philip G., and Norman Riley. *The Navier–Stokes equations: a classification of flows and exact solutions*. No. 334. Cambridge University Press, 2006.

M. B. Glauert. The laminar boundary layer on oscillating plates and cylinders. *Journal of fluid mechanics*, pages 97–110, 1956.

C. E. Grosch and H. Salwen. Oscillating stagnation point flow. *Proceedings of the Royal Society of London. Series A, Mathematical and Physical Sciences*, 384:175–190, 1982.

P. Hall and D. T. Papageorgiou, *The onset of chaos in a class of Navier–Stokes solutions*, *J. Fluid Mech.*, 393 (1999), pp. 59–87.

A. L. Hazel and T. J. Pedley. Alteration of Mean Wall Shear Stress Near an Oscillating Stagnation Point. *Journal of Biomechanical Engineering*, 120:227, 1998.

K. Hiemenz. Die Grenzschicht an einem in den gleichformigen Flüssigkeitsstrom eingetauchten geraden Kreiszyylinder. *Dinglers Polytech. J.*, 326:321–410, 1911.

Homann, Fritz. "Der Einfluss grosser Zähigkeit bei der Strömung um den Zylinder und um die Kugel." *ZAMM-Journal of Applied Mathematics and Mechanics/Zeitschrift für Angewandte Mathematik und Mechanik* 16.3 (1936): 153–164.

Howarth, Leslie. On the calculation of steady flow in the boundary layer near the surface of a cylinder in a stream. No. ARC-R/M-1632. AERONAUTICAL RESEARCH COUNCIL LONDON (UNITED KINGDOM), 1934.

M. Ishigaki, *Periodic boundary layer near a two-dimensional stagnation point*, *J. Fluid Mech.*, 43 (1970), pp. 477–486.

Libby, Paul A. "Laminar flow at a three-dimensional stagnation point with large rates of injection." *AIAA Journal* 14.9 (1976): 1273–1279.

M. J. Lighthill, *The response of laminar skin friction and heat transfer to fluctuations in stream velocity*, Proc. Roy. Soc. London A, 224 (1954), pp. 1–23.

G. J. Merchant and S. H. Davis, *Modulated stagnation point flow and steady streaming*, *J. Fluid Mech.*, 198 (1989), pp. 543–555.

Y. Matunobu, *Structure of pulsatile Hiemenz flow and temporal variations of wall shear stress near the stagnation point II*, *J. Phys. Soc. Japan*, 43 (1977), pp. 326–329.

T. J. Pedley. Two-dimensional boundary layers in a free stream which oscillates without reversing. *Journal of Fluid Mechanics*, 55:359–383, 1972.

N. Riley. Oscillating Viscous Flows. *Mathematika*, 12:165–175, 1965.

N. Riley and R. Vasantha. An unsteady stagnation-point flow. *Quarterly Journal of Mechanics and Applied Mathematics*, 42:511–521, 1989.

N. Rott. Unsteady viscous flow in the vicinity of a stagnation point. *Quarterly of Applied Mathematics*, 13(4):444–451, 1956.

SCHOFIELD, D. & DAVEY, A. 1967 Dual solutions of the boundary-layer equations at a point of attachment. *J. Fluid Mech.* 30, 809–811.h

H. Schlichting, *Berechnung ebener periodischer Grenzschichtströmungen*, *Phys. Z.*, 33 (1932), pp. 327–335

J. T. Stuart. The viscous flow near a stagnation point when the external flow has uniform vorticity. *Journal of Aerospace Science*, 26:124–125, 1959.

J. T. Stuart. Double boundary layers in oscillatory viscous flow. *Journal of Fluid Mechanics*, 24(4):673–687, 1966.

Stuart, J. T. "The viscous flow near a stagnation point when the external flow has uniform vorticity." *Journal of the Aerospace Sciences* (2012).

K. Tamada. Two-dimensional stagnation point flow impinging obliquely on a plane wall. *Journal of the Physical Society of Japan*, 46(2):310–311, 1979. BIBLIOGRAPHY 164

R. M. Tooke and M. G. Blyth. A note on oblique stagnation-point flow. *Physics of Fluids*, 20:033101, 2008.

J. Watson. The two-dimensional laminar flow near the stagnation point of a cylinder which has an arbitrary transverse motion. *The Quarterly Journal of Mechanics and Applied Mathematics*, 12(2):175, 1959.

Wang, C. Y. (1973). Axisymmetric Stagnation Flow Towards a Moving Plate. *American Institute of Chemical Engineering Journal*, 19(5), 1080-1082.

Wang, C. Y. "Stagnation flow on the surface of a quiescent fluid—an exact solution of the Navier–Stokes equations." *Quarterly of applied mathematics* 43.2 (1985): 215–223.

Weidman, P.D. and Mahalingam, S. (1997), Axisymmetric stagnation point flow impinging on a transversely oscillating plate with suction, *J. Engg. Math.* 31, No. 4, pp. 305-318.

CURRICULUM VITAE

PERSONAL INFORMATION

Surname, Name: Belhaj, Ali Mohamed

Nationality: Libyan

Date and Place of Birth: 19 November 1967, Alsabiah – Libya

Marital Status: Married with 4 children

Phone: +218922307055

email: ali.belhag@yhoo.com



EDUCATION

MS Kazan University Mechanical Engineering, 2002

BS Tripoli University Engineering, 1993

High School Alzahra for boys

WORK EXPERIENCE

2018 Present University Teacher

2005 – 2012 University Teacher and Human development coach

1997 – 2004 Engineer at the Technical Research Center

LANGUAGES

Arabic (Native), English (V.Good), Russian (Little)

HOBBIES

Reading and writing, Tourism and exploration, Photography.